

Conformally curved binary black hole initial data including tidal deformations and outgoing radiation

Nathan K. Johnson-McDaniel,¹ Nicolás Yunes,² Wolfgang Tichy,³ and Benjamin J. Owen¹

¹*Institute for Gravitation and the Cosmos, Center for Gravitational Wave Physics,
Department of Physics, The Pennsylvania State University, University Park, PA 16802, USA*

²*Department of Physics, Princeton University, Princeton, NJ 08544, USA*

³*Department of Physics, Florida Atlantic University, Boca Raton, FL 33431, USA*

(Dated: July 10, 2009)

By asymptotically matching a post-Newtonian (PN) metric to two perturbed Schwarzschild metrics, we generate approximate initial data (in the form of an approximate 4-metric) for a nonspinning black hole binary in a circular orbit. We carry out this matching through $O(v^4)$ in the binary's orbital velocity v , and thus the resulting data, like the $O(v^4)$ PN metric, are conformally curved. The matching procedure also fixes the quadrupole and octupole tidal deformations of the holes, including the 1PN corrections to the quadrupole fields. Far from the holes, we use the appropriate PN metric that accounts for retardation, which we construct using the highest-order PN expressions available to compute the binary's past history. The data set's uncontrolled remainders are thus $O(v^5)$ throughout the timeslice; we also generate an extension to the data set that has uncontrolled remainders of $O(v^6)$ in the purely PN portion of the timeslice (i.e., not too close to the holes). This extension also includes various other readily available higher-order terms. The addition of these terms decreases the constraint violations in certain regions, even though it does not increase the data's formal accuracy. The resulting data are smooth, since we join all the metrics together by smoothly interpolating between them. We perform this interpolation using transition functions constructed to avoid introducing excessive additional constraint violations. Due to their inclusion of tidal deformations and outgoing radiation, these data should substantially reduce both the high- and low-frequency components of the initial spurious ("junk") radiation observed in current simulations that use conformally flat initial data. Such reductions in the nonphysical components of the initial data will be necessary for simulations to achieve the accuracy required to supply Advanced LIGO and LISA with the templates necessary for parameter estimation.

PACS numbers: 04.25.Nx, 04.25.dg, 04.30.Db

I. INTRODUCTION

A. Motivation and overview of results

At present, several years after the initial breakthroughs in the evolution of binary black hole spacetimes [1, 2, 3], numerical relativity has matured to the point where successful binary black hole simulations are now commonplace (see, e.g., [4] for a review). Recent progress in the nonspinning case includes simulations of systems with mass ratios of up to 10 : 1 [5, 6] and longer, more accurate simulations of equal-mass systems [7, 8].

It is now time to consider what improvements need to be made to these simulations so that they are accurate enough to provide gravitational wave detectors such as LIGO [9] with the model waveforms they need to detect and study binary black holes. The accuracy required of such waveforms has been studied by Lindblom, Owen, and Brown (LOB) [10]. Their results imply that current simulations are sufficiently accurate to supply the waveforms necessary for detection with either LIGO or LISA [11]. This conclusion is supported by the Samurai [12] and NINJA [13] projects, which indicate that currently used data analysis pipelines (including some not based on matched filtering) can easily detect a wide variety of numerical relativity waveforms at essentially

the same level in stationary gaussian noise. The Samurai project also performs a more detailed comparison of a subset of waveforms for parameter estimation, and finds that they are all indistinguishable if used for estimation of intrinsic parameters (i.e., not sky position or arrival time) at a signal-to-noise ratio (SNR) of less than 14 (25 if one eliminates the code that disagrees the most with the others).

However, Advanced LIGO may detect binary black hole signals with SNRs of order 100 [10]. According to LOB [10], if a waveform's phase error (suitably averaged in the frequency domain) is less than 0.007 radians, then it is suitable for use in parameter estimation with Advanced LIGO with such an SNR. However, even the Caltech/Cornell group's simulations (which are arguably the most accurate yet) have maximum phase errors (in the time domain) of order 0.01 radians or more (see [7, 14] for some discussion of their error budget). Converting such error measures to the criteria of LOB is more subtle than it looks and we do not attempt it here. (See [15] for a discussion of some possible pitfalls, along with suggestions for successful applications of the standards from LOB.) However it seems likely that even the Caltech/Cornell group's simulations may not satisfy the LOB conditions for parameter estimation, at least for binaries whose masses place the worst phase error in the detector's most sensitive frequency band.

All current binary black hole simulations incur some error from the initial data used. These data sets’ lack of astrophysical realism is clearly announced by the burst of spurious (or “junk”) radiation present at the beginning of these simulations. This junk radiation is also responsible for various deleterious effects on simulations. First, one wastes the computer time required for the spurious radiation to propagate off the computational grid. Second, the system that remains after that time has been perturbed by the spurious radiation. This radiation’s most prominent effect is to increase the binary’s eccentricity,¹ though it also slightly increases the masses of the holes—see [19]. Additionally, in the unequal-mass case, the initial junk radiation is emitted anisotropically, giving the system a small “kick” transverse to the holes’ initial orbital motion [20]. The high-frequency component of the spurious radiation is a particular problem for spectral codes. For instance, the Caltech/Cornell group finds that the high-frequency component of the initial pulse of spurious radiation generates secondary spurious waves that propagate throughout the computational domain for two light-crossing times after the initial junk radiation has exited [7, 14].

Currently employed initial data’s omission of significant features of the spacetime can also be seen analytically. Except for occasional tests of initial data (discussed in Sec. IB), all current simulations use initial data sets that assume *conformal flatness* (i.e., that the spatial metric is a scalar multiple of the flat 3-metric). The assumption of conformal flatness is convenient, since it allows one to get simple, mostly analytic expressions for initial data that exactly solve the constraint equations and include orbiting black holes (see, e.g., [21, 22] for reviews).

In general, these sets are geared either towards the puncture or excision approaches. The majority of the community uses punctures, with initial data stemming from [23]. These data are very flexible, as they contain parameters with which one can directly set the momentum and spin of each hole. For instance, for evolutions with spinning holes, one can simply set these parameters using post-Newtonian (PN) results as in [24, 25, 26, 27]. For nonspinning configurations in a circular orbit, parameter choices based on the assumption of a helical Killing vector [28, 29] are possible as well. The Caltech/Cornell and Princeton groups use excision [30, 31], with initial data constructed using the conformal thin-sandwich method (see, e.g., [32]). These data are slightly harder to construct than puncture data are, since one has to solve a larger number of elliptic equations. However, excision data have the advantage of a direct connection to the isolated horizon formalism [33], which allows one to construct holes with well-defined masses and spins. Additionally, the excision approach is applicable to a wider

array of initial data construction methods: It is used in all of the extant evolutions of superposed black hole data sets except for one specifically tailored to the puncture approach. (See Sec. IB for a discussion of these evolutions.) The data we present here also require evolutions using excision or the turducken approach [34].

Conformally flat initial data cannot accurately represent some features of a binary black hole spacetime, since the PN metric for a binary system stops being spatially conformally flat at $O(v^4)$, where v is the binary’s orbital velocity in units of c , the speed of light (see Sec. IV A for discussion). This is the same order at which gravitational radiation enters the PN metric (see Sec. IV B for discussion). The order at which this fundamental disagreement with PN predictions first occurs gives a rough indication of the error committed in using conformally flat initial data. At present, the simulation for which this error is the smallest is the longest of the Caltech/Cornell runs (in [7]), for which $v_{\text{initial}} \simeq 0.24$, where v_{initial} is the binary’s initial orbital velocity. We expect the initial data’s conformal flatness to only affect the waveform at $O(v_{\text{initial}}^4)$, which for this run is comparable to the phase error allowed for a waveform to be used for parameter estimation with Advanced LIGO. It is thus possible (though perhaps not likely) that conformally flat initial data would be suitable for use in the simulations that will generate such waveforms.

It is unlikely that conformally flat initial data can be used to generate the waveforms required for parameter estimation with LISA. Here the required (appropriately averaged frequency domain) phase accuracy is 2×10^{-4} radians [10], 20 times smaller than v_{initial}^4 for the longest of Caltech/Cornell’s simulations. One can reduce the error in the initial data by starting the simulation with a larger separation. However, $v_{\text{initial}}^4 \simeq 2 \times 10^{-4}$ implies an initial (PN coordinate) separation of ~ 71 times the binary’s mass, and thus a merger time that is over 400 times as long as the Caltech/Cornell group’s longest simulations to date, which start from a (PN coordinate) separation of ~ 15.3 times the binary’s mass. It is thus necessary to improve the accuracy of the initial data. Evolutions of more accurate initial data will also give a direct measure of the errors introduced in using current, conformally flat initial data.

This paper provides initial data that include more of the physics present in the binary’s spacetime than any previous constructions. In particular, our data’s accurate description of certain properties of the spacetime should substantially reduce *both* components of the aforementioned spurious radiation. These two components are thought to come from different physical effects. The long-wavelength component is thought to correspond to the initial data’s lack of outgoing gravitational radiation, whose wavelength would be somewhat longer than the orbital separation. Of course, one expects the junk to be generated predominantly in the strong-field region near the holes, where the binary’s gravitational radiation cannot be disentangled from the rest of its gravitational field.

¹ In practice, the eccentricity can be reduced by various means [16, 17, 18].

However, one also expects the pieces that one wants in the strong-field region to appear at $O(v^4)$, just as the true gravitational waves do in the radiation (or far) zone (defined in Sec. II). Our data include all the $O(v^4)$ terms in the strong and weak field regions. The short-wavelength component is thought to come from the holes' quasinormal modes ringing down, emitting gravitational radiation with wavelengths on the order of their masses, as they relax from their initial, close to spherical state to their desired tidally deformed state (see, e.g., [14]). Our data include the Newtonian quadrupole and octupole tidal deformations each hole induces on the other, as well as the 1PN corrections to the quadrupole deformations.

The tidal deformations are contained in perturbed Schwarzschild metrics, given (in the horizon-penetrating coordinate system we use) in Eqs. (3.5) and (3.6). The tidal fields are fixed by asymptotically matching these Schwarzschild metrics to an $O(v^4)$ PN metric, given in Eqs. (4.1); expressions for the tidal fields around hole 1 are given in Eqs. (B1). One also needs to introduce a coordinate transformation in order to put the black hole metrics in the same coordinate system as the PN metric. This transformation is also determined (perturbatively) by the matching; instructions for putting it together around hole 1 are given in Sec. V G. Instructions for converting all of these results to the region around hole 2 are given at the beginning of Sec. V.

The PN metric mentioned above treats retardation perturbatively and thus becomes inaccurate far from the binary. In that region, we thus use a version of the PN metric that includes retardation explicitly (but also uses a multipolar decomposition, so it does not provide the desired accuracy closer to the holes). This metric is given in Eqs. (6.6). Due to retardation, one needs to know the binary's past history accurately in order to obtain the far zone metric accurately far from the binary. This past history is computed in Sec. VI A to the highest PN order possible with current results. The contributions of these terms are of equal or higher order than some of our uncontrolled remainders, but their inclusion is necessary if one wishes to obtain, e.g., the correct phasing for the outgoing radiation.

We have also added other formally higher-order terms to the metrics, including all the readily available PN results, along with a resummation of the black hole backgrounds in the PN metric. We found that certain of these terms improved the constraint violations in various regions; other of these additional terms are expected to improve evolutions of the data. The resummation is given in Sec. VIII A; all the remaining higher-order terms are discussed in Sec. VII. The transition functions that we use to stitch the metrics together smoothly are given in Sec. VIII B. We have constructed these transition functions so that they satisfy the so-called Frankenstein theorems [35]. The resulting merged metric is thus guaranteed to have constraint violations whose formal order is no larger than the constraint violations of the individual metrics. See Appendix D for the technical details of

	$m^{3/2}\ H\ _2$ (10^{-2})	$m^2\ H\ _\infty$ (10^{-2})	$m^{3/2}\ \vec{M}\ _2$ (10^{-3})	$m^2\ \vec{M}\ _\infty$ (10^{-3})
This paper	1.565	0.631	2.973	1.879
Paper II	1.566	0.758	4.627	2.065
Paper I	9.149	4.466	5.837	2.531

TABLE I: The L^2 and sup norms (denoted by $\|\cdot\|_2$ and $\|\cdot\|_\infty$, respectively) of the Hamiltonian and momentum constraints (H and \vec{M}) for an equal-mass binary with a coordinate separation of 10 times its total mass, m . (The norms of the momentum constraint include the L^2 3-vector norm $\sqrt{M^k M_k}$, where the index is lowered using the metric under consideration.) These are computed along the x -axis outside the unperturbed horizons of the holes, but inside the interval $[-16.4m, 16.4m]$.

how we compute the metrics. We have generated MAPLE scripts and C code that produce initial data for a non-spinning binary of any mass ratio and initial separation in a quasicircular orbit. These are available at [36].

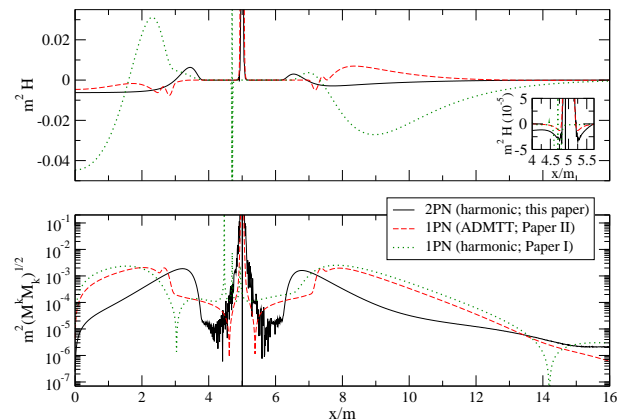


FIG. 1: The Hamiltonian constraint and norm of the momentum constraint along the x -axis around hole 1 for this paper's data along with the data from Papers I and II. (In the norm of the momentum constraint, the index is lowered using the metric in question.) All of these were computed for an equal-mass binary with a coordinate separation of 10 times its mass. In the inset, we zoom in to show how the Hamiltonian constraint violations behave close to the horizon. Note that the data from Paper II are in a different coordinate system throughout, and that the black hole background in Paper I's data is in a different (and not horizon penetrating) coordinate system.

The constraint violations give a measure of how much more accurate this paper's data are compared with those constructed in previous papers (viz., [37] and [38], which we refer to as Papers I and II). We plot the constraint violations of the three sets of data in Fig. 1. [See, e.g., Eqs. (14)–(15) in [21] for expressions for the constraint equations.] N.B.: While the Hamiltonian constraint violations of this paper's data are larger close to the hole than those of either of the previous papers' data, this is due to our inclusion of the full time dependence of the tidal fields, as discussed in Appendix D 1; the motivation

for doing this, even at the cost of larger constraint violations, is given in Sec. VII. If one does not include these higher-order terms, then the new data’s constraint violations are smaller close to the hole than those of either of the previous papers’ data. See Fig. 20 for a comparison of the constraint violations of the inner zone metric with and without full time dependence in the tidal fields. For a simple, quantitative comparison of the overall constraint violations, we can consider their L^2 and sup norms. These are presented for all three sets of data in Table I and show, as expected, that the new data have smaller overall constraint violations than either of the previous papers’ data. Of course, the L^2 norm of the new data’s Hamiltonian constraint violations is only very slightly less than that of the data from Paper II, but this is probably to be expected: See Sec. VIII C for some discussion of this, as well as further details about the comparison plot and table.

B. Conformally curved initial data

The problems with conformally flat data have inspired a variety of constructions of conformally curved binary black hole data, for which there are two general approaches. One approach—the one we have taken—is primarily motivated by a desire for astrophysical realism, seeing the spurious radiation as an indicator of the failure of conformally flat initial data to model the desired spacetime accurately enough. These constructions so far have restricted their attention to nonspinning binaries and used the PN approximation to include the binary’s physics. (Of course, true astrophysical binaries are expected to have significant spins, so the consideration of nonspinning binaries is merely a technical convenience appropriate for initial attempts at constructing astrophysically realistic data.) The other approach is primarily concerned with reducing the junk radiation in practice with relatively simple choices for initial data (viz., a superposition of boosted black holes). This approach is often geared primarily towards spinning black holes, since the amount of spurious radiation increases with the spin of the holes. (This is due to the nonexistence of a conformally flat slicing even of an isolated Kerr black hole with nonzero spin—see [39, 40].)

Besides our present work, other constructions in the first category are this work’s antecedents ([37, 38, 41], discussed in the next subsection), along with the approaches of Nissanke [42] and Kelly *et al.* [43]. (The latter two only use the PN approximation in their construction, so the resulting data cannot accurately describe the spacetime near the holes.) Nissanke, building on the work of Blanchet [44] (who constructed initial data for a head-on collision of initially stationary holes), obtains explicit analytic expressions for the 3-metric and extrinsic curvature from the 2PN metric. (N.B.: These constructions only use the version of the PN metric that treats retardation perturbatively, so the resulting data rapidly lose

accuracy away from the binary.) Kelly *et al.* [43] extend the work of Tichy *et al.* [45] to give initial data from the 2.5PN ADMTT metric that are valid through $O(v^4)$ and thus contain the binary’s outgoing radiation in the far zone. (See Sec. IV B for a discussion of why gravitational radiation is present at that order.) They do not obtain data that are valid through $O(v^5)$, even though the 2.5PN metric contains the $O(v^5)$ terms in all its components, since one would need the $O(v^6)$ terms in the spatiotemporal components to obtain initial data valid through $O(v^5)$: See Sec. I C 1 for further details. In order to obtain these data, they have to evaluate an integral numerically, so their data are not completely analytic. The original data in Tichy *et al.* [45] are completely analytic, though they use the version of the ADMTT metric available in the literature, which gives expressions for the $O(v^4)$ and $O(v^5)$ pieces of the transverse-traceless (TT) part of the metric that are only valid in the near zone. Tichy *et al.*’s data were thus only valid through $O(v^3)$ far from the holes. Kelly *et al.* calculated the additional terms necessary for the TT pieces to be valid through $O(v^4)$ in the far zone.

The most recent progress in the second category for nonspinning black holes is Lovelace’s [46] construction and evolution of superposed Schwarzschild data. (There is a companion construction and evolution of superposed spinning black hole data in Lovelace *et al.* [47].) Lovelace uses the superposed black hole data as free data for a constraint solver and finds that the resulting data produce less spurious radiation than conformally flat data. There are also older constructions in a similar vein [48, 49, 50], though their data have only been evolved in head-on collisions without first solving the constraints [51]. In this case, it was found that there was *more* spurious radiation with the superposed data than with Brill-Lindquist data. The Kerr puncture data presented by Hannam *et al.* [52] (who use Dain’s work in [53, 54] to construct superposed Kerr free data in puncture form for a constraint solver) have been shown to reduce the junk radiation for head-on collisions of spinning black holes. However, the given construction is only applicable to the case of a head-on collision of initially stationary holes: It has not been extended to give the holes linear momenta. The freedom inherent in these superposed black hole initial data constructions has been studied in [55], and a helical Killing vector version of superposed data is constructed in [56]. But neither of those papers’ data sets have been evolved, to our knowledge.

While the use of a conformally curved Kerr metric near each of the holes is likely responsible for most of the reduction of spurious radiation seen in the case of a spinning binary, it is not clear, physically, what feature of Lovelace’s data is reducing the spurious radiation in the Schwarzschild case. Furthermore, it is known [42] that the superposed nonspinning Kerr-Schild metric differs from the PN metric at 2PN, due to the lack of interaction terms (e.g., terms that involve products of the distances from the field point to each of the holes). Such

a disagreement with the PN metric is probably characteristic of all superposed initial data constructions, thus limiting their ability to substantially reduce the junk radiation.

Evolutions of conformally curved binary initial data are uncommon, and most have restricted their attention to the computationally cheap case of head-on collisions, as seen above. Only Lovelace [46] and Lovelace *et al.* [47] have evolved superposed black hole data for an orbiting binary. For the PN data, such head-on tests are mostly inapplicable: Only Nissanke’s data set is not already specialized to a (quasi)circular orbit. But even though her data (which reduce to Blanchet’s in the limit of a head-on collision of initially stationary black holes) could be tested using a head-on collision, they have not been evolved, to our knowledge.

In fact, the only evolution of PN initial data of which we are aware is that of Kelly *et al.* [57]. They evolved the data they obtained in [43] (as well as the original version without waves from [45]), necessarily doing so for an orbiting binary, since their data were derived under the assumption of a quasicircular orbit. They found what naïvely appears to be a slightly better reduction of the initial spurious radiation than that seen with Lovelace’s superposed black hole initial data, even without first solving the constraint equations. (Their data satisfy the constraints approximately, but not exactly.) However, the results are not directly comparable: Most importantly, Lovelace begins his evolution with a separation of about twice that with which Kelly *et al.* begin their evolution. Thus, while Kelly *et al.* see a slightly larger reduction in the maximum amplitude of their junk radiation, even their smallest amplitude is larger than that from the conformally flat data with which Lovelace is comparing his data’s performance. In addition, Kelly *et al.* are comparing their data’s performance with puncture data, while Lovelace is using conformal thin-sandwich excision data (constructed in the manner of Cook and Pfeiffer [32]) as a benchmark. (There are also other important differences, such as the extraction radius used and the mode of the junk radiation that is reduced most substantially.)

It is also important to realize that Kelly *et al.*’s data only reduce the low-frequency component of the junk radiation: The high-frequency component visible when using conformally flat puncture data is still present in the evolution of Kelly *et al.*’s data. This is not surprising, since their initial data make no attempt to include accurate tidal deformations on the holes. (And, indeed, their data’s constraint violations are largest near the holes.) In addition, they obtain nearly identical junk radiation when evolving the data with and without waves: The only difference is that the spurious radiation is superposed over the outgoing wave train when they evolve the data with waves; the spurious radiation itself appears to be unchanged. This, again, is what should be anticipated, since one expects the junk to be generated primarily in the strong field region near the holes, and Kelly *et al.*’s data (with waves in the far zone) have the same ac-

curacy in the strong field region as Tichy *et al.*’s original data (without waves in the far zone).

As mentioned in the previous subsection, the data set we construct here should help reduce *both* components of the junk radiation, since it includes an accurate description of the spacetime near the holes (including the quadrupolar and octupolar tidal deformations), matched to the PN metric through $O(v^4)$. We also offer an extension to these data that are accurate through $O(v^5)$ in the PN portions of the timeslice (i.e., not too close to the holes). This extension includes certain other higher-order terms, as well, including higher-order corrections to the trajectories. While these “extra” higher-order terms do not increase the data’s formal accuracy, even in just the PN portions, such terms will likely improve the accuracy of the data in practice. This extension will also allow for a more direct comparison with Kelly *et al.*’s results, since they included the $O(v^5)$ terms in the spatial metric in the near zone (though not the matching $O(v^6)$ terms in the extrinsic curvature, which we have). Such a comparison would reveal how much of the spurious radiation is due to the initial data’s failure to include the correct tidal deformations.

C. Specifics of our approach and its relation to other work

With currently available technology, if one wishes to generate initial data that include the holes’ tidal deformations or the binary’s outgoing radiation, it is necessary to allow the initial data (as first constructed) to be merely an approximate solution of the constraint equations. (One can always use these approximate data as free data for a constraint solver and thus obtain an exact solution of the constraints, to numerical precision.) Since the post-Newtonian approximation has been developed to a very high order, it is an obvious choice for the description of the binary’s spacetime. Indeed, an explicit expression for the metric to 2.5PN order (with a perturbative treatment of retardation) is given by Blanchet, Faye, and Ponsot (BFP) [58].

However, one cannot obtain accurate initial data throughout a timeslice of the binary’s spacetime using just the PN metric, since the PN approximation breaks down near the holes: The PN approximation is a weak-field approximation (due to the post-Minkowskian iteration in powers of G , Newton’s gravitational constant), in addition to being a slow-motion approximation (the post-Newtonian expansion proper, which formally proceeds as an expansion in $1/c$, where c is the speed of light). Moreover, the standard PN approximation (as presented, e.g., in BFP) treats retardation perturbatively. It thus becomes inaccurate quite rapidly as one enters the radiation zone (i.e., when one is further than about a reduced gravitational wavelength away from the binary’s center of mass).

The resolution of both of these problems is to realize

that there is an appropriate approximate description of the spacetime in each of the regions where the standard PN metric is no longer a good approximation: Near each of the holes, in the regions known as the *inner zones*, spacetime is well described by a perturbed black hole metric. (These zones, as well as the others we mention here, are defined more precisely in Sec. II.) In the radiation zone (or *far zone*) there is another version of the PN metric that incorporates retardation nonperturbatively. These are all readily available in the literature to the order we need them. For the reasons described below, we choose to use Detweiler’s perturbed black hole metric [59] in addition to BFP’s PN metric. We also choose to put together the far zone metric following the recipe and ingredients supplied by Pati and Will [60, 61]. (In addition, we use Blanchet’s results [62] for the evolution of the binary’s phase with radiation reaction: These secular effects are important in obtaining the far zone metric accurately, due to its dependence upon retarded time—see Sec. VIA.)

One then has to stitch all these spacetimes—the far zone, inner zones, and the *near zone* where the standard PN metric is valid—together into one global approximate metric. (Of course, this metric will be global in space, but not in time—i.e., it will only be accurate in a temporal neighborhood of a timeslice of the binary’s spacetime.) This stitching-together proceeds in two steps: First, one uses the technique of matched asymptotic expansions to match the metrics at a formal level. This puts all the metrics in the same coordinate system (up to uncontrolled remainders) and fixes any previously undetermined parameters (e.g., the holes’ tidal perturbations) so that the metrics are asymptotic to each other in their regions of mutual validity (the *buffer zones*). The final, numerical merging of the metrics is effected by *transition functions* that smoothly interpolate between the metrics in their mutual buffer zones. The resulting merged metric is guaranteed to satisfy the Einstein equations to the same order as its constituent metrics because the transition functions are constructed following the so-called Frankenstein theorems [35]. (We have checked this scaling explicitly in Sec. VIIC.)

Once one has obtained such approximate initial data, it is, of course, possible to use them as the input to a numerical constraint solver, and thus obtain an exact solution, to numerical precision. In fact, it is probably desirable to do so. The idea when doing this is that if the input to the constraint solver satisfies the constraints to some reasonably good tolerance, and describes the desired physics, the “exact” solution one obtains after solving the constraints will not differ too much from the input in its physical content. This is probably true regardless of how one chooses to produce the “exact” solution to the constraints, as long as the procedure modifies the initial guess in a reasonable way. (For instance, the York-Lichnerowicz decomposition [21] multiplies the initial data by an appropriate conformal factor and modifies the extrinsic curvature by the gradient of a vector field

so that the data satisfy the constraint equations—both Pfeiffer *et al.* [63] and Tichy *et al.* [45] have implemented this numerically without the assumption of conformal flatness.) However, it may be preferable to project the approximate initial data onto the closest “point” on the constraint hypersurface (as measured by some appropriate norm), possibly using the results of [64].

If one chooses to evolve without solving the constraints (as did Kelly *et al.*), then one will not have a true vacuum evolution: The constraint violations will act as matter (which may not satisfy any of the standard energy conditions). For instance, Bode *et al.* [65] investigated the evolution of initial data that only approximately satisfied the Hamiltonian constraint (though the momentum constraint was satisfied exactly). They found that the holes accreted the negative Hamiltonian constraint violations that surrounded them, decreasing their masses. Additionally, the initial apparent horizon masses were larger than the irreducible masses for the constraint-violating data, but equaled them for the constraint-satisfying data.

1. Comparisons with similar constructions

Alvi [41] was the first to attempt to construct binary black hole initial data by matching perturbed black hole metrics onto a PN metric, considering, for simplicity, two nonspinning black holes in a circular orbit. (All subsequent attempts using this procedure, including the present one, have also restricted their attention to this simplest case.) In performing this calculation, he fixed the perturbation (encoded in multipolar tidal fields) on the holes *a priori*, using its expected Newtonian quadrupole value, instead of reading it off from the matching as we do here. This gives the same result for the lowest-order pieces of the tidal fields as our method, though it does not offer the opportunity of reading off the higher-order corrections, as we can.

Numerical experiments with Alvi’s initial data [66] demonstrated that they were not suitable for use in evolutions. This inspired Yunes *et al.* [37] (Paper I) to revisit the problem and correct various deficiencies in Alvi’s method, such as an inconsistent order counting (due to not including the terms needed to compute the extrinsic curvature to the appropriate order; this is discussed below) and a lack of smoothness at the joins of the global metric (due to not actually performing asymptotic matching). Yunes and Tichy [38] (Paper II) then improved this initial data construction (in the sense of getting better numerical agreement between the metrics) by putting the near zone metric in a form that is very close to the inner zone metric near the holes. This was done by applying some resummation and using ADMTT coordinates instead of harmonic coordinates for the PN metric. They also constructed horizon-penetrating coordinates to give the first usable initial data generated with this method. However, in both cases the initial data were only valid through $O(v^2)$ and the tidal fields were still

just the lowest-order ones Alvi had obtained.

The present calculation builds on all these previous attempts, computing fully matched initial data through $O(v^4)$, so as to include the pieces of the PN metric that break conformal flatness (and contain gravitational radiation), and reading off the tidal fields (including the 1PN corrections to the quadrupole fields) from the matching. (We also demonstrate that the mass parameters of the PN metric are equal to those of the perturbed Schwarzschild metrics to the order considered: This is established here more firmly than in Papers I and II in addition to being extended to higher order.) In addition, we have included the radiation zone portion of the metric to accommodate the larger grid sizes common in current simulations. This was done explicitly by Alvi and implicitly in Paper II, due to its use of the ADMTT PN metric, though neither of them included the effects of radiation reaction on the binary’s past evolution in their far zone metric. The radiation zone was neglected completely in Paper I, which used a harmonic metric, as we do here. Additionally, all the previous versions used a corotating coordinate system, while the current calculation stays in inertial coordinates.

While we only obtain fully matched initial data through $O(v^4)$, we actually have to carry out the matching of the 4-metric through $O(v^5)$ in order to do so: We need to match the $O(v^5)$ pieces of the spatiotemporal components of the 4-metrics in order to obtain the extrinsic curvature consistently [see the discussion after Eq. (2) in Paper I], and one needs to carry out the matching of all the components in order to obtain the $O(v^5)$ piece of the coordinate transformation.

Additionally, while our goal was simply to keep terms of quadrupolar order overall in the multipole expansion, as was done previously, we found that it was necessary to match the lowest-order octupolar pieces in order to match the 1PN corrections to the quadrupole pieces consistently. This is discussed in Sec. V A. In fact, we have carried out the matching of quadrupole pieces to the highest possible order to which it can be done consistently without the inclusion of the hexadecapole tidal fields. (These hexadecapole pieces can only be included with input from nonlinear black hole perturbation theory, as the “quadrupole squared” pieces are of hexadecapole order.) We also obtained the 1PN correction to the electric octupole and the associated piece of the coordinate transformation as a further application of our matching procedure. However, we cannot obtain the other $O(v^4)$ octupole pieces in the initial data (since they include the hexadecapole tidal fields), so our knowledge of these corrections does not allow us to increase the formal order to which our data are valid.

Building on the work done in Paper II, we have used horizon-penetrating coordinates for the black holes from the outset. This requirement of horizon penetration is necessary for numerical purposes. The coordinates need to be regular and the lapse positive in a neighborhood of the horizon: Even though the spacetime near the singu-

larity will be excised or filled with matter, one needs to be able to evolve at least a small portion of the spacetime inside the horizon.

At the same time, we want the coordinates for the black hole and PN metric to agree as closely as possible before the matching has been performed: Close agreement makes for simple matching algebraically and improves the numerical agreement of the resulting matched metrics. Ideally, the coordinates would agree exactly for an unperturbed black hole, though this is not compatible with the requirement of horizon penetration, as standard PN coordinates (harmonic or ADMTT) are not horizon penetrating. We thus attempted instead to obtain agreement between the two coordinate systems to as high a PN order as possible.

These desiderata are satisfied if we use the fully harmonic version of Cook-Scheel coordinates [67] for the black hole and standard (PN) harmonic coordinates for the PN metric:² Cook-Scheel coordinates are horizon-penetrating, and in their fully harmonic version only differ from PN harmonic coordinates for an unperturbed black hole at $O(v^4)$. See Appendix A for an explicit comparison. This agreement was the best of any of the horizon-penetrating coordinate systems present in the literature we consulted (even if we also consider ADMTT coordinates for the PN metric). Of course, we then adjust this coordinate system perturbatively so that it agrees with the near zone coordinate system to the order we have matched. However, we have checked that this adjustment does not affect the coordinates’ horizon penetration. The agreement between the coordinate systems used in Paper II was exact in the unperturbed case, while it is not here. However, we decided against converting the PN metric to horizon-penetrating coordinates for this version of the data—see Sec. VIII A for further details.

The other choices for our ingredients were made for computational ease. We selected Detweiler’s perturbed black hole metric [59] instead of Poisson’s [68] because Detweiler expresses the tidal fields in the Thorne-Hartle-Zhang (THZ) harmonic specialization of locally inertial coordinates [69, 70]. This gauge choice agrees better with the PN metric in harmonic coordinates than does Poisson’s light-cone gauge. For the far zone, the results from the direct integration of the relaxed Einstein equations (DIRE) approach were the obvious choice: Pati and Will [60, 61] give an explicit recipe for computing the far zone metric to the order we need it, along with all the nec-

² We use the term *harmonic coordinates* to refer to *any* coordinates x^α that satisfy $\nabla_\alpha \nabla^\alpha x^\beta = 0$, not just PN harmonic coordinates. (Here ∇_α is the covariant derivative associated with the metric under consideration and indices are raised using that metric.) For an unperturbed Schwarzschild black hole of mass M , PN harmonic coordinates are obtained by transforming the Schwarzschild radial coordinate \mathcal{P} to $R_{\text{PN}} = \mathcal{P} - M$ and thus retain the coordinate singularity at the horizon present in Schwarzschild coordinates.

essary ingredients (except for a few that can be obtained from Will and Wiseman [71]). Even more conveniently, their expression is in the same (harmonic) coordinate system as BFP’s PN metric, so we do not have to determine a coordinate transformation for the matching between the near and far zones. [We have checked explicitly that the near and far zone metrics match through $O(v^5)$ in all components.] One also needs to know the binary’s past history in order to obtain the far zone metric accurately, due to retardation: We calculate this in the PN approximation using Blanchet’s results [62].

We could have used Alvi’s result for the far zone metric [41] if we had only been interested in obtaining initial data valid through $O(v^4)$: Alvi’s metric, computed following Will and Wiseman, is in the same coordinate system as Pati and Will’s (and thus BFP’s near zone metric), and is computed through $O(v^5)$ in all its components. However, we needed higher-order results than he obtained, or Will and Wiseman’s results could give, to construct our extended data. This is also why BFP’s metric was preferable to the ADMTT metric given by Jaranowski and Schäfer [72]: One needs to calculate several integrals (one of which Kelly *et al.* [43] had to resort to numerical techniques to evaluate) to obtain even the $O(v^4)$ pieces of the far zone metric in this approach, while it is possible to obtain the $O(v^5)$ pieces of the far zone metric merely by taking derivatives using Pati and Will’s results. [One is also able to obtain initial data through $O(v^5)$ in the near zone using BFP’s results, since they give the $O(v^6)$ pieces of the spatiotemporal components of the metric. This is not possible with Jaranowski and Schäfer’s results.]

2. Comparison with Taylor and Poisson’s determination of the tidal fields

Our method for determining the tidal fields can be compared and contrasted with that employed in the recent calculation by Taylor and Poisson [73]. Most importantly, Taylor and Poisson’s aims are slightly different and more general: They have carried out the matching of a single black hole to an arbitrary 1PN metric (expressed in terms of potentials), and used the standard PN prescription (for obtaining equations of motion) for which orders to keep in the various components, as opposed to our “initial data prescription.” They thus keep terms through $O(v^4)$ in the purely temporal component of the metric, $O(v^3)$ in the spatiotemporal components, and $O(v^2)$ in the purely spatial components, while we keep terms through $O(v^5)$ in all components. [While the $O(v^5)$ terms in the purely temporal and purely spatial components are needed to obtain the $O(v^5)$ piece of the coordinate transformation, which itself is necessary for obtaining the initial data to a formal accuracy of $O(v^4)$, those components themselves do not increase the formal accuracy of the resulting initial data.] We also expand the near zone metric in multipoles before matching, while

Taylor and Poisson do not.

But the general setups have some superficial similarities: Both approaches use harmonic coordinates for the PN metric and THZ coordinates [69, 70] for the black hole perturbation. However, Taylor and Poisson transform Poisson’s perturbed black hole metric [68] to the THZ gauge instead of using Detweiler’s result [59] directly. Additionally, they use PN harmonic coordinates for the black hole background, since they have no need for their coordinates to be horizon penetrating.

The actual determination of the tidal fields is carried out in a very different manner in the two calculations: Taylor and Poisson first introduce the most general coordinate transformation that preserves the post-Newtonian form of the metric. They then specialize it so that it transforms harmonic coordinates to harmonic coordinates, and apply it to the PN potentials. After this, they decompose the transformed potentials into irreducible pieces, and can then finally use the matching conditions to determine expressions for the tidal fields in terms of the potentials. They also obtain the black hole’s equations of motion and the previously undetermined pieces of the coordinate transformation from the matching conditions.

We, however, have adopted a more brute force approach that assumes nothing about the coordinate transformation *a priori*, except its zeroth-order value. (In fact, even the zeroth-order value can be shown to be constrained by the matching.) However, it *does* assume that the PN point particle trajectories are valid for black holes, as is required by the strong equivalence principle: Taylor and Poisson demonstrate that this is indeed the case (to the order they have matched). Our method also requires no decomposition, though it makes heavy use of the computer algebra system MAPLE and the associated tensor manipulation package GRTENSORII [74]. We use the gauge invariance of the linearized Riemann tensor and linear independence to separate out the portions of the equations that determine the tidal fields from those that determine the coordinate transformation. See Sec. V A for a detailed presentation of our algorithm.

With this method, we obtained expressions for the tidal fields that can be compared with those of Taylor and Poisson: The pieces that we both computed agree exactly. See Appendix B 1 for a comparison, including explicit expressions for the tidal fields we obtained. While our expressions do not have the full generality of Taylor and Poisson’s, they *do* include the 1PN corrections to the magnetic quadrupole and electric octupole fields (for a circular orbit), neither of which Taylor and Poisson computed.

D. Structure of the paper

We begin by giving an overview of our matching procedure in Sec. II and then present expressions for the inner and near zone metrics in Secs. III and IV. In Sec. IV, we

also consider two relevant aspects of the PN metric, viz., conformal flatness breaking and gravitational radiation effects. Next we discuss the specifics of our matching procedure and read off the matching parameters and coordinate transformation order-by-order in Sec. V. We compute the far zone metric in Sec. VI, where we also discuss the PN results we use to obtain the effects of radiation reaction on the binary’s evolution. In Sec. VII we give an overview of the construction of an extension of this data set that is valid through $O(v^5)$ in the near and far zones, in addition to including various other higher-order terms. Then we stitch the metrics together numerically in Sec. VIII, first resumming the near zone metric to improve its strong field behavior (and thus the matching), then constructing transition functions to stitch all the metrics together smoothly, and finally considering the constraint violations of the resulting merged metric. Lastly, we conclude and summarize in Sec. IX.

We present various ancillary results and technical details in the appendices: Appendix A compares Cook-Scheel and PN harmonic coordinates. We provide explicit expressions for the tidal fields and some related discussion in Appendix B, along with the calculation of the fourth order pieces of the octupole tidal fields and the polynomial part of the associated coordinate transformation. In Appendix C, we give the details of our calculation of the higher-order extension to the data, and in Appendix D the precise details of how the metrics are implemented numerically.

E. Notation and Conventions

Units: We use geometrized units with $G = c = 1$ throughout. (G is Newton’s constant and c is the speed of light.)

Binary parameters: The binary’s orbital velocity is v , its orbital angular velocity is ω , and its coordinate separation is b . The masses of the holes are m_1 and m_2 ; their total mass is $m := m_1 + m_2$.

Orbit terminology: When we are only considering terms through $O(v^4)$ and the PN equations of motion are thus conservative, we shall refer to the binary’s orbit as circular. When we are considering nonconservative terms [at $O(v^5)$ and higher] but find that their effects can be ignored in the current portion of our calculation, we shall refer to the binary’s orbit as (quasi)circular. When we construct the extension to our data in Sec. VII and Appendix C or are considering the binary’s past history as encoded in the far zone metric in Sec. VIA and can no longer ignore radiation reaction, we refer to quasicircular orbits.

Indices: We use the standard convention that Greek letters denote spacetime indices, while lowercase Roman letters (here k, l, p, s, u , and v) denote spatial indices. In Sec. III, uppercase Roman letters denote indices on the 2-sphere, but in Secs. II, IV, and VIIIB they label the holes, as well as, by extension, the zones into which

we divide the data’s timeslice. [In the latter context, the notation “ $+(1 \leftrightarrow 2)$ ” denotes that the preceding expression is to be added to itself with the labels 1 and 2 switched.] In Sec. VI and Appendix C, Q denotes a multi-index. Except where otherwise noted (e.g., in Secs. IV A, VI, and VIII), spacetime indices are raised and lowered using the Minkowski metric $\eta_{\alpha\beta}$, so spatial indices are raised and lowered using the Kronecker delta $\delta_{kl} := \text{diag}(1, 1, 1)$ (the symbol “ $=$ ” indicates a definition). We may even freely raise and lower spatial indices within expressions for notational convenience, particularly in Sec. IV. The summation convention is always in force, and may even be applied to spatial indices that are at the same level, particularly in Sec. VI. Parentheses, square brackets, and angle brackets on indices denote symmetrization, antisymmetrization, and the symmetric trace-free projection, respectively. For instance, $A_{(\alpha\beta)} := (A_{\alpha\beta} + A_{\beta\alpha})/2$, $A_{[\alpha\beta]} := (A_{\alpha\beta} - A_{\beta\alpha})/2$, and $A_{<kl>} := (A_{kl} + A_{kl})/2 - A^p{}_p \delta_{kl}/3$. We use vertical bars to exclude indices from these operations—e.g., $A_{(\alpha|\beta|\gamma)} := (A_{\alpha\beta\gamma} + A_{\gamma\beta\alpha})/2$.

Arrays: In addition to the ordinary 3-dimensional Kronecker delta defined above, we also define a “lowered 4-dimensional Kronecker delta,” $\Delta_{\alpha\beta} := \text{diag}(1, 1, 1, 1)$. Our conventions for the three- and four-dimensional Levi-Civita symbols ϵ_{klp} and $\epsilon_{\alpha\beta\gamma\delta}$ are that $\epsilon_{123} = \epsilon_{0123} = 1$.

Metrics: As is usual, $\eta_{\alpha\beta}$ denotes the Minkowski metric; our signature is $(-, +, +, +)$. In Secs. IV and V (and Appendix B) $g_{\alpha\beta}$ denotes the near zone (PN) metric and $h_{\alpha\beta}$ denotes the inner zone (perturbed black hole) metric. In Sec. VIII A and Appendix A, $g_{\alpha\beta}$ (sometimes with decorations) is also used for the unperturbed Schwarzschild metric. In Sec. VI (and the associated Appendix C), $g_{\alpha\beta}$ denotes the far zone metric, and $h_{\alpha\beta}$ its associated metric perturbation.

Coordinates: Inner zone coordinates are $\mathcal{X}^\alpha = (T, \mathcal{X}^k)$, with $\mathcal{P} := \sqrt{\mathcal{X}_k \mathcal{X}^k}$ (Schwarzschild); $X^\alpha = (T, X^k) = (T, X, Y, Z)$, with $R := \sqrt{X_k X^k}$ (Cook-Scheel). PN harmonic coordinates (used in the near and far zones) are $x^\alpha = (t, x^k) = (t, x, y, z)$, with $r := \sqrt{x_k x^k}$; r^α denotes just the spatial coordinates [i.e., $r^\alpha = (0, x^k)$]. Unit vectors are denoted by “hats.” For instance, $\hat{t}^\alpha, \hat{x}^\alpha, \hat{y}^\alpha$, and \hat{z}^α are the Cartesian PN coordinate basis vectors corresponding to indices 0, 1, 2, and 3, respectively. Because we are interested in expanding in the distance from hole 1, we also define “tilded” coordinates with their origin at hole 1’s position at $t = 0$, viz., $\tilde{x}^\alpha := x^\alpha - (m_2/m)b\hat{x}^\alpha$, $\tilde{x} := x - (m_2/m)b$, $\tilde{r} := \sqrt{\tilde{x}_k \tilde{x}^k}$, and $\tilde{r}^\alpha := r^\alpha - (m_2/m)b\hat{x}^\alpha$. Spatial vectors (or the spatial parts of spacetime vectors) will be denoted either with an arrow or a spatial index.

Norms: The Euclidean norm for spatial vectors is denoted by $\|\cdot\|$ (so, e.g., we could write the definition of R above as $R := \|\vec{X}\|$).

Derivatives: All partial derivatives are taken with respect to harmonic PN coordinates, so $\partial_\alpha := \partial/\partial x^\alpha$. Overdots denote differentiation with respect to t (i.e.,

PN harmonic time). While in Sec. III, overdots properly denote differentiation with respect to T (i.e., the Cook-Scheel time coordinate), as we shall see, this is equivalent to differentiation with respect to t to the order we are considering. We use the shorthand $\partial_{\alpha\beta} := \partial_\alpha \partial_\beta$.

Order counting: We have to deal with two expansions here, since we are performing asymptotic matching. For our purposes, the PN expansion can be treated as an expansion in $\sqrt{m_2/b}$. We use m_2 (instead of m_1 or m) for convenience, as we concentrate on matching around hole 1. (We can do this without loss of generality, by the symmetry of exchanging labels 1 and 2.) The black hole perturbation expansion is in multipoles, so around hole 1 it can be treated as an expansion in \tilde{r}/b . Here we treat t/b as the same order as \tilde{r}/b , as required by the slow time variation assumption made in the derivation of the perturbed black hole metric. This means that we only match in a neighborhood of $t = 0$.

Order notation: It will be important for us to have a compact notation for, e.g., the j th term of the expansion of some arbitrary quantity. For this, we use the “order projection” notation, which has three different flavors: Since the slow-motion PN expansion can be considered our primary expansion (and is the expansion to which we refer when we simply call something j th order), the most commonly used flavor will be $(\cdot)_j$. This denotes the coefficient of $(m_2/b)^{j/2}$ in the (asymptotic) power series expansion of its argument. For the reasons discussed in Sec. V A, this includes multipoles through octupolar order for $j \in \{2, 3\}$ but only through quadrupole order for $j \in \{4, 5\}$. (In principle, we include all the multipoles for $j \in \{0, 1\}$, since there are only monopole contributions.) For the times when we need to single out a particular multipole for consideration, we shall use $(\cdot)_{j,n}$, which denotes the 2^n th multipole-order piece of $(\cdot)_j$. Finally, when we want to include all of the multipolar orders through 2^n we shall use $(\cdot)_{j,\leq n}$.

Polynomial and nonpolynomial parts: All the expressions we consider when performing the matching of the inner and near zones can be written as the sum of a polynomial in \tilde{x}^α and nonpolynomial terms of a particular form, viz., polynomials in \tilde{x}^α multiplied by \tilde{r}^n , $n \in \mathbb{Z} \setminus \{0, 2, 4, \dots\}$. It will often be convenient to divide expressions up into their polynomial and nonpolynomial parts, since these can be treated separately, by linear independence. We shall thus denote the polynomial and nonpolynomial parts of an expression by the superscripts P and NP, respectively.

References: [37] and [38] will be referred to as Papers I and II, respectively.

II. ASYMPTOTIC MATCHING

The technique of asymptotic matching is a standard one in the analysis of multiscale and singular perturbation problems, allowing one to relate and combine approximate solutions that are valid on different scales [75].

It has been used in general relativity to obtain, e.g., PN equations of motion—[73] contains the most recent of these calculations—and the radiation zone metric of a binary system [76]. (See Paper I and [73] for further discussion and references.) Here we specialize our discussion to the case of a binary black hole.

A timeslice of a binary black hole spacetime divides naturally into four primary zones and three secondary *buffer zones*: See Fig. 2 for an illustration. In practical work, the boundaries of all of these zones are necessarily only given approximately, since we do not currently possess sharp estimates for the error bars of the approximations used to describe this spacetime. There are two *inner zones* around the black holes, given by $r_A \ll b$, where r_A is the distance from (the point particle associated with) hole A : Here the spacetime is well described by a perturbed black hole. Surrounding (and partially overlapping) these is the *near zone*, where the standard (harmonic coordinate) PN metric is valid—i.e., not too close to the holes, yet not so far away that retardation cannot be treated perturbatively. This is given by $r_A \gg m_A$ and $r \lesssim \lambda$, where m_A is the mass of hole A , r is the distance from the system’s center-of-mass, and $\lambda = b/2v$ is the reduced characteristic wavelength of the binary’s gravitational radiation. Finally, the remainder of the timeslice (along with a little bit of the outer portion of the near zone) comprise the *far zone*, given by $r \gtrsim \lambda$, where retardation can no longer be treated perturbatively, and spacetime is described by a separate PN metric that accounts for this. (N.B.: Different relations were given for the outer edge of the near zone and inner edge of the far zone in Papers I and II, but the ones used here are more accurate.) See Table III (in Sec. VIII B) for numerical values for the boundaries of the zones for a particular equal-mass binary.

The three buffer zones are the portions of the timeslice where the preceding four regions overlap. (Due to the “fuzziness” inherent in \lesssim and \gtrsim , the near and far zone can have a substantial overlap, despite formal appearances.) We restrict our attention to cases in which the specified zones overlap in the manner we shall describe, but in no other fashion (e.g., we do not want the two inner zones to overlap). There are two buffer zones where the two inner zones overlap the near zone (thus these are given by $m_A \ll r_A \ll b$), and another buffer zone where the near zone overlaps the far zone, which is very roughly an annulus whose radius and thickness are both of order λ . (The order of the thickness of the annulus is our choice—see Sec. VIII B: All that is required formally is that it increase as v decreases, corresponding to a larger realm of validity of the near zone metric’s perturbative treatment of retardation. Additionally, as is indicated in the figure, this buffer zone would not be spherical in a more nuanced description.) These buffer zones are where we perform the formal matching that determines the coordinate transformation and relations between parameters as well as where we stitch the metrics together numerically.

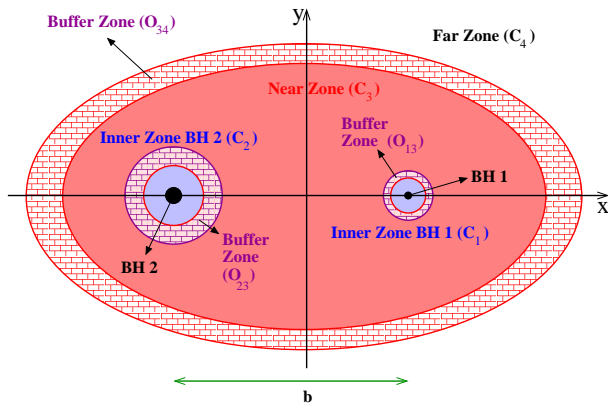


FIG. 2: A diagram of the zones into which we divide the binary black hole timeslice. The two black holes (BH 1 and BH 2, denoted by filled-in circles) lie on the x -axis, surrounded by their respective inner zones (C_1 and C_2) and inner-to-near buffer zones (O_{13} and O_{23}). (In actuality, the black holes should be tidally distorted, along with their associated inner and buffer zones. We neglect this distortion in the above diagram for simplicity.) The near zone, C_3 , covers the orbit of the binary and is surrounded by the far zone, C_4 , and the near-to-far buffer zone, O_{34} .

This matching and stitching relies on the observation that if the metrics that are valid in the various zones are all to be different approximations to the same (unknown) global exact metric, then, considered as abstract tensors, they should agree with each other in their realms of mutual validity. More specifically, assume that there exists a buffer zone in which two approximate metrics $\mathbf{g}^{(1)}$ and $\mathbf{g}^{(2)}$ are both valid. (We write these metrics without indices to emphasize that they are currently being considered as abstract tensors.) Take their associated small parameters to be ϵ_1 and ϵ_2 , respectively. (The buffer zone is then defined to be the region in which these parameters are indeed small.) Then make a bivariate expansion of the metrics in both small parameters. That is, take $\mathbf{g}^{(1)}$, which is already an expansion in ϵ_1 , and expand it in ϵ_2 as well; similarly expand $\mathbf{g}^{(2)}$ in ϵ_1 . The coefficients of both bivariate expansions, considered as abstract tensors, should then be equal if the metrics describe the same spacetime. The resulting equations relate the parameters of the two metrics.

While the statement of this result in terms of abstract metrics is simple, in practice one works with the metrics' coordinate components. In general, the coordinate systems in which the metrics' components are known will not agree, so one first chooses the coordinate system in which one of the metrics is expressed to be the primary coordinate system. (For us, this will be the near zone's PN harmonic coordinate system.) One then applies an arbitrary coordinate transformation to the other metric in order to put it in the same coordinate system as the first (to the order one matches). Equating coefficients of the bivariate expansions of the components of the metrics (including the coordinate transformation) is then equiv-

alent to equating the coefficients of the expansions of the abstract tensors. In this case, the resulting equations will determine not only the relations between the metrics' parameters, but also the arbitrary coordinate transformation. In our calculation, each order's contribution to the coordinate transformation contains some arbitrary pieces—i.e., pieces that can be set to any value without affecting that order's matching. We have found that most of these are determined by the matching at two orders higher.

III. INNER ZONE METRIC

Detweiler's perturbed black hole metric [59] is derived under the slow-motion and weak-curvature assumptions of Thorne and Hartle [69]. Here one characterizes the strength of the perturbation by the length scale \mathcal{R} , defined to be the smallest of the radius of curvature, inhomogeneity scale, and scale of time variation of the external universe. For convenience, these are generally all taken to be formally of the same order. (In the nomenclature of Thorne and Hartle, the “external universe” refers to the perturbing spacetime in which the black hole is placed, here consisting of the tidal fields generated by the hole's binary companion.) For a post-Newtonian binary we have $\mathcal{R} \sim \sqrt{b^3/m_2}$ [see, e.g., the discussion following Eq. (1.4b) in [69]]. Here b is the coordinate separation of the holes and m_2 is the mass of the hole's companion (the one responsible for the perturbing tidal fields). (We are thus specializing to the inner zone surrounding hole 1 in giving this scaling, as well as the scalings of the tidal fields below. One can obtain the scalings for the inner zone surrounding hole 2 using the substitution $1 \leftrightarrow 2$.)

With these assumptions, the time derivative of a quadrupole field is of octupolar order. Since one is only able to include quadrupole and octupole perturbations in linear black hole perturbation theory, the time dependence of the tidal fields in the metric is restricted to the quadrupole fields, and even there it is only linear. Of course, it is possible to obtain the complete time dependence of the tidal fields (for times much less than the radiation reaction timescale), as Taylor and Poisson [73] did, since we can compute the tidal fields at any point in the orbit. (See Appendix B for further discussion.) However, knowing this dependence does not let us compute the metric to a higher formal accuracy.

In Detweiler's metric, the tidal perturbations are encoded by symmetric trace-free electric and magnetic tidal fields \mathcal{E}_{kl} (electric quadrupole), \mathcal{E}_{klp} (electric octupole), \mathcal{B}_{kl} (magnetic quadrupole), and \mathcal{B}_{klp} (magnetic octupole). These come from the Thorne-Hartle-Zhang (THZ) harmonic specialization of locally inertial coordinates (from [69, 70]), which Detweiler uses to express the perturbation of Minkowski space that his metric approaches in the buffer zone.

As their names suggest, the quadrupole and octupole tidal fields formally scale as \mathcal{R}^{-2} and \mathcal{R}^{-3} , respectively.

However, this is only a formal scaling, since it requires that one treat the radius of curvature, inhomogeneity scale, and scale of time variation of the external universe as being of the same order [see, e.g., Eq. (1.4b) in [69]]. For a post-Newtonian binary, these are not of the same order: The magnetic moments are a factor of v smaller than the corresponding electric moments; the octupole moments are a factor of v *larger* than the formal scaling would suggest—see Eqs. (2.1) and (2.2) in [73] and the surrounding discussion. Specifically, the magnetic quadrupole tidal field on hole 1 is actually $\sim (m_2/b)^{1/2}(m_2/b^3)$ [cf. the expression given in Eqs. (5.45b) and (5.56b) of [77]], and the electric octupole tidal field on hole 1 is actually $\sim m_2/b^4$ [cf. Eqs. (5.50) and (5.56a) in [77]]. In order to simplify later expressions and make their expansion in \tilde{r}/b explicit (\tilde{r} denotes the

distance from hole 1), we define “barred” versions of the tidal fields around hole 1 with the scaling taken out, viz.,

$$\begin{aligned}\bar{\mathcal{E}}_{kl} &:= (b^3/m_2)\mathcal{E}_{kl}, & \bar{\mathcal{B}}_{kl} &:= (b/m_2)^{1/2}(b^3/m_2)\mathcal{B}_{kl}, \\ \bar{\mathcal{E}}_{klp} &:= (b^4/m_2)\mathcal{E}_{klp}, & \bar{\mathcal{B}}_{klp} &:= (b/m_2)^{1/2}(b^4/m_2)\mathcal{B}_{klp}.\end{aligned}\tag{3.1}$$

Detweiler [59] presents the metric perturbation in Schwarzschild coordinates, giving the portion involving the quadrupole fields, including their time derivatives (which are actually of octupolar order), in his Eqs. (G.6)–(G.11), and the portion with the octupole fields in his Eq. (58). Putting this all together, along with the background unperturbed Schwarzschild metric, we obtain a line element of

$$\begin{aligned}h_{\alpha\beta}^{(S)}d\mathcal{X}^\alpha d\mathcal{X}^\beta &= -H_{T^2}^{(S)}dT^2 + H_k^{(S)}dTd\mathcal{X}^k - \frac{2}{3}\left[2\mathcal{P} + M - \frac{4M^2}{\mathcal{P} - 2M} + \frac{6M^3}{\mathcal{P}(\mathcal{P} - 2M)}\right]\mathcal{E}'_{kl}\mathcal{X}^k\mathcal{X}^l dT d\mathcal{P} \\ &\quad + \frac{\mathcal{P}^2}{3(\mathcal{P} - 2M)}\mathcal{C}'_{klp}\mathcal{X}^l\mathcal{X}^p d\mathcal{X}^k d\mathcal{P} + H_{\mathcal{P}^2}^{(S)}d\mathcal{P}^2 + H_\sigma^{(S)}\mathcal{P}^2\sigma_{AB}d\mathcal{X}^A d\mathcal{X}^B + O(\mathcal{P}^4/\mathcal{R}^4),\end{aligned}\tag{3.2}$$

where the “(S)” acts as a reminder that this is in Schwarzschild coordinates $\mathcal{X}^\alpha = (T, \mathcal{X}^k)$, with a radial coordinate of $\mathcal{P} := \sqrt{\mathcal{X}_k\mathcal{X}^k}$. Additionally, M is the mass of the hole, σ_{AB} denotes the metric on the 2-sphere, and we have defined

$$\begin{aligned}H_{T^2}^{(S)} &:= 1 - 2\frac{M}{\mathcal{P}} + \left[1 - 2\frac{M}{\mathcal{P}}\right]^2 \left[\mathcal{E}_{kl} - 2M \log\left(\frac{\mathcal{P}}{2M}\right)\mathcal{E}'_{kl}\right]\mathcal{X}^k\mathcal{X}^l - \left[\mathcal{P} - 4M + 12\frac{M^3}{\mathcal{P}^2} - \frac{16}{3}\frac{M^4}{\mathcal{P}^3} - \frac{8}{3}\frac{M^5}{\mathcal{P}^4}\right]\mathcal{E}'_{kl}\mathcal{X}^k\mathcal{X}^l \\ &\quad + \frac{1}{3}\left[1 - 2\frac{M}{\mathcal{P}}\right]^2 \left[1 - \frac{M}{\mathcal{P}}\right]\mathcal{E}_{klp}\mathcal{X}^k\mathcal{X}^l\mathcal{X}^p, \\ H_k^{(S)} &:= \frac{4}{3}\left[1 - 2\frac{M}{\mathcal{P}}\right] \left[\mathcal{C}_{klp} - 2M \log\left(\frac{\mathcal{P}}{2M}\right)\mathcal{C}'_{klp}\right]\mathcal{X}^l\mathcal{X}^p - \frac{4}{3}\left[\mathcal{P} - 2M - 4\frac{M^2}{\mathcal{P}} + 4\frac{M^3}{\mathcal{P}^2} + \frac{8}{3}\frac{M^4}{\mathcal{P}^3} + \frac{8}{3}\frac{M^5}{\mathcal{P}^4}\right]\mathcal{C}'_{klp}\mathcal{X}^l\mathcal{X}^p \\ &\quad + \frac{2}{3}\left[1 - 2\frac{M}{\mathcal{P}}\right] \left[1 - \frac{4}{3}\frac{M}{\mathcal{P}}\right]\mathcal{C}_{klps}\mathcal{X}^l\mathcal{X}^p\mathcal{X}^s, \\ H_{\mathcal{P}^2}^{(S)} &:= \left[1 - 2\frac{M}{\mathcal{P}}\right]^{-1} - \left[\mathcal{E}_{kl} - 2M \log\left(\frac{\mathcal{P}}{2M}\right)\mathcal{E}'_{kl}\right]\mathcal{X}^k\mathcal{X}^l - \frac{1}{3}\left[1 - \frac{M}{\mathcal{P}}\right]\mathcal{E}_{klp}\mathcal{X}^k\mathcal{X}^l\mathcal{X}^p \\ &\quad + \left[\mathcal{P} - \frac{4M^2}{\mathcal{P} - 2M} + \frac{4M^3}{(\mathcal{P} - 2M)^2} - \frac{16}{3}\frac{M^4}{\mathcal{P}(\mathcal{P} - 2M)^2} - \frac{8}{3}\frac{M^5}{\mathcal{P}^2(\mathcal{P} - 2M)^2}\right]\mathcal{E}'_{kl}\mathcal{X}^k\mathcal{X}^l, \\ H_\sigma^{(S)} &:= 1 - \left[1 - 2\frac{M^2}{\mathcal{P}^2}\right] \left[\mathcal{E}_{kl} - 2M \log\left(\frac{\mathcal{P}}{2M}\right)\mathcal{E}'_{kl}\right]\mathcal{X}^k\mathcal{X}^l + \left[\mathcal{P} - 6\frac{M^2}{\mathcal{P}} - 4\frac{M^3}{\mathcal{P}^2} + \frac{8}{3}\frac{M^4}{\mathcal{P}^3}\right]\mathcal{E}'_{kl}\mathcal{X}^k\mathcal{X}^l \\ &\quad - \frac{1}{3}\left[1 - 2\frac{M}{\mathcal{P}} + \frac{4}{5}\frac{M^3}{\mathcal{P}^3}\right]\mathcal{E}_{klp}\mathcal{X}^k\mathcal{X}^l\mathcal{X}^p.\end{aligned}\tag{3.3}$$

We have also defined $\mathcal{C}_{klp} := \epsilon_{kls}\mathcal{B}^s_p$ and $\mathcal{C}_{klps} := \epsilon_{klu}\mathcal{B}^u_{ps}$, for convenience, as the magnetic tidal fields only appear in the perturbation in these dual forms. (The “barred” versions of these quantities are defined analogously to $\bar{\mathcal{B}}_{kl}$ and $\bar{\mathcal{B}}_{klp}$.) Here ϵ_{klp} is the 3-dimensional Levi-Civita symbol, with $\epsilon_{123} = 1$. While we have not

indicated this explicitly, \mathcal{E}_{kl} and \mathcal{C}_{klp} both depend (linearly) on the null ingoing Eddington-Finkelstein coordinate $V := T + \mathcal{P} + 2M \log(\mathcal{P}/2M - 1)$. (The octupole fields are treated as constants, since their time derivatives are of hexadecapole order.) Thus, primes denote derivatives with respect to V . We include the \mathcal{B}'_{kl} contri-

butions here, even though they do not increase the formal accuracy of our initial data: We fix the lowest-order piece of \mathcal{B}'_{kl} when we read off the 1PN correction to the electric octupole (in Appendix B 2) as an application of our matching procedure. We also are able to obtain the full time dependence of the tidal fields (up to radiation reaction effects) *a posteriori*—see the discussion in Appendix B 2. (Including such formally higher-order pieces can improve the accuracy of the data in practice.)

There is one gauge subtlety here that Detweiler [59] does not address in his paper: If one compares the expression for the THZ tidal perturbation in his Eq. (53) to that of the metric perturbation in his Eqs. (56)–(57), it appears that the portions of the metric perturbation involving time derivatives of the tidal fields do not approach the analogous portions of the THZ tidal perturbation. The resolution of this apparent discrepancy is that Detweiler made a tacit gauge transformation (away from the pure THZ gauge, though only affecting the time derivatives of the tidal fields, to the order considered) to obtain the given compact expressions for the metric per-

turbation [78].

We now transform this metric to the quasi-Cartesian form of Cook-Scheel harmonic coordinates (from [67]), which we denote by $X^\alpha = (T, X^k)$, with $R := \sqrt{X_k X^k}$. The transformation is given by

$$\begin{aligned}\mathcal{T} &= T - 2M \log \left| \frac{R - M}{R + M} \right|, \\ \mathcal{X}^k &= \left[1 + \frac{M}{R} \right] X^k,\end{aligned}\tag{3.4}$$

so $\mathcal{P} = R + M$. This comes from Cook and Scheel's Eqs. (20), (41), and (43) upon noting that Boyer-Lindquist coordinates reduce to Schwarzschild coordinates for a Schwarzschild hole. In order to simplify our transformation, we use the relation $\mathcal{P}^2 \sigma_{AB} d\mathcal{X}^A d\mathcal{X}^B = (1 + M/R)^2 (dX_p dX^p - dR^2)$, obtained from $d\mathcal{X}_k d\mathcal{X}^k = d\mathcal{P}^2 + \mathcal{P}^2 \sigma_{AB} d\mathcal{X}^A d\mathcal{X}^B$, to eliminate σ_{AB} , thus obtaining a full transformed line element of

$$\begin{aligned}h_{\alpha\beta} dX^\alpha dX^\beta &= -H_{T^2} dT^2 + H_{RT} dR dT + \frac{16}{3} \frac{M^2}{R} \left[1 + \frac{M}{R} - \frac{2}{3} \frac{M^2}{R^2} - \frac{2}{3} \frac{M^3}{R^2(R+M)} \right] \dot{C}_{klp} X^l X^p dX^k dT \\ &\quad + H_k^{[1]} dX^k \left[\left(1 - \frac{M^2}{R^2} \right) dT - 4 \frac{M^2}{R^2} dR \right] + H_k^{[2]} dX^k dR + H_{R^2} dR^2 + H_{\text{trc}} dX_s dX^s + O(R^4/\mathcal{R}^4),\end{aligned}\tag{3.5}$$

where

$$\begin{aligned}H_{T^2} &:= \frac{R - M}{R + M} + \left[1 - \frac{M}{R} \right]^2 \left[(\mathcal{E}_{kl} + T \dot{\mathcal{E}}_{kl}) X^k X^l + \frac{1}{3} \mathcal{E}_{klp} X^k X^l X^p \right] + \frac{4M^2}{(R + M)^2} \left[R - \frac{5}{3} \frac{M^2}{R} \right] \dot{\mathcal{E}}_{kl} X^k X^l, \\ H_{RT} &:= \frac{8M^2}{(R + M)^2} + 8 \frac{M^2}{R^2} \frac{R - M}{R + M} \left[(\mathcal{E}_{kl} + T \dot{\mathcal{E}}_{kl}) X^k X^l + \frac{1}{3} \mathcal{E}_{klp} X^k X^l X^p \right] \\ &\quad - \left[\frac{4}{3} R + \frac{14}{3} M + \frac{8}{3} \frac{M^2}{R} - 2 \frac{M^3}{R^2} - \frac{104}{3} \frac{M^4}{R^2(R + M)} + \frac{80}{3} \frac{M^5}{R^2(R + M)^2} + \frac{32}{3} \frac{M^6}{R^2(R + M)^3} \right] \dot{\mathcal{E}}_{kl} X^k X^l, \\ H_k^{[1]} &:= \frac{2}{3} \left[1 + \frac{M}{R} \right] \left[2(\mathcal{C}_{klp} + T \dot{\mathcal{C}}_{klp}) X^l X^p + \left(1 - \frac{1}{3} \frac{M}{R} \right) \mathcal{C}_{klps} X^l X^p X^s \right], \\ H_k^{[2]} &:= \left[\frac{R}{3} + 2M + \frac{16}{3} \frac{M^2}{R} + \frac{26}{3} \frac{M^3}{R^2} - 11 \frac{M^4}{R^3} - \frac{32}{3} \frac{M^5}{R^3(R + M)} - \frac{64}{9} \frac{M^6}{R^3(R + M)^2} \right] \dot{C}_{klp} X^l X^p, \\ H_{R^2} &:= \sum_{n=1}^3 \left(\frac{2M}{R + M} \right)^n - \frac{2M}{R} - \frac{M^2}{R^2} + \left[2 \frac{M}{R} + 3 \frac{M^2}{R^2} - \frac{M^4}{R^4} - \frac{16M^4}{R^2(R + M)^2} \right] (\mathcal{E}_{kl} + T \dot{\mathcal{E}}_{kl}) X^k X^l \\ &\quad + \left[\frac{1}{3} \frac{M}{R} + \frac{1}{3} \frac{M^2}{R^2} - \frac{2}{5} \frac{M^3}{R^3} - \frac{7}{15} \frac{M^4}{R^4} - \frac{1}{15} \frac{M^5}{R^5} - \frac{16}{3} \frac{M^4}{R^2(R + M)^2} \right] \mathcal{E}_{klp} X^k X^l X^p + \left[\frac{16}{3} \frac{M^2}{R} + \frac{80}{3} \frac{M^3}{R^2} \right. \\ &\quad \left. + 28 \frac{M^4}{R^3} + \frac{40}{3} \frac{M^5}{R^4} - \frac{176}{3} \frac{M^6}{R^4(R + M)} + \frac{72M^7}{R^4(R + M)^2} - \frac{32}{3} \frac{M^8}{R^4(R + M)^3} - \frac{32}{3} \frac{M^9}{R^4(R + M)^4} \right] \dot{\mathcal{E}}_{kl} X^k X^l, \\ H_{\text{trc}} &:= \left[1 + \frac{M}{R} \right]^2 \left[1 - \left(1 + 2 \frac{M}{R} - \frac{M^2}{R^2} \right) (\mathcal{E}_{kl} + T \dot{\mathcal{E}}_{kl}) X^k X^l - \frac{1}{3} \left(1 + \frac{M}{R} - \frac{M^2}{R^2} - \frac{1}{5} \frac{M^3}{R^3} \right) \mathcal{E}_{klp} X^k X^l X^p \right. \\ &\quad \left. - 4 \frac{M^2}{R^2} \left(R + 2M - \frac{2}{3} \frac{M^2}{R + M} \right) \dot{\mathcal{E}}_{kl} X^k X^l \right].\end{aligned}\tag{3.6}$$

We have used the fact that the time dependence of \mathcal{E}_{kl} and \mathcal{C}_{klp} is only linear (to the multipolar order we are

considering) to write $\mathcal{E}'_{kl} = \dot{\mathcal{E}}_{kl}$ and $\mathcal{E}_{kl}(V) = \mathcal{E}_{kl} + [T + R + M + 2M \log(\mathcal{P}/2M)]\dot{\mathcal{E}}_{kl}$, with analogous expressions involving \mathcal{C}_{klp} . [This expansion removes the logarithms present in the expression for the metric in Eq. (3.2).] Here an overdot denotes a derivative with respect to T , and the tidal fields on the right are constant, so \mathcal{E}_{kl} and $\dot{\mathcal{E}}_{kl}$ are treated formally as independent tidal fields, despite the notation. That is, \mathcal{E}_{kl} just denotes the constant part of $\mathcal{E}_{kl}(T) = \mathcal{E}_{kl} + T\dot{\mathcal{E}}_{kl}$. Finally, despite appearances, this expression for the metric is in fact in a quasi-Cartesian form: dR should just be considered a shorthand for $X_k dX^k/R$.

IV. NEAR ZONE METRIC

We take the harmonic coordinate metric to the order needed from Eqs. (7.2) in Blanchet, Faye, and Ponsot [58] and specialize it to a circular orbit, obtaining

$$g_{00} + 1 = \frac{2m_1}{r_1} + \frac{m_1}{r_1} [4v_1^2 - (\hat{n}_1 \cdot \vec{v}_1)^2] - 2\frac{m_1^2}{r_1^2} - m_1 m_2 \left[\frac{2}{r_1 r_2} + \frac{r_1}{2b^3} - \frac{r_1^2}{2r_2 b^3} + \frac{5}{2r_2 b} \right] + (1 \leftrightarrow 2) + O(v^6), \quad (4.1a)$$

$$\begin{aligned} g_{0k} = & -\frac{4m_1}{r_1} v_1^k - \left\{ \frac{m_1^2}{r_1^2} (\hat{n}_1 \cdot \vec{v}_1) + \frac{m_1 m_2}{S^2} [16(\hat{n}_2 \cdot \vec{v}_1) - 12(\hat{n}_2 \cdot \vec{v}_2)] \right\} n_1^k - m_1 m_2 \left\{ 4\frac{\hat{n}_1 \cdot \vec{v}_1}{b^2} - 12\frac{\hat{n}_1 \cdot \vec{v}_1}{S^2} \right\} n_{12}^k \\ & + \left\{ \frac{m_1}{r_1} [2(\hat{n}_1 \cdot \vec{v}_1)^2 - 4v_1^2] + \frac{m_1^2}{r_1^2} + \frac{m_1 m_2}{b^3} [3r_1 - 2r_2] - m_1 m_2 \left[\frac{r_2^2}{r_1 b^3} + \frac{3}{r_1 b} - \frac{8}{r_2 b} + \frac{4}{bS} \right] \right\} v_1^k \\ & + (1 \leftrightarrow 2) + O(v^6), \end{aligned} \quad (4.1b)$$

$$\begin{aligned} g_{kl} - \delta_{kl} = & \left\{ 2\frac{m_1}{r_1} - \frac{m_1}{r_1} (\hat{n}_1 \cdot \vec{v}_1)^2 + \frac{m_1^2}{r_1^2} + m_1 m_2 \left[\frac{2}{r_1 r_2} - \frac{r_1}{2b^3} + \frac{r_1^2}{2r_2 b^3} - \frac{5}{2r_1 b} + \frac{4}{bS} \right] \right\} \delta_{kl} \\ & + 4\frac{m_1}{r_1} v_1^k v_1^l + \frac{m_1^2}{r_1^2} n_1^k n_1^l - m_1 m_2 \left[\frac{4}{S^2} + \frac{4}{bS} \right] n_{12}^k n_{12}^l + 4\frac{m_1 m_2}{S^2} \left[n_1^{(k} n_2^{l)} + 2n_1^{(k} n_{12}^{l)} \right] + 8\frac{m_1 m_2}{b^2} n_{12}^{(k} v_{12}^{l)} \\ & + (1 \leftrightarrow 2) + O(v^6). \end{aligned} \quad (4.1c)$$

Here $\vec{x}_A(t)$, $A \in \{1, 2\}$ denotes the position of (the point particle associated with) hole A .³ Thus $\vec{r}_A := \vec{x} - \vec{x}_A(t)$ gives the displacement from hole A , with $r_A := \|\vec{r}_A\|$ giving the distance from hole A and $\hat{n}_A := \vec{r}_A/r_A$ the associated unit vector. Similarly, $\vec{v}_A := \dot{\vec{x}}_A$ denotes the velocity of hole A . The displacement vector from hole B to hole A is given by $\vec{r}_{AB} := \vec{r}_A - \vec{r}_B$, with an associated unit vector of $\hat{n}_{AB} := \vec{r}_{AB}/\|\vec{r}_{AB}\|$. Thus, specializing to a (quasi)circular orbit, $\|\vec{r}_{12}\| = b$, where b is the separation of the holes and is therefore constant up to orbital shrinkage (which we can neglect when performing the matching, given the order to which we are calculating, though we include it when implementing the metrics numerically—see Sec. VIA). Additionally, we shall usually use the shorthand $\vec{b} := \vec{r}_{12}$. (We do not use it in the above expression for the metric since \vec{r}_{12} changes sign under $1 \leftrightarrow 2$, while \vec{b} does not.) Similarly, $\vec{v}_{AB} := \vec{v}_A - \vec{v}_B$; we also have $S := r_1 + r_2 + b$. Finally, the notation

“ $+(1 \leftrightarrow 2)$ ” denotes that the preceding expression is to be added to itself with the labels 1 and 2 switched.

For a circular orbit, we have $\vec{b} = -\omega^2 \vec{b}$, by definition, where

$$\omega = \sqrt{\frac{m}{b^3}} \left[1 + \frac{m}{2b} (\eta - 3) + O\left(\frac{m^2}{b^2}\right) \right] \quad (4.2)$$

is the (harmonic coordinate) angular velocity [obtained from Eq. (8.6) in [58]], and $\eta := m_1 m_2 / m^2$ is the symmetric mass ratio. Assuming a (quasi)circular orbit [so that the separation vector of the point particles is orthogonal to their velocities up to $O(v^5)$ radiation reaction effects] also allows us to make the simplifications $\hat{n}_{12} \cdot \hat{v}_1 = \hat{n}_{12} \cdot \hat{v}_2 = \hat{n}_{12} \cdot \hat{v}_{12} = O(v^5)$ in obtaining the expression for the metric given in Eqs. (4.1). We take the explicit expression for the orbit to be $\vec{b} = b(\hat{x} \cos \omega t + \hat{y} \sin \omega t)$. From the definition of the center-of-mass coordinates used in the PN metric, the positions of (the point particles associated with) the holes are given, to the order we need them, by

$$\vec{x}_1 = \frac{m_2}{m} \vec{b}, \quad \vec{x}_2 = -\frac{m_1}{m} \vec{b}. \quad (4.3)$$

[For a circular orbit, the first PN corrections to these are $O(v^4)$ and are thus not needed here.] The expressions

³ We shall henceforth refrain from belaboring the distinction between the PN point particles and true black holes, except where we feel that it is important to emphasize this point.

for the holes' velocities are obtained by taking a time derivative.

The explicit expansions of the near zone metric at various orders given in the next section were obtained using the expansions

$$\begin{aligned} \frac{1}{r_2^n} = & \frac{1}{b^n} \left\{ 1 - n \frac{\vec{r}_1 \cdot \hat{b}}{b} + \frac{1}{2b^2} [n(n+2)(\vec{r}_1 \cdot \hat{b})^2 - nr_1^2] \right. \\ & + \frac{1}{6b^3} [3n(n+2)r_1^2(\vec{r}_1 \cdot \hat{b}) - n(n+2)(n+4)(\vec{r}_1 \cdot \hat{b})^3] \\ & \left. + O\left(\left[\frac{r_1}{b}\right]^4\right) \right\} \end{aligned} \quad (4.4)$$

and

$$\begin{aligned} \frac{1}{S^n} = & \left[2b + r_1 + \vec{r}_1 \cdot \hat{b} + \frac{r_1^2 - (\vec{r}_1 \cdot \hat{b})^2}{2b} + O\left(\left[\frac{r_1}{b}\right]^3\right) \right]^{-n} \\ = & \frac{1}{(2b)^n} \left\{ 1 - \frac{n}{2} \left[\frac{r_1}{b} + \frac{\vec{r}_1 \cdot \hat{b}}{b} \right] + \frac{n(n-1)}{8} \frac{r_1^2}{b^2} \right. \\ & + \frac{n(n+1)}{4} \frac{r_1(\vec{r}_1 \cdot \hat{b})}{b^2} + \frac{n(n+3)}{8} \frac{(\vec{r}_1 \cdot \hat{b})^2}{b^2} \\ & \left. + O\left(\left[\frac{r_1}{b}\right]^3\right) \right\}. \end{aligned} \quad (4.5)$$

Here we include the octupole pieces in the expression for $1/r_2^n$ because they become of quadrupole order when, e.g., multiplied by m_1/r_1 in the $-2m_1m_2/r_1r_2$ piece of g_{00} . We do not need to expand $1/S^n$ to octupolar order as it is not multiplied by m_1/r_1 at the PN order we are working.

A. The PN metric and conformal flatness

At $O(v^4)$, the spatial PN metric is no longer conformally flat: That is, there does not exist a coordinate system in which the 3-metric can be written as $g_{kl} = \Psi \delta_{kl}$. This can be guessed from a cursory inspection of the PN metric, as nondiagonal spatial components first appear at $O(v^4)$, but was established more firmly in [79], and then further studied in [80]. In both cases, this result was an offshoot of a comparison of the predictions of a post-Newtonian analysis of the Isenberg-Mathews-Wilson (IMW) approximation [81, 82] with those of the full PN approximation: They were found to differ starting at $O(v^4)$. Such a comparison gives the desired result because the IMW approximation assumes spatial conformal flatness (along with maximal slicing—i.e., a vanishing trace of the extrinsic curvature) in an attempt to remove the dynamical degrees of freedom from the gravitational field.

However, the comparison with the IMW approximation is not exact. The post-Newtonian analyses use the ADMTT gauge, for which we have $\delta_{kl}\pi^{kl} = 0$, where π^{kl} is the canonical momentum conjugate to the 3-metric,

g_{kl} , while maximal slicing sets $g^{lp}K_{lp} = 0$, where K_{lp} is the extrinsic curvature of the slice. Of course, these two slicings agree as long as g_{kl} is a multiple of the flat space metric, since then $\delta_{kl}\pi^{kl} = 0 \Leftrightarrow g_{kl}\pi^{kl} = 0 \Leftrightarrow g^{lp}K_{lp} = 0$. [See, e.g., Eq. (E.2.31) in Wald [83] for the relation between π^{lp} and K^{lp} .] But in general, the two slicings will differ at the higher, non-conformally flat orders we are interested in.

It is also possible to demonstrate this lack of spatial conformal flatness directly, and we shall do so here for the harmonic slicing we are using. In four or more dimensions, the Weyl tensor settles questions of conformal flatness: It vanishes if and only if a space is conformally flat [84]. However, in three dimensions the Weyl tensor vanishes identically, and its analogue for settling questions of conformal flatness is the Bach or Cotton-York tensor, C_{kl} . This is defined (with indices raised by the 3-metric) by

$$C_{kl} := 2\epsilon_k{}^{ps}\nabla_s R_{lp} - \frac{1}{2}\epsilon_{kl}{}^p\nabla_p R. \quad (4.6)$$

Here ∇_k , R_{kl} , and R are, respectively, the (three-dimensional) covariant derivative, Ricci tensor, and Ricci scalar associated with g_{kl} . In fact, the nonvanishing of the Cotton-York tensor is a necessary and sufficient condition to render its associated 3-metric non-conformally flat [39, 84] (for a proof, see Chap. VI, §5 in [85]).

We have computed the formal $O(c^{-4})$ portions of this tensor [i.e., those that correspond to the $O(c^{-4}) \Leftrightarrow O(v^4)$ pieces of the spatial metric] symbolically using MAPLE and GRTENSORII and verified that certain components are nonvanishing at various points of the timeslice. As an illustration, we have plotted the lowest-order piece of the norm of the Cotton-York tensor, $\sqrt{\delta^{kp}\delta^{ls}C_{kl}C_{ps}}$ along the axis passing through the holes in Fig. 3 for the standard equal-mass test system of $m_1 = m_2 = m/2$, $b = 10m$. As expected, the values are largest in the region around the holes, showing that this is the region in which the largest perturbation would be required to make the 2PN metric conformally flat.

There is, however, a more intuitive way of understanding the breaking of spatial conformal flatness of the PN metric (here returning to the ADMTT slicing). This approach relates explicitly to the failure of the PN metric to be manifestly conformally flat at $O(v^4)$ and comes from the work of Nissanke [42].⁴ From the study of PN theory in the canonical ADM formalism [87], one knows that the PN metric can be rewritten as

$$g_{kl} = \Psi \delta_{kl} + h_{kl}, \quad (4.7)$$

⁴ This argument was suggested to one of us by Luc Blanchet [86]. Additional intuition can be obtained from Valiente Kroon's result [40] that stationary spacetimes only admit conformally flat slices if certain "obstructions," constructed out of Geroch-Hansen quadrupoles, vanish.

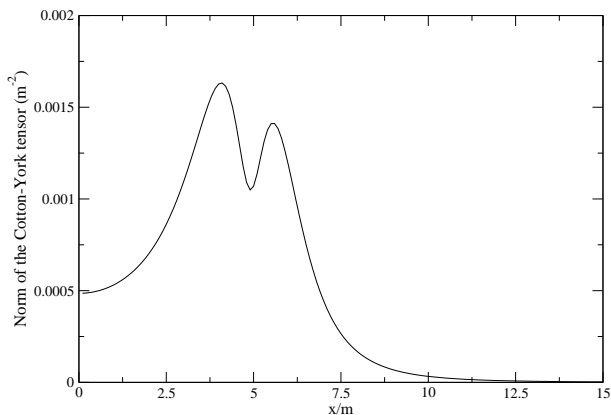


FIG. 3: The norm of the Cotton-York tensor for the test system $m_1 = m_2 = m/2$, $b = 10m$ along the x -axis (i.e., the axis passing through both holes). (We only show it around hole 1 because it is symmetric about $x = 0$.)

where Ψ is some conformal factor, while h_{kl} is not proportional to the flat metric. In fact, h_{kl} must be symmetric and trace-free and contains a piece that is proportional to

$$\frac{\partial^2}{\partial x_1^{<k} \partial x_2^{l>}} \log S, \quad (4.8)$$

where S was defined in the previous subsection and the angle brackets stand for the symmetric trace-free projection. [See, e.g., Eq. (3.1) in [42]; we have left off pieces of the form $v_1^{<k} v_1^{l>}$.] This is clearly not a manifestly conformally flat contribution to the metric, so we can use it to connect with the heuristic that “the 2PN metric is not spatially conformally flat because it contains various pieces that are not manifestly conformally flat.”

To do so, we shall demonstrate how the presence in h_{kl} of the term given in Eq. (4.8) prevents the obvious sort of coordinate transformation from rendering g_{kl} conformally flat. For the purposes of illustration, we take our coordinate transformation to be of the form $x^k \rightarrow x'^k = x^k + \xi^k$, where $\xi^k = O(v^4)$, and ask that it remove the h_{kl} piece from the 3-metric. (Of course, in general the coordinate transformation would just need to turn h_{kl} into a scalar multiple of δ_{kl} , and would not have to be of the form above, but our assumptions suffice for a heuristic argument.) Thus, ξ^k should satisfy

$$\partial_{(k} \xi_{l)} = -\frac{1}{2} h_{kl}, \quad (4.9)$$

but this equation has no solution when the right-hand side is given by Eq. (4.8). To show that this is the case, it is sufficient [by the gauge invariance of the linearized Riemann tensor—see the discussion surrounding Eq. (5.5)] to show that the (three-dimensional) flat space linearized Riemann tensor associated with h_{kl} does not vanish. We have computed this tensor [with h_{kl} given by Eq. (4.8)] and verified that several components are indeed generically nonzero.

B. Gravitational radiation in the PN metric

The order at which the effects of gravitational radiation appear in the PN metric is different for different effects, which can easily lead to confusion. We thus offer a brief discussion of these orders here. To avoid even further confusion, since we shall discuss some pieces that are not dimensionless, we shall describe all orders in terms of the formal slow motion expansion in $1/c$, as do Blanchet, Faye, and Ponsot (BFP) [58]. [Since the metric is dimensionless, an $O(c^{-n})$ contribution to it can be unambiguously identified as being $O(v^n)$.] It is well known that the effects of gravitational radiation reaction first enter the equations of motion at $O(c^{-5})$ for a circular orbit. [See, e.g., Eq. (189) in Blanchet [62].] This is also the leading order of the binary’s gravitational wave luminosity. [See, e.g., Eq. (171) in Blanchet.] However, the lowest-order “quadrupole formula” piece of the gravitational waveform appears in the PN far zone metric at one order lower, viz., $O(c^{-4})$. This can be seen in Blanchet’s Eq. (238); his x variable is $O(c^{-2})$. These terms can also be seen in Eqs. (6.10) and (6.11a) of [71]. Here they are presented in a form that allows for a more direct comparison with our expression for the far zone metric, though this expression does not show the factors of c^{-1} explicitly. The terms in question appear as the final two terms in the curly brackets in our expression for the far zone spatial metric in Eq. (6.6c). Explicitly, they are $4(m_1/r)(v_1^{kl} - \omega^2 x_1^{kl}) + (1 \leftrightarrow 2)$.

Our initial data should thus contain the binary’s outgoing gravitational radiation (whether one uses the extension that adds on various higher-order terms or not), since we have included all the $O(v^4)$ pieces in the spatial metric, along with the matching $O(v^5)$ pieces in the extrinsic curvature. This explains why Kelly *et al.* obtain the outgoing wave train when they evolve [57], since their data set [43] contains only terms in the far zone through $O(v^4)$ [in the spatial metric, with the matching $O(v^5)$ pieces in the extrinsic curvature], even though they do not have the $O(v^5)$ terms in the spatial metric.

The factor of $1/c$ one obtains in going from the terms in the near zone that give the lowest-order piece of the waveform when expanded in the far zone (i.e., in b/r), which are $O(c^{-4})$, to the lowest-order $O(c^{-5})$ radiation reaction contribution to the equations of motion is explained by Blanchet in [88]: Radiation reaction effects arise from antisymmetric waves—i.e., those that are time-odd—and such waves will come from expressions involving at least one more time derivative (and thus factor of $1/c$) than their symmetric (and time-even) counterparts. Explicitly, these near zone terms that match onto the lowest-order gravitational wave terms in the far zone are $4(m_1/r_1)v_1^k v_1^l - 4(m_1 m_2 / b S) n_{12}^k n_{12}^l + (1 \leftrightarrow 2)$, since $r_A = r[1 + O(b/r)]$ and $S = 2r[1 + O(b/r)]$. The (multipolar expansion of the) first time derivative of these terms gives the lowest-order radiation reaction contribution to the metric given in [88]. These terms themselves are also some of the contributions to the near zone metric that

cause it to be conformally curved.

V. THE MATCHING CALCULATION

A. The setup

By symmetry, we can concentrate on performing the matching around hole 1: All our results in this case can be directly translated to the matching around hole 2 by taking $1 \leftrightarrow 2$, $(t, x, y, z) \rightarrow (t, -x, -y, z)$, and $(T, X, Y, Z) \rightarrow (T, -X, -Y, Z)$, along with $\hat{x}_\alpha \rightarrow -\hat{x}_\alpha$ and $\hat{y}_\alpha \rightarrow -\hat{y}_\alpha$ in the tidal fields. Here \hat{x}_α and \hat{y}_α denote the unit vectors in the x_1 - and x_2 -directions, respectively. (Similarly, \hat{t}_α and \hat{z}_α denote unit vectors in the x_0 - and x_3 -directions—we shall use these later.) In other words, we switch the masses to turn m_1 into m_2 , and then rotate by π radians around the z -axis to move the new m_2 into the same position as the old m_2 . However, we also need to rotate the inner zone coordinates so that they have the same relation to the new near zone coordinates that they did when we performed the original matching around hole 1. Finally, the tidal fields transform as Cartesian tensors under this rotation, and this transformation is taken care of by the final two substitutions.

Since our matching calculation will determine the coordinate transformation, the relations between the metrics' mass parameters, and the inner zone metric's tidal fields, we need to posit expansions for all of these. For the coordinate transformation, we make nearly the same ansatz as in Papers I and II, viz.,

$$X^\alpha(x^\beta) = \sum_{j=0}^5 \left(\frac{m_2}{b}\right)^{j/2} (X^\alpha)_j(x^\beta) + O(v^6). \quad (5.1)$$

(This is slightly more general than the ansatz used in the previous papers because we do not fix the zeroth order coordinate transformation from the outset.) We choose $\sqrt{m_2/b}$ as our expansion parameter because it makes for slightly simpler notation than either $v = \sqrt{m/b}$ or $\sqrt{m_1/b}$ when expanding in the buffer zone around hole 1, as we are doing here. We can make this choice without loss of generality: The resulting coordinate transformation will be the same regardless of which of these three possibilities we choose to use as our expansion parameter, though the coefficients of the expansion parameter will differ by ratios of the masses. As in the previous papers, we implicitly assume that $(X_\alpha)_j$ is a power series in \tilde{r}/b , including negative powers—i.e., a Laurent series—so we can write, e.g., $m_2/r = (m_2/b)(b/r)$. However, $(X_\alpha)_j$ should not depend on m_2/b , by definition.

We also need to worry about the multipole expansion of each $(X_\alpha)_j$. This would seem to be straightforward, since we only want to keep terms through quadrupole order overall. However, the structure of the inner zone metric creates some complications: In order to obtain data that include all the quadrupole $[O([\tilde{r}/b]^2)]$ pieces

at fourth and fifth orders,⁵ one needs to obtain the octupole $[O([\tilde{r}/b]^3)]$ pieces of the coordinate transformation when matching at second and third orders. This is due to the appearance of b/\tilde{r} terms in $(h_{\alpha\beta})_j$ for $j \geq 2$. These enter the fourth and fifth order coordinate transformation equations, where they multiply the second and third order pieces of the coordinate transformation and thus produce quadrupolar contributions from octupolar pieces of the coordinate transformation. The octupole fields themselves also enter, as they are multiplied by b/\tilde{r} in the fourth and fifth order pieces of the inner zone metric. However, we shall see that the octupole piece of the second order coordinate transformation vanishes, and that of the third order one only appears in the time coordinate. Thus, the only place where the octupole pieces of the coordinate transformation appear is in the $(h_{(\alpha|\gamma)})_2 (A_{|\beta})^\gamma)_3$ piece of the fifth order coordinate transformation equations [given in full in Eq. (5.30)].

This increase in the number of multipoles that have to be kept as one proceeds to higher and higher orders in v is a general feature of the matching of these two metrics. It is thus a source of significant technical difficulty: One would need to include the hexadecapole pieces in the matching calculation if one wanted to include all of the quadrupole pieces at sixth and higher orders. This follows since at sixth order the hexadecapole pieces start to be multiplied by b^2/\tilde{r}^2 , making them of quadrupole order. (It would still be possible to obtain all the dipole pieces at fifth and sixth orders if one had an expression for the near zone metric through seventh order, but one would not be able to include any new higher-order corrections to the tidal fields this way.)

We posit the same expansion in $\sqrt{m_2/b}$ for the mass parameter of the inner zone metric, M_1 , as we did for the coordinate transformation, so

$$M_1 = \sum_{j=0}^3 \left(\frac{m_2}{b}\right)^{j/2} (M_1)_j + O(v^4). \quad (5.2)$$

However, it will turn out that we did not need to allow this freedom, as we shall find that the mass parameters of the two metrics agree to the highest order to which our matching fixes them—i.e., $M_1 = m_1 + O(v^4)$. Similarly,

⁵ We count orders using our primary expansion in v (or, equivalently, $\sqrt{m_2/b}$).

we asymptotically expand the tidal fields in $\sqrt{m_2/b}$, so

$$\begin{aligned}
\mathcal{E}_{kl} &= \frac{m_2}{b^3} \sum_{j=0}^3 \left(\frac{m_2}{b}\right)^{j/2} (\bar{\mathcal{E}}_{kl})_j + O(v^6), \\
\dot{\mathcal{E}}_{kl} &= \frac{m_2}{b^3} \sum_{j=1}^2 \left(\frac{m_2}{b}\right)^{j/2} (\dot{\bar{\mathcal{E}}}_{kl})_j + O(v^5), \\
\mathcal{E}_{klp} &= \frac{m_2}{b^4} \sum_{j=0}^2 \left(\frac{m_2}{b}\right)^{j/2} (\bar{\mathcal{E}}_{klp})_j + O(v^5), \\
\mathcal{B}_{kl} &= \left(\frac{m_2}{b}\right)^{3/2} \frac{1}{b^2} \sum_{j=0}^2 \left(\frac{m_2}{b}\right)^{j/2} (\bar{\mathcal{B}}_{kl})_j + O(v^6), \\
\dot{\mathcal{B}}_{kl} &= \left(\frac{m_2}{b}\right)^2 \frac{1}{b^2} (\dot{\bar{\mathcal{B}}}_{kl})_1 + O(v^5), \\
\mathcal{B}_{klp} &= \left(\frac{m_2}{b}\right)^{3/2} \frac{1}{b^3} \sum_{j=0}^1 \left(\frac{m_2}{b}\right)^{j/2} (\bar{\mathcal{B}}_{klp})_j + O(v^5).
\end{aligned} \tag{5.3}$$

[The expansions of the duals of the magnetic fields—e.g., \mathcal{C}_{klp} —are defined analogously. Also recall that the “barred” tidal fields are defined in Eq. (3.1). Additionally, the tidal fields and their time derivatives—e.g., \mathcal{E}_{kl} and $\dot{\mathcal{E}}_{kl}$ —are treated as formally independent.] We do not include the $O(v^5)$ pieces of the octupole tidal fields here because we did not fix them in the matching: We only had to match the octupole fields through $O(v^3)$ to obtain initial data with formal uncontrolled remainders of $O(v^5)$ and $O([r/b]^3)$ (i.e., octupolar order). We also chose to read off the $O(v^4)$ pieces of the octupole fields separately (in Appendix B 2), but did not do so for the $O(v^5)$ parts.

In order to read off the matching parameters (and any undetermined pieces of the lower-order coordinate transformations) as efficiently as possible, we note that all of our equations for the coordinate transformation at orders beyond the zeroth will be of the form

$$\partial_{(\alpha} X_{\beta)} = S_{\alpha\beta} \equiv S_{(\alpha\beta)}. \tag{5.4}$$

Here $\partial_\alpha := \partial/\partial x^\alpha$ (i.e., all partial derivatives are taken with respect to PN harmonic coordinates), X^α is a function of x^α , and $S_{\alpha\beta}$, the equation’s source, is some (symmetric) matrix function of x^α (either explicitly, or implicitly though X^α) which is C^2 in the buffer zone. The integrability condition for this equation is that the flat-space linearized Riemann tensor associated with $S_{\alpha\beta}$ vanish, i.e., that we have

$$\mathcal{I}_{\alpha\beta\gamma\delta} := \partial_{\alpha\beta} S_{\gamma\delta} + \partial_{\gamma\delta} S_{\alpha\beta} - \partial_{\alpha\delta} S_{\gamma\beta} - \partial_{\gamma\beta} S_{\alpha\delta} = 0. \tag{5.5}$$

[N.B.: For convenience, we have defined $\mathcal{I}_{\alpha\beta\gamma\delta}$ with a slightly different index ordering than the linearized Riemann tensor—given in, e.g., Eq. (5.44) of [77]—and without the factor of $1/2$.] This follows from the gauge invariance of the linearized Riemann tensor. (See, e.g., §4.1 in Straumann [89] for a proof and discussion of that result.

In [90], Blanchet and Damour use this gauge invariance for the same purpose we do.)

For future use, we note that the homogeneous equation, $\partial_{(\alpha} X_{\beta)} = 0$, is the flat space Killing equation, and its most general solution is given by

$$X_\alpha = F_{\beta\alpha} x^\beta + C_\alpha, \tag{5.6}$$

where $F_{\alpha\beta} \equiv F_{[\alpha\beta]}$ is some constant (antisymmetric) 4×4 matrix and C_α is some constant 4×1 matrix. See, e.g., §13.1 in Weinberg [91] for a proof. (Our X_α , $F_{\alpha\beta}$, and C_α correspond to Weinberg’s ξ_α , $b_{\beta\alpha} = -b_{\alpha\beta}$, and a_α , respectively.) We shall primarily employ this result tacitly at each order beyond the zeroth to ensure that we have the most general expression for that order’s contribution to the coordinate transformation.

Our general approach to the nontrivial matching that occurs at second order and beyond will be as follows: We first use the above integrability condition to read off the matching parameters, exploiting the linear independence of various terms to simplify the process and justify our claims of uniqueness. We start with the nonpolynomial terms, which determine many of the previously undetermined parts of the coordinate transformation from two orders lower, as well as the inner zone mass parameter; the polynomial part then determines the tidal fields.⁶ The nonpolynomial part consists of all the terms that are not polynomials in $\tilde{x}^\alpha := x^\alpha - (m_2/m)b\hat{x}^\alpha$. For this calculation, these are all of the form of a polynomial in \tilde{x}^α multiplied by \tilde{r}^n , where $n \in \mathbb{Z} \setminus \{0, 2, 4, 6, \dots\}$. After we have fixed all the parameters that can be fixed at a given order, we can then solve for that order’s contribution to the coordinate transformation (and the polynomial part can be solved for separately from the nonpolynomial part that first appears at fourth order). In all of this, MAPLE and GRTENSORII proved very helpful: They work extremely well for all aspects of the polynomial part, while requiring more care when applied to the nonpolynomial part.

B. Zeroth Order $O([m_2/b]^0)$

To lowest (zeroth) order in $(m_2/b)^{1/2}$, we have

$$(g_{\alpha\beta})_0 = (A_\alpha{}^\gamma)_0 (h_{\gamma\delta})_0 (A_\beta{}^\delta)_0, \tag{5.7}$$

where we have defined $A_\alpha{}^\beta := \partial_\alpha X^\beta$. Since $(g_{\alpha\beta})_0 = (h_{\alpha\beta})_0 = \eta_{\alpha\beta}$, matching just tells us that $(A_\alpha{}^\beta)_0$ must be a (general) Lorentz transformation—i.e., not necessarily

⁶ It is intuitively reasonable that the polynomial and nonpolynomial parts should determine the parameters that they do: If one neglects all gauge subtleties and the like, the nonpolynomial terms can be thought of as being those associated with hole 1, and the polynomial terms with (the tidal fields of) hole 2. We discuss this more fully in Sec. V G.

one continuously connected to the identity—which we call L_α^β . We also pick up a 4×1 matrix “constant of integration” $(C^\alpha)_0$ in obtaining $(X^\alpha)_0$, so we are finally left with

$$(X^\alpha)_0 = L_\beta^\alpha x^\beta + (C^\alpha)_0. \quad (5.8)$$

For simplicity, we shall take this lowest-order piece to be the expected translation due to the position of m_2 at $t = 0$, viz.,

$$L_\alpha^\beta = \delta_\alpha^\beta, \quad (C_\alpha)_0 = -\frac{m_2}{m} b \hat{x}_\alpha. \quad (5.9)$$

In fact, one can show that matching through third order requires that the spatial part of $(C_\alpha)_0$ be as given above (though the temporal part can still be freely specified). Similarly, that matching requires L_α^β to differ from the identity only by a possible rotation about the y -axis, along with possible spatial and temporal reflections. These are combined with a rotation that takes $+y$ to $-y$ if we have an odd number of reflections. We thus conjecture that matching at higher orders will further constrain this lowest-order coordinate transformation to be as given above. At the very least, the matching at fourth and fifth orders is independent of the remaining freedom.

C. First Order [$O(\sqrt{m_2/b})$]

We have $(g_{\alpha\beta})_1 = (h_{\alpha\beta})_1 = 0$. Thus, the first order matching gives us

$$(A_{(\alpha\beta)})_1 = 0, \quad (5.10)$$

using the fact that $(h_{\alpha\beta})_0 = \eta_{\alpha\beta}$. As was given in Eq. (5.6), the most general solution of this equation is

$$(X_\alpha)_1 = (F_{\beta\alpha})_1 \tilde{x}^\beta + (C_\alpha)_1, \quad (5.11)$$

where we have written this in terms of $\tilde{x}^\alpha := x^\alpha - (m_2/m)b\hat{x}^\alpha$ because $\tilde{r}/b := \sqrt{\tilde{x}_k \tilde{x}^k}/b$ is one of our small parameters. We can do this without loss of generality, as it simply entails a different value for C_α .

This result differs from that given in Eq. (21) of Paper I; the latter suffers from some sign errors introduced during transcription. However, this does not affect that paper’s final coordinate transformation, as the relevant constants were all taken to be zero. This is appropriate for Papers I and II, since they were using a corotating coordinate system: The boost encoded in our $(F_{\alpha\beta})_1$ [seen in Eq. (5.25)] would thus not be expected to appear in the coordinate transformation.

D. Second Order [$O(m_2/b)$]

Proceeding to the next order, we have, recalling that $(\dot{\mathcal{E}}_{kl})_0 = 0$,

$$(h_{\alpha\beta})_2 = \left[\frac{2(M_1)_0}{m_2} \frac{b}{(R)_0} - \frac{(\bar{\mathcal{E}}_{kl})_0}{b^2} (X^k)_0 (X^l)_0 - \frac{(\bar{\mathcal{E}}_{klp})_0}{3b^3} (X^k)_0 (X^l)_0 (X^p)_0 \right] \Delta_{\alpha\beta}. \quad (5.12)$$

Similarly, noting that $(\dot{b}_k)_0 = 0$,

$$(g_{\alpha\beta})_2 = \left[\frac{2m_1}{m_2} \frac{b}{(r_1)_0} + 2 - \frac{2}{b} \{(\vec{r}_1)_0 \cdot (\hat{b})_0\} + \frac{1}{b^2} \{3[(\vec{r}_1)_0 \cdot (\hat{b})_0]^2 - [(r_1)_0]^2\} + \frac{1}{b^3} \{3[(r_1)_0]^2 [(\vec{r}_1)_0 \cdot (\hat{b})_0] - 5[(\vec{r}_1)_0 \cdot (\hat{b})_0]^3\} \right] \Delta_{\alpha\beta}. \quad (5.13)$$

Here $\Delta_{\alpha\beta} := \text{diag}(1, 1, 1, 1)$ is the “lowered 4-dimensional Kronecker delta.” Also, we have $(\hat{b}_k)_0 = \hat{x}_k$ and, with our choice for the zeroth order coordinate transformation, $(r_1^k)_0 = \tilde{r}^k$. The equations for the coordinate transformation at this order are thus

$$(g_{\alpha\beta})_2 = (A_\alpha^\gamma)_0 (h_{\gamma\delta})_2 (A_\beta^\delta)_0 + (A_\alpha^\gamma)_1 (h_{\gamma\delta})_0 (A_\beta^\delta)_1 + 2 (A_{(\alpha|\gamma})_0 (h_{\gamma\delta})_0 (A_{|\beta)}^\delta)_2, \quad (5.14)$$

since $(h_{ab})_1 = 0$, or, using our previous results,

$$(g_{\alpha\beta})_2 = (h_{\alpha\beta})_2 + (F_\alpha^\gamma)_1 (F_{\beta\gamma})_1 + 2 (A_{(\alpha\beta)})_2. \quad (5.15)$$

Thus, at this order, the source of the differential equation [cf. Eq. (5.4)] is given by

$$2 (S_{\alpha\beta})_2 = 2 (A_{(\alpha\beta)})_2 = (g_{\alpha\beta})_2 - (h_{\alpha\beta})_2 - (F_\alpha^\gamma)_1 (F_{\beta\gamma})_1. \quad (5.16)$$

We now apply the integrability condition from Eq. (5.5) and focus on the nonpolynomial piece of $(S_{\alpha\beta})_2$; here this is the one that diverges [as $(R)_0 = (r_1)_0 = \tilde{r} \rightarrow 0$]. It must satisfy the integrability condition independently of the other pieces, by linear independence, and [considering, e.g., $(T_{kl00})_2$] gives $(M_1)_0 = m_1$, as expected. The polynomial piece of the integrability conditions tells us that

$$(\bar{\mathcal{E}}_{kl})_0 = \delta_{kl} - 3\hat{x}_k \hat{x}_l, \quad (\bar{\mathcal{E}}_{klp})_0 = 15\hat{x}_k \hat{x}_l \hat{x}_p - 9\delta_{(kl} \hat{x}_{p)}, \quad (5.17)$$

using linear independence to read off the quadrupole and octupole tidal fields separately. Solving for the coordinate transformation, we obtain

$$(X_\alpha)_2 = \left[1 - \frac{\tilde{x}}{b}\right] \Delta_{\alpha\beta} \tilde{x}^\beta + \frac{\Delta_{\beta\gamma} \tilde{x}^\beta \tilde{x}^\gamma}{2b} \hat{x}_\alpha - \frac{1}{2} (F_\alpha{}^\gamma)_1 (F_{\beta\gamma})_1 \tilde{x}^\beta + (F_{\beta\alpha})_2 \tilde{x}^\beta + (C_\alpha)_2. \quad (5.18)$$

E. Third Order $[O([m_2/b]^{3/2})]$

At this order, the inner zone metric is

$$(h_{00})_3 = \frac{2(M_1)_0 b}{m_2} \left(\frac{1}{R}\right)_1 + \frac{2(M_1)_1 b}{m_2} \frac{b}{(R)_0} - 2 \frac{(\bar{\mathcal{E}}_{kl})_0}{b^2} (X^k)_0 (X^l)_1 - \frac{(\bar{\mathcal{E}}_{kl})_1}{b^2} (X^k)_0 (X^l)_0 \\ - \frac{(\dot{\bar{\mathcal{E}}}_{kl})_1}{b^2} (T)_0 (X^k)_0 (X^l)_0 - \frac{(\bar{\mathcal{E}}_{klp})_0}{b^3} (X^k)_0 (X^l)_0 (X^p)_1 - \frac{(\bar{\mathcal{E}}_{klp})_1}{3b^3} (X^k)_0 (X^l)_0 (X^p)_0, \quad (5.19a)$$

$$(h_{0k})_3 = \frac{2}{3} \frac{(\bar{\mathcal{C}}_{klp})_0}{b^2} (X^l)_0 (X^p)_0 + \frac{1}{3} \frac{(\bar{\mathcal{C}}_{klps})_0}{b^3} (X^l)_0 (X^p)_0 (X^s)_0 - \frac{2}{3} \frac{(\dot{\bar{\mathcal{E}}}_{lp})_1}{b^2} (X^l)_0 (X^p)_0 (X_k)_0, \quad (5.19b)$$

$$(h_{kl})_3 = (h_{00})_3 \delta_{kl}, \quad (5.19c)$$

and the near zone metric is

$$(g_{00})_3 = \frac{2m_1}{m_2} b \left(\frac{1}{r_1}\right)_1 - \frac{2}{b} [(\vec{r}_1)_0 \cdot (\hat{b})_1] + \frac{2}{b^2} \{3[(\vec{r}_1)_0 \cdot (\hat{b})_1][(\vec{r}_1)_0 \cdot (\hat{b})_0] - (\vec{r}_1)_1 \cdot (\vec{r}_1)_0\} + \frac{6}{b^3} [(\vec{r}_1)_0 \cdot (\vec{r}_1)_1][(\vec{r}_1)_0 \cdot (\hat{b})_0], \quad (5.20a)$$

$$(g_{0k})_3 = 4 \frac{m_1}{m} \left\{1 - \frac{b}{(r_1)_0} - \frac{1}{b} [(\vec{r}_1)_0 \cdot (\hat{b})_0] + \frac{1}{2b^2} [3\{(\vec{r}_1)_0 \cdot (\hat{b})_0\}^2 - \{(r_1)_0\}^2] \right. \\ \left. + \frac{1}{2b^3} [3\{(r_1)_0\}^2 \{(\vec{r}_1)_0 \cdot (\hat{b})_0\} - 5\{(\vec{r}_1)_0 \cdot (\hat{b})_0\}^3] \right\} (\dot{b}_k)_1, \quad (5.20b)$$

$$(g_{kl})_3 = (g_{00})_3 \delta_{kl}. \quad (5.20c)$$

Here we have $(\vec{b})_1 = \sqrt{m/m_2} t \hat{y}$, so $(\vec{r}_1)_1 = - (m_2/m) (\vec{b})_1 = -\sqrt{m_2/mt} \hat{y}$, and thus $(\vec{r}_1)_1 \cdot (\hat{b})_0 = 0$. Additionally, $(\hat{b})_1 = \sqrt{m/m_2} (t/b) \hat{y}$ and $(\dot{b}_k)_1 = \sqrt{m/m_2} \hat{y}_k$. We also have

$$\left(\frac{1}{R}\right)_1 = -\frac{1}{(R)_0} \frac{(X_k)_0 (X^k)_1}{[(R)_0]^2} \\ = -\frac{\tilde{r}^k [(F_{\alpha k})_1 \tilde{x}^\alpha + (C_k)_1]}{\tilde{r}^3}, \quad (5.21)$$

and

$$\left(\frac{1}{r_1}\right)_1 = -\frac{1}{(r_1)_0} \frac{(\vec{r}_1)_0 \cdot (\vec{r}_1)_1}{[(r_1)_0]^2} = \sqrt{\frac{m_2}{m}} \frac{yt}{\tilde{r}^3}, \quad (5.22)$$

where $\tilde{r}^\alpha := r^\alpha - (m_2/m) b \hat{x}^\alpha$.

At this order, the equations for the coordinate trans-

formation are

$$2(S_{\alpha\beta})_3 = 2(A_{(\alpha\beta)})_3 = (g_{\alpha\beta})_3 - (h_{\alpha\beta})_3 \\ - 2(h_{(\alpha|\gamma})_2 (F_{|\beta)}^\gamma)_1 - 2(F_{(\alpha|\gamma})_1 (A_{|\beta)\gamma})_2, \quad (5.23)$$

recalling that $(h_{\alpha\beta})_1 = 0$ and utilizing our lower-order results. To obtain $(F_{\alpha\beta})_1$, we look at the \tilde{r}^{-7} piece of $(\mathcal{I}_{kl00})_3$. Such a piece can only come from two spatial derivatives both acting on \tilde{r}^{-3} in the \tilde{r}^{-3} pieces of $(S_{00})_3$; those pieces, in turn, only come from $(1/R)_1$ and $(1/r_1)_1$. Therefore, using Eqs. (5.21) and (5.22), the integrability conditions require that we have

$$\tilde{r}^k [(F_{\alpha k})_1 \tilde{x}^\alpha + (C_k)_1] = -\sqrt{\frac{m_2}{m}} yt, \quad (5.24)$$

from which we immediately see that

$$(C_k)_1 = 0, \quad (F_{\alpha\beta})_1 = 2\sqrt{\frac{m_2}{m}} \hat{t}_{[\alpha} \hat{y}_{\beta]}, \quad (5.25)$$

using the antisymmetry of $F_{\alpha\beta}$. (Recall that $\hat{t}_0 = -1$.) By similar logic, the \tilde{r}^{-5} piece of $(\mathcal{I}_{kl00})_3$ only comes from the $(M_1)_1$ piece of $(h_{00})_3$ and gives us $(M_1)_1 = 0$. The remaining nonpolynomial pieces cancel, so we have extracted all the information we can from the nonpolynomial part of the integrability condition.

From the polynomial part of the integrability conditions, we first read off the octupole parts of the tidal fields, which are

$$\begin{aligned} (\dot{\mathcal{E}}_{kl})_1 &= -\frac{6}{b}\sqrt{\frac{m}{m_2}}\hat{x}_{(k}\hat{y}_{l)}, & (\bar{\mathcal{E}}_{klp})_1 &= 0, \\ (\bar{\mathcal{B}}_{klp})_0 &= \frac{9}{2}\sqrt{\frac{m}{m_2}}[5\hat{x}_{(k}\hat{x}_l\hat{z}_p) - \delta_{(kl}\hat{z}_{p)}], \end{aligned} \quad (5.26)$$

and then the quadrupole parts, which are

$$(\bar{\mathcal{E}}_{kl})_1 = 0, \quad (\bar{\mathcal{B}}_{kl})_0 = -6\sqrt{\frac{m}{m_2}}\hat{x}_{(k}\hat{z}_{l)}. \quad (5.27)$$

The third order coordinate transformation is thus

$$\begin{aligned} (X_\alpha)_3 &= \sqrt{\frac{m}{m_2}}\left\{-\frac{yt}{b^2}\Delta_{\alpha\beta}\tilde{x}^\beta + \left[\frac{\tilde{x}_\mu\tilde{x}^\mu - 4\tilde{x}^2}{2b^2} + \left(2 - \frac{m_2}{m}\right)\frac{\tilde{x}}{b} + \left(2 + \frac{1}{2}\frac{m_2}{m}\right)\frac{m_2}{m}\right]y\hat{t}_\alpha + 2\left[1 - \frac{m_2}{m}\right]\frac{yt}{b}\hat{x}_\alpha\right. \\ &\quad \left.+ \left[\frac{3\tilde{r}^2 + t^2}{6b^2} + \left(\frac{m_2}{m} - 2\right)\frac{\tilde{x}}{b} + \frac{1}{2}\left(\frac{m_2}{m}\right)^2 + 4\right]t\hat{y}_\alpha\right\} + \left\{\sqrt{\frac{m_2}{m}}[\hat{y}_{(\alpha}(F_{\beta)0})_2 - \hat{t}_{(\alpha}(F_{\beta)2})_2] + (F_{\beta\alpha})_3\right\}\tilde{x}^\beta \\ &\quad + (C_\alpha)_3 + \frac{1}{2b^3}\sqrt{\frac{m}{m_2}}\tilde{x}y(4\tilde{x}^2 - y^2 - z^2)\hat{t}_\alpha, \end{aligned} \quad (5.28)$$

where the octupole part is the final term.

F. Fourth and Fifth Orders $[O([m_2/b]^2)]$ and $O([m_2/b]^{5/2})]$

The matching at fourth and fifth orders proceeds in the same way as it did at lower orders, though the algebraic complexity increases substantially. We shall thus give far fewer details of the calculations than we did before, and mostly concern ourselves with pointing out the new features of the calculation that arise at these orders. The most prominent new feature, and the one responsible for much of the algebraic complexity, is the presence of a nonpolynomial part in the coordinate transforma-

tion. We know to expect this at fourth order because the transformation between Cook-Scheel and PN harmonic coordinates is nonpolynomial, and its lowest-order piece is $O(v^4)$ —see Sec. V G. However, there are various other nonpolynomial pieces present in the coordinate transformation at fourth and fifth orders. We have to solve for these nonpolynomial parts of the coordinate transformation by inspection (though we can still use MAPLE to obtain the polynomial part). It is reasonably easy to do so if one first breaks the source into pieces by multipolar order.

The other subtleties involve the multipole expansion and are best illustrated by giving two examples: First looking at the fourth order piece of the inner zone metric component, we have

$$\begin{aligned} (h_{00})_4 &= 2\frac{(M_1)_2}{m_2}\frac{b}{(R)_0} + 2\frac{(M_1)_0}{m_2}b\left(\frac{1}{R}\right)_2 - 2\frac{[(M_1)_0]^2}{m_2^2}\frac{b^2}{[(R)_0]^2} - \frac{(\bar{\mathcal{E}}_{kl})_2}{b^2}(X^k)_0(X^l)_0 - \frac{(\bar{\mathcal{E}}_{kl})_0}{b^2}(X^k)_1(X^l)_1 \\ &\quad - 2\frac{(\bar{\mathcal{E}}_{kl})_0}{b^2}(X^k)_0(X^l)_{2,0} + 2\frac{(M_1)_0}{m_2}\frac{(\bar{\mathcal{E}}_{kl})_0}{b(R)_0}(X^k)_0(X^l)_0 + \frac{2}{3}\frac{(M_1)_0}{m_2}\frac{(\bar{\mathcal{E}}_{klp})_0}{b^2(R)_0}(X^k)_0(X^l)_0(X^p)_0. \end{aligned} \quad (5.29)$$

The terms to notice are the ones involving $(X^k)_{2,0}$

and \mathcal{E}_{klp}/R . The first of these reflects the necessity

of avoiding “hidden octupole” pieces (i.e., pieces of octupolar order that arise when multiplying together pieces of lower multipolar order) when looking at corrections to lower-order terms: We only want to include $(X^k)_{2,0}$, the monopole (zeroth-order-in- \tilde{x}/b) piece of $(X^k)_2$, in $(\bar{\mathcal{E}}_{kl})_0 (X^k)_0 (X^l)_{2,0}/b^2$; the dipole contribution to $(X^k)_2$ would give an octupole contribution to

h_{00} . Contrariwise, we do not want to leave out any terms of quadrupolar order, even if they arise from, e.g., octupolar tidal fields. The \mathcal{E}_{klp}/R contribution is such a term.

These subtleties arise in a slightly different form in the equation for the fifth order piece of the coordinate transformation:

$$\begin{aligned} 2(S_{\alpha\beta})_5 &= 2(A_{(\alpha\beta)})_5 = (g_{\alpha\beta})_5 - (h_{\alpha\beta})_5 - 2(h_{(\alpha|\gamma})_4 (F_{|\beta)}^\gamma)_1 - (F_{\alpha}^\gamma)_1 (h_{\gamma\delta})_3 (F_{\beta}^\delta)_1 - 2(h_{(\alpha|\gamma})_3 (A_{|\beta)}^\gamma)_{2,0} \\ &\quad - 2(h_{(\alpha|\gamma)}^{\text{NP}})_3 (A_{|\beta)}^\gamma)_2 - 2(F_{(\alpha|\gamma)}^\gamma)_1 (h_{\gamma\delta}^{\text{P}})_2 (A_{|\beta)}^\delta)_{2,0} - 2(F_{(\alpha|\gamma)}^\gamma)_1 (h_{\gamma\delta}^{\text{NP}})_2 (A_{|\beta)}^\delta)_2 - 2(h_{(\alpha|\gamma)}^{\text{P}})_2 (A_{|\beta)}^\gamma)_{3,0} \\ &\quad - 2(h_{(\alpha|\gamma)}^{\text{NP}})_2 (A_{|\beta)}^\gamma)_{3,\leq 3} - 2(A_{(\alpha|\gamma)}^\gamma)_2 (A_{|\beta)}^\gamma)_{3,\leq 1} - 2(A_{(\alpha|\gamma)}^\gamma)_{2,0} (A_{|\beta)}^\gamma)_{3,2} - 2(F_{(\alpha|\gamma)}^\gamma)_1 (A_{|\beta)}^\gamma)_4. \end{aligned} \quad (5.30)$$

Here we have to avoid “hidden octupole” terms in many of the contractions: For instance, we only want the quadrupole-and-lower pieces of $(A_{(\alpha|\gamma)}^\gamma)_2 (A_{|\beta)}^\gamma)_3$, which are given by $(A_{(\alpha|\gamma)}^\gamma)_2 (A_{|\beta)}^\gamma)_{3,\leq 1} + (A_{(\alpha|\gamma)}^\gamma)_{2,0} (A_{|\beta)}^\gamma)_{3,2}$. However, it is also necessary to split up the inner zone metric’s contributions into polynomial and nonpolynomial parts to keep from excluding quadrupole pieces as well [since the nonpolynomial parts of the second and third order pieces of the inner zone metric are all $O(b/R)$]. In fact, this behavior means that we need to include the octupole part of the third order piece of coordinate transformation [in $(h_{(\alpha|\gamma)}^{\text{NP}})_2 (A_{|\beta)}^\gamma)_{3,\leq 3}$]. (One would also need to include the octupole part of the second order piece of the coordinate transformation, but it vanishes.)

The rest of the calculation proceeds as before, with the same general results: We obtain the next two orders’ contributions to the matching parameters, with the non-

polynomial pieces giving $(F_{\alpha\beta})_2 = 0$ and

$$(F_{\alpha\beta})_3 = \left[\left(\frac{m_2}{m} \right)^{3/2} + 3\sqrt{\frac{m_2}{m}} + 5\sqrt{\frac{m}{m_2}} \right] \hat{t}_{[\alpha} \hat{y}_{\beta]}, \quad (5.31)$$

along with $(C_k)_j = 0$ and $(M_1)_j = 0$ for $j \in \{2, 3\}$. Similarly, the polynomial pieces give

$$\begin{aligned} (\bar{\mathcal{E}}_{kl})_2 &= \frac{1}{2} \left[3\hat{x}_k \hat{x}_l - \delta_{kl} + \frac{m}{m_2} (4\hat{x}_k \hat{x}_l - 5\hat{y}_k \hat{y}_l + \hat{z}_k \hat{z}_l) \right], \\ (\bar{\mathcal{B}}_{kl})_2 &= \left[5 \left(\frac{m}{m_2} \right)^{3/2} + 7\sqrt{\frac{m}{m_2}} - 3\sqrt{\frac{m_2}{m}} \right] \hat{x}_{(k} \hat{z}_{l)}, \end{aligned} \quad (5.32)$$

along with $(\bar{\mathcal{B}}_{kl})_1 = (\bar{\mathcal{E}}_{kl})_3 = 0$. The fourth order piece of the coordinate transformation is

$$\begin{aligned} (X_\alpha)_4 &= -(\mathcal{A}_t)_4 \hat{t}_\alpha + \frac{1}{2} \frac{m_1}{m_2} \frac{\tilde{x}}{b} \left[5 \frac{\tilde{x}^2}{b\tilde{r}} - 6 \frac{\tilde{x}}{\tilde{r}} - \frac{\tilde{r}}{b} \right] \tilde{r}_\alpha + (\mathcal{A}_x)_4 \hat{x}_\alpha + (\mathcal{A}_y)_4 \hat{y}_\alpha + (\mathcal{A}_z)_4 \hat{z}_\alpha \\ &\quad + \left\{ \sqrt{\frac{m_2}{m}} [\hat{y}_{(\alpha} (F_{\beta)0})_3 - \hat{t}_{(\alpha} (F_{\beta)2})_3] + (F_{\beta\alpha})_4 \right\} \tilde{x}^\beta + (C_\alpha)_4, \end{aligned} \quad (5.33)$$

where

$$\begin{aligned}
(\mathcal{A}_t)_4 &:= 4 \frac{m_1^2 b^2}{m_2^2 \tilde{r}} + t \left[\frac{t^2}{6b^2} + \frac{5(y^2 - \tilde{x}^2) + z^2}{2b^2} + 2 \frac{m}{m_2} \frac{\tilde{x}^2 - y^2}{b^2} - \left(\frac{1}{2} \frac{m_2}{m} + \frac{m}{m_2} - 2 \right) \frac{\tilde{x}}{b} \right. \\
&\quad \left. + 1 + \frac{m}{2m_2} + \frac{3}{2} \frac{m_2}{m} + \frac{5}{8} \left(\frac{m_2}{m} \right)^2 \right], \\
(\mathcal{A}_x)_4 &:= \frac{1}{2} \frac{m_1}{m_2} \left[\frac{\tilde{r}^2}{b^2} - 5 \frac{\tilde{x}^2}{b^2} + 6 \frac{\tilde{x}}{b} + 4 \right] \tilde{r} + \left[\left(\frac{t^2 - z^2}{b^2} + \frac{m}{m_2} \frac{z^2 - y^2}{b^2} + 4 - \frac{7}{2} \frac{m}{m_2} \right) \tilde{x} + \left(\frac{m}{2m_2} - 1 \right) \frac{\tilde{x}^2}{b} \right. \\
&\quad \left. + \left(\frac{m_2}{m} - \frac{m}{2m_2} \right) \frac{y^2}{b} - \left(1 + \frac{3}{2} \frac{m}{m_2} - \frac{m_2}{m} \right) \frac{t^2}{b} + \left(2 - \frac{3}{2} \frac{m}{m_2} \right) \frac{z^2}{b} \right], \\
(\mathcal{A}_y)_4 &:= y \left[\frac{m_1}{m_2} \frac{3\tilde{x}^2 - y^2}{b^2} - \left(\frac{1}{2} \frac{m_2}{m} + 2 \frac{m}{m_2} - 2 \right) \frac{\tilde{x}}{b} + \frac{5}{2} \frac{m}{m_2} - \frac{9}{2} - \frac{m_2}{2m} - \frac{5}{8} \left(\frac{m_2}{m} \right)^2 \right], \\
(\mathcal{A}_z)_4 &:= z \left[\frac{t^2 + z^2 + 3y^2 - 5\tilde{x}^2}{2b^2} + \frac{m}{m_2} \frac{\tilde{x}^2 - y^2}{b^2} + \frac{m}{2m_2} - \frac{1}{2} \right].
\end{aligned} \tag{5.34}$$

The fifth order piece is

$$\begin{aligned}
(X_\alpha)_5 &= (\mathcal{A}_t)_5 \hat{t}_\alpha - \left\{ \mathcal{M}_0 \left(6, \frac{1}{2} \right) \frac{\tilde{x} y t}{b^2 \tilde{r}} + \mathcal{K} \left[3 - \frac{5}{2} \frac{\tilde{x}}{b} \right] \frac{\tilde{x}^2 y t}{b \tilde{r}^3} \right\} \tilde{r}_\alpha + \frac{5}{2} \mathcal{K} \frac{\tilde{x}^2 t}{b^2 \tilde{r}} \epsilon_{0\alpha k 3} \tilde{r}^k + (\mathcal{A}_x)_5 \hat{x}_\alpha + (\mathcal{A}_y)_5 \hat{y}_\alpha \\
&\quad + \frac{y z t}{2b^2} \mathcal{M}(3, 3, -5) \hat{z}_\alpha + \left\{ \sqrt{\frac{m_2}{m}} [\hat{y}_{(\alpha} (F_{\beta)0})_4 - \hat{t}_{(\alpha} (F_{\beta)2})_4] + (F_{\beta\alpha})_5 \right\} \tilde{x}^\beta + (C_\alpha)_5.
\end{aligned} \tag{5.35}$$

Here $\epsilon_{\alpha\beta\gamma\delta}$ is the 4-dimensional Levi-Civita symbol, with $\epsilon_{0123} = 1$. Additionally, for notational convenience, we have defined

$$\begin{aligned}
(\mathcal{A}_t)_5 &:= \mathcal{M}_0(1, 0) \left[1 + \frac{14}{3} \frac{\tilde{x}}{b} \right] \frac{y}{b} \tilde{r} - 4 \mathcal{M}_0(1, 1) \frac{y t b^2}{\tilde{r}^3} - \frac{y}{4} \left[\mathcal{M}(1, 11, -10) \frac{t^2}{b^2} + \mathcal{M} \left(\frac{35}{3}, -\frac{35}{3}, 10 \right) \frac{\tilde{x}^2}{b^2} \right. \\
&\quad \left. - \mathcal{M} \left(3, -\frac{17}{3}, 6 \right) \frac{y^2}{b^2} - \mathcal{M} \left(\frac{5}{3}, \frac{7}{3}, 2 \right) \frac{z^2}{b^2} - \mathcal{M}(4, -6, 6) \frac{\tilde{x}}{b} - \mathcal{M} \left(4, \frac{17}{3}, -\frac{17}{3}, 10 \right) \frac{m_2}{m} \right], \\
(\mathcal{A}_x)_5 &:= \mathcal{M}_0 \left(3, \frac{3}{2} \right) \frac{y t}{b^2} \tilde{r} - \mathcal{K} \left[2 + 3 \frac{\tilde{x}}{b} \right] \frac{y t}{\tilde{r}} - \frac{y t}{b} \left[\frac{1}{2} \mathcal{M}(-11, 9, 1) \frac{\tilde{x}}{b} + \mathcal{M}(8, -11, 2, 1) \right], \\
(\mathcal{A}_y)_5 &:= \left[\mathcal{M}_0(2, 0) + \mathcal{M}_0 \left(3, -\frac{1}{2} \right) \frac{\tilde{x}}{b} \right] \frac{t}{b} \tilde{r} + 3 \mathcal{K} \frac{\tilde{x}^2 t}{b \tilde{r}} - \frac{t}{4} \left[\mathcal{M} \left(3, \frac{7}{3}, -\frac{4}{3} \right) \frac{t^2}{b^2} - \mathcal{M}_0(7, 12) \frac{\tilde{x}^2}{b^2} + \mathcal{M}_0(7, 8) \frac{y^2}{b^2} \right. \\
&\quad \left. + \mathcal{M}(9, -5, 0) \frac{z^2}{b^2} + \mathcal{M}_0(16, 6) \frac{\tilde{x}}{b} - \mathcal{M} \left(0, \frac{47}{3}, -\frac{17}{3}, 10 \right) \frac{m_2}{m} \right] - \mathcal{M}_0(8, 0) \tilde{x},
\end{aligned} \tag{5.36}$$

and

$$\begin{aligned}
\mathcal{M}(A, B, C, D) &:= A \left(\frac{m}{m_2} \right)^{3/2} + B \sqrt{\frac{m}{m_2}} + C \sqrt{\frac{m_2}{m}} + D \left(\frac{m_2}{m} \right)^{3/2}, \\
\mathcal{M}(A, B, C) &:= A \left(\frac{m}{m_2} \right)^{3/2} + B \sqrt{\frac{m}{m_2}} + C \sqrt{\frac{m_2}{m}}, \\
\mathcal{M}_0(A, B) &:= \mathcal{M}(A, -A - B, B) = A \left(\frac{m}{m_2} \right)^{3/2} - (A + B) \sqrt{\frac{m}{m_2}} + B \sqrt{\frac{m_2}{m}}, \\
\mathcal{K} &:= \mathcal{M}_0(0, -1) = \sqrt{\frac{m}{m_2}} - \sqrt{\frac{m_2}{m}},
\end{aligned} \tag{5.37}$$

where $\mathcal{M}_0(A, B)$ and \mathcal{K} vanish in the limit $m_1 \rightarrow 0$ ($\Rightarrow m \rightarrow m_2$).

G. Summary of matching results

The final output of the matching is a set of expressions for the tidal fields, which are given explicitly in Eqs. (B1);

a relation between the mass parameters M and m_1 , which we found to be equal [up to uncontrolled remainders of $O(v^4)$]; and the coordinate transformation necessary to

place the inner zone metric in the same coordinate system as the near zone metric to the order we matched. To obtain the full coordinate transformation, we start from Eq. (5.1) and insert the various pieces we have read off or chosen. We shall take anything we were unable to fix by matching to be zero—here this will be C_0 (to all orders), along with $(F_{\alpha\beta})_j$ and $(C_k)_j$ for $j \in \{4, 5\}$. With the results of our matching, this means that we have $C_\alpha = 0$ (to all orders). We took the zeroth-order piece of the coordinate transformation to simply be the expected translation of the origin from the binary’s center-of-mass to hole 1, so

$$(X_\alpha)_0 = \tilde{x}_\alpha := x_\alpha - (m_2/m)b\hat{x}_\alpha. \quad (5.38)$$

With $(C_\alpha)_1 = 0$, we also have

$$(X_\alpha)_1 = (F_{\beta\alpha})_1 \tilde{x}^\beta, \quad (5.39)$$

where

$$(F_{\alpha\beta})_1 = 2\sqrt{\frac{m_2}{m}}\hat{t}_{[\alpha}\hat{y}_{\beta]}. \quad (5.40)$$

Continuing onward, $(X_\alpha)_2$ is given by Eq. (5.18), where $(F_{\alpha\beta})_2 = 0$ and $(C_\alpha)_2 = 0$; $(X_\alpha)_3$ comes from Eq. (5.28), where

$$(F_{\alpha\beta})_3 = \mathcal{M}(0, 5, 3, 1)\hat{t}_{[\alpha}\hat{y}_{\beta]}, \quad (5.41)$$

and $(C_\alpha)_3 = 0$. [$\mathcal{M}(A, B, C, D)$ is defined in Eq. (5.37).] Similarly, $(X_\alpha)_4$ can be obtained from Eq. (5.33), and we take $(F_{\alpha\beta})_4 = 0$ and $(C_\alpha)_4 = 0$. Finally, $(X_\alpha)_5$ is given in Eq. (5.35); again, we set $(F_{\alpha\beta})_5 = 0$ and $(C_\alpha)_5 = 0$.

Looking back over this coordinate transformation, it is possible to gain some physical intuition about what it is accomplishing: The expected Lorentz boost due to the holes’ orbital motion is present (through third order, which is the highest order at which we have fixed all the coordinate transformation, up to a possible temporal shift). We also have the lowest-order piece of the transformation between Cook-Scheel and harmonic PN coordinates for an unperturbed Schwarzschild black hole. [This is given by the first term in $(\mathcal{A}_t)_4$ in Eq. (5.34).] The remainder of the coordinate transformation is probably mostly concerned with effecting the transformation from locally inertial coordinates centered on the black hole to PN barycentric coordinates. In addition, as we noted previously, the polynomial and nonpolynomial parts of the full coordinate transformation are related to the individual holes in the expected manner: The nonpolynomial parts are associated with hole 1 and vanish in the limit $m_1 \rightarrow 0$. The polynomial pieces are associated with hole 2—indeed, everything except for the piece of the background Cook-Scheel-to-PN-harmonic transformation vanishes in the limit $m_2 \rightarrow 0$.

VI. FAR ZONE METRIC

The direct integration of the relaxed Einstein equations (DIRE) approach [60, 61] can be used to compute the full

4-metric $g_{\alpha\beta}$ (in harmonic coordinates) in both the near and far zones. The resulting far zone metric is expressed in terms of derivatives of multipole moments obtained by integrating the “effective” stress-energy pseudotensor over the near zone. One also obtains nonlinear contributions from integrating over the far zone (known as the *outer integral* in the DIRE approach), though only two of the resulting terms appear in the metric perturbation $h^{\alpha\beta}$ [defined in Eq. (2.2) of [60]] to the order we are considering.

In this formalism, the metric perturbation in the far zone can be expressed in terms of the source multipoles \mathcal{I}^Q and \mathcal{J}^Q via [Eqs. (5.12) in [60]]⁷

$$h^{00} = 4\frac{\mathcal{I}}{r} + 2\partial_{kl}\left[\frac{\mathcal{I}^{kl}(u)}{r}\right] - \frac{2}{3}\partial_{klm}\left[\frac{\mathcal{I}^{klm}(u)}{r}\right] + 7\frac{\mathcal{I}^2}{r^2} + O(v^6), \quad (6.1a)$$

$$h^{0k} = -2\partial_l\left[\frac{\dot{\mathcal{I}}^{kl}(u)}{r}\right] + 2\epsilon^{lkp}\frac{n^l\mathcal{J}^p}{r^2} + \frac{2}{3}\partial_{lp}\left[\frac{\dot{\mathcal{I}}^{klp}(u)}{r}\right] + \frac{4}{3}\epsilon^{lkp}\partial_{ls}\left[\frac{\mathcal{J}^{ps}(u)}{r}\right] + O(v^6), \quad (6.1b)$$

$$h^{kl} = 2\frac{\ddot{\mathcal{I}}^{kl}(u)}{r} - \frac{2}{3}\partial_p\left[\frac{\ddot{\mathcal{I}}^{klp}(u)}{r}\right] - \frac{8}{3}\epsilon^{ps(k)}\partial_s\left[\frac{\dot{\mathcal{J}}^{p(l)}(u)}{r}\right] + \frac{\mathcal{I}^2}{r^2}\hat{n}^k\hat{n}^l + O(v^6). \quad (6.1c)$$

Here $r := \|\vec{x}\|$ is the distance from the binary’s center-of-mass to the field point and $\hat{n}^k := x^k/r$ is its associated unit vector. The $(\mathcal{I}/r)^2$ terms are the two contributions from the outer integrals mentioned previously. We have included all the terms Pati and Will give, even though some of the ones in the purely temporal and spatial components only contribute terms that are of a higher order than we need here. We do this for completeness and also because we shall need these higher-order terms when we construct the extension to this data set (in Appendix C).

The source multipoles \mathcal{I}^Q and \mathcal{J}^Q (Q is a multi-index) are defined in Eqs. (4.5) of [60]. With these definitions, the mass monopole \mathcal{I} is simply (a PN corrected version of) the total mass of the system, the dipole moment \mathcal{I}^k is the center of mass vector (so it vanishes in our coordinate system), and the current dipole \mathcal{J}^k is the total angular momentum. One can show that these three quantities are conserved up to radiative losses.

⁷ We have corrected a sign error in Pati and Will’s expression for h^{kl} : They give coefficients of $+2/3$ and $+8/3$ for the second and third terms. The correct signs can be obtained from Pati and Will’s Eqs. (2.13) and (4.7b) in [60].

The source multipoles can be expanded in the PN approximation to find

$$\mathcal{I} = m_1 \left(1 + \frac{1}{2}v_1^2 - \frac{m_2}{2b} \right) + (1 \leftrightarrow 2) + O(bv^4), \quad (6.2a)$$

$$\mathcal{J}^k = \epsilon^{klp} m_1 x_1^l v_1^p + (1 \leftrightarrow 2) + O(b^2 v^3), \quad (6.2b)$$

$$\mathcal{I}^{kl} = m_1 x_1^{kl} \left(1 + \frac{1}{2}v_1^2 - \frac{m_2}{2b} \right) + \frac{7}{4} m_1 m_2 b \delta^{kl} + (1 \leftrightarrow 2) + O(b^3 v^4), \quad (6.2c)$$

$$\mathcal{J}^{kl} = \epsilon^{kps} m_1 v_1^s x_1^{pl} + (1 \leftrightarrow 2) + O(b^3 v^3), \quad (6.2d)$$

$$\mathcal{I}^{klp} = m_1 x_1^{klp} + (1 \leftrightarrow 2) + O(b^4 v^2). \quad (6.2e)$$

The first two come from Will and Wiseman's Eqs. (4.16) [71], and the remainder from Pati and Will's Eq. (D1) [61]. (Even though we only need the lowest-order piece of \mathcal{I}^{kl} here, we include the 1PN corrections that Pati and Will give since we will need them in our construction of the higher-order extension in Appendix C.) Here the notation is mostly the same as for the near zone metric and was defined in Sec. IV. One new definition is $x_1^{kl} := x_1^k x_1^l$ (with similar definitions holding for different vectors, as well as larger collections of indices).

Even though this structure is somewhat obscured in the expression Pati and Will give for it, the far zone PN expansion of the metric perturbation is clearly a bivariate expansion. There is a post-Minkowskian expansion in powers of G , given by radiative multipole moments, and a post-Newtonian expansion in v (or, more formally, $1/c$) of these radiative multipole moments in terms of source moments computed in the near zone (see, e.g., [62]). Although formally the near and far zone expansions are independent, in practice there is a relation between their expansion parameters. This is given by the definition of the far zone, $r \gtrsim \lambda = b/2v$, from which one finds that

$$\frac{b}{r} \lesssim 2v. \quad (6.3)$$

As explained in Sec. IV C of [60], formal consistency requires that we treat each *additional* inverse power of r as raising the effective order by *at least* one factor of v . [This order counting is also equivalent to the order counting Alvi [41] uses in computing the far zone metric, though he keeps terms through $O(v^5)$ in all components.] For example, with this far zone order counting

$$\begin{aligned} \frac{\mathcal{I}}{r} &\propto \frac{m}{r} = O(v^2), \\ \mathcal{I}^{kl} \partial_{kl} r^{-1} &\propto \frac{m}{r} \frac{x_1^2}{r^2} = O(v^4), \\ \mathcal{I}^{klp} \partial_{klp} r^{-1} &\propto \frac{m}{r} \frac{x_1^3}{r^3} = O(v^5), \end{aligned} \quad (6.4)$$

since m/r comes with a factor of G due to the post-Minkowskian expansion while x_1/r does not. This also means that we treat the $(\mathcal{I}/r)^2 \propto (m/r)^2$ term as $O(v^4)$, not $O(v^5)$.

With this order counting in mind, we now determine the order of each source multipole moment. This leads to the following orders for the components of the metric perturbation in the far zone: $h^{00} = O(v^2)$, $h^{0k} = O(v^4)$, and $h^{kl} = O(v^4)$. Note that this is not the standard order counting of the metric perturbation in the near zone, since there we have $b/r = O(v^0)$, which thus leads to $h^{00} = O(v^2)$, $h^{0k} = O(v^3)$, and $h^{kl} = O(v^4)$. The far zone order counting allows us to expand the full 4-metric in the far zone to obtain [from Eqs. (4.2) in [60]]

$$g_{00} = - \left[1 - \frac{1}{2}h^{00} + \frac{3}{8}(h^{00})^2 \right] + \frac{1}{2}h^{kk}, \quad (6.5a)$$

$$g_{0k} = - \left[1 - \frac{1}{2}h^{00} \right] h^{0k}, \quad (6.5b)$$

$$g_{kl} = \left[1 + \frac{1}{2}h^{00} - \frac{1}{8}(h^{00})^2 - \frac{1}{2}h^{pp} \right] \delta^{kl} + h^{kl}, \quad (6.5c)$$

with remainders of $O(v^6)$. Here we have kept the $-(1/2)h^{00}$ term in the expression for g_{0k} for formal consistency. It only gives terms of $O(v^6)$ with our order counting (which we neglect here), but would give terms of $O(v^5)$ if we had used the standard near zone order counting, where $h^{0k} = O(v^3)$. This is the only $O(v^6)$ term in the expression for g_{0k} , so the uncontrolled remainder in that expression is thus actually $O(v^7)$.

We can now easily compute the full metric by carrying out all the differentiation in the expression for the metric perturbation, Eqs. (6.1a). In doing this, it is important to realize that the multipoles depend on retarded time, which must be carefully accounted for when differentiating. Eqs. (6.5) then give the full metric. In performing this calculation, we assume a (quasi)circular orbit, so the acceleration and the trajectories are parallel or antiparallel to each other and the velocity is perpendicular to either of them to $O(v^5)$. We thus have $\vec{x}_1 \cdot \vec{v}_1 = O(v^5) = \vec{a}_1 \cdot \vec{v}_1$ and $\vec{a}_A = -\omega^2 \vec{x}_A + O(v^5)$, where $a_A^k := \dot{v}_A^k$ is the acceleration of point particle A . [The latter leads to expressions such as $(\vec{v}_1 \cdot \vec{j}_1) = -\omega^2 v_1^2 + O(v^5)$, where $j_A^k := \dot{a}_A^k$ is the jerk of point particle A .] After much algebra, we finally obtain the full metric in the far zone:

$$g_{00} + 1 = \frac{2m_1}{r} + \frac{m_1}{r} \left\{ v_1^2 - \frac{m_2}{b} + 2(\vec{v}_1 \cdot \hat{n})^2 - \frac{2m}{r} + 6 \frac{(\vec{x}_1 \cdot \hat{n})}{r} (\vec{v}_1 \cdot \hat{n}) - \frac{x_1^2}{r^2} + \frac{(\vec{x}_1 \cdot \hat{n})^2}{r^2} (3 - 2r^2 \omega^2) \right\} \quad (6.6a)$$

$$+ (1 \leftrightarrow 2) + O(v^5),$$

$$g_{0k} = -\frac{m_1}{r} \left\{ 4(\vec{v}_1 \cdot \hat{n}) + 4(\vec{v}_1 \cdot \hat{n})^2 - 6(\vec{x}_1 \cdot \hat{n})^2 \omega^2 + 4 \frac{(\vec{x}_1 \cdot \hat{n})}{r} + 12 \frac{(\vec{x}_1 \cdot \hat{n})}{r} (\vec{v}_1 \cdot \hat{n}) - 2 \frac{x_1^2}{r^2} + 6 \frac{(\vec{x}_1 \cdot \hat{n})^2}{r^2} \right\} v_1^k$$

$$+ \frac{m_1}{r} \left\{ 4(\vec{x}_1 \cdot \hat{n}) + 8(\vec{x}_1 \cdot \hat{n})(\vec{v}_1 \cdot \hat{n}) - 2 \frac{x_1^2}{r} + 6 \frac{(\vec{x}_1 \cdot \hat{n})^2}{r} \right\} \omega^2 x_1^k + (1 \leftrightarrow 2) + O(v^6), \quad (6.6b)$$

$$g_{kl} - \delta_{kl} = \frac{2m_1}{r} \delta_{kl} + \frac{m_1}{r} \left\{ \left[v_1^2 - \frac{m_2}{b} + 2(\vec{v}_1 \cdot \hat{n})^2 + \frac{m}{r} + 6 \frac{(\vec{x}_1 \cdot \hat{n})}{r} (\vec{v}_1 \cdot \hat{n}) - \frac{x_1^2}{r^2} + \frac{(\vec{x}_1 \cdot \hat{n})^2}{r^2} (3 - 2\omega^2 r^2) \right] \delta_{kl} \right.$$

$$\left. + \frac{m}{r} \hat{n}^{kl} + 4v_1^{kl} - 4\omega^2 x_1^{kl} \right\} + (1 \leftrightarrow 2) + O(v^5), \quad (6.6c)$$

where everything is evaluated at the retarded time $u := t - r$. [This expression agrees with Alvi's result, given in his Eq. (2.17) [41], though he also includes the $O(v^5)$ terms in the purely temporal and spatial components. We include these pieces—as well as even higher-order ones—when we construct the extension to the data in Sec. VII and have checked that we agree with Alvi about all the $O(v^5)$ terms.]

A. Evolution of the binary's phase and separation

Even though the effects of radiation reaction on the binary's orbital separation and phase are formally small, only beginning at $O(v^5)$, they produce large corrections to the far zone metric when one is far away from the binary, since the retarded time at which one is evaluating the binary's parameters becomes large. For instance, even as close as $r = 50m$, which is inside the outermost extraction radius (usually well inside) for all the simulations used in the Samurai project [12], the phase difference between a circular orbit [using the 3PN expression for ω given in Eq. (190) of [62]] and 3.5PN inspiral (the computation of which is detailed below) is ~ 0.015 radians for an equal-mass binary with a separation of $10m$. (This phase difference should be compared with the averaged frequency domain phase accuracy required for parameter estimation with Advanced LIGO, viz., 0.007 radians, from [10]. While such a comparison is not really warranted—see [15] for some discussion—it gives a rough idea of the required accuracy.) See Sec. IV A in Kelly *et al.* [43] for further discussion of the necessity of using formally higher-order PN results in obtaining the far zone metric.

We thus use the most accurate (3.5PN) expression for the inspiral, as given by Blanchet [62], who obtains it from an energy balance argument. The phase itself is given by Blanchet's Eq. (234) [62], where it is expressed in terms of the dimensionless time variable Θ , defined in

his Eq. (232) [62]. Since we are evaluating everything at the retarded time u , we have $\Theta = (\eta/5m)(t_c - u)$. Here the “coalescence time” t_c is defined as the time at which the binary's frequency goes to infinity (or, equivalently, its separation goes to zero). One can calculate this in the PN approximation by using the energy balance relation $dE/dt = -\mathcal{L}$, where E and \mathcal{L} are the binary's energy and gravitational wave luminosity, respectively. These are given in terms of $\gamma := m/b$ though 3.5PN in Blanchet's Eqs. (191) and (230) [62], respectively. We can then compute t_c by integrating $dt/db = (dE/db)(dt/dE) = -(dE/db)/\mathcal{L}$ from $b = 0$ to $b = b_0$ (where b_0 is the binary's separation at $t = 0$). Here we expand the quotient as a power series (to 3.5PN) rather than using a Padé approximant (or performing any resummation of the energy or luminosity), as is sometimes done in the literature (see, e.g., [92]).

With the 3.5PN expression for t_c in hand, we can simply substitute it into Blanchet's Eq. (234) [62] to obtain the phase as a function of u , making sure to expand to 3.5PN order after substituting. We add a constant to the phase so that it is zero when $t = 0$, to be consistent with our choice of initial phase in the matching (i.e., so the holes initially lie on the x -axis, with our expression for the orbit). We also take the freely specifiable gauge constant r'_0 and constant of integration Θ_0 to be m and 1, respectively. (The dependence of ω on u is then obtained by differentiating the phase with respect to time.) To obtain the retarded time dependence of b , we use $b = m/\gamma$, along with the expressions for γ in terms of x [Blanchet's Eq. (193) [62]] and x in terms of Θ [Blanchet's Eq. (233) [62]], expanding the quotient consistently to 3.5PN. (We take the appearance of b in a logarithm in the expression for γ to consist only of b 's lowest-order dependence on Θ , viz., $4m\Theta^{1/4}$.) N.B.: The final expansions of the expressions for ϕ and b are important. If they are not performed, then one does not recover the expected values for b and ω at $u = 0$ [viz., b_0 and ω_0 , respectively—here ω_0 is the binary's 3PN angular veloc-

ity for $b = b_0$ obtained from Blanchet's Eq. (190) [62]. We do not display the resulting expressions, as they are quite lengthy, and best handled entirely within a computer algebra system. (We have carried out the calculations in MAPLE and our scripts are available at [36].) Our results can be seen graphically in Fig. 4, where we plot the past history of an equal-mass binary's separation (starting from $b_0 = 10m$) along with the fractional deviations of its phase from $\omega_0 u$.

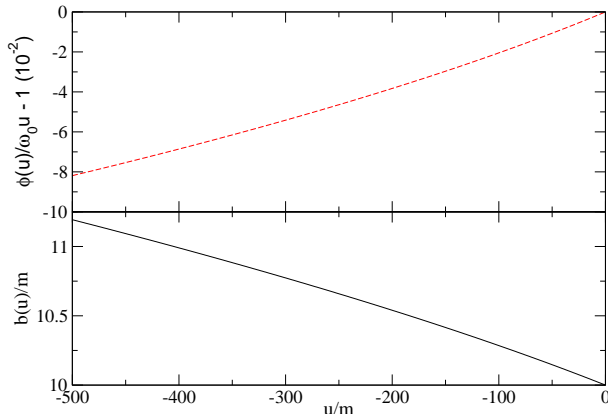


FIG. 4: The 3.5PN results for the past history of an equal-mass binary's separation, starting from $10m$ at $u = 0$, along with the fractional deviations of its phase from $\omega_0 u$.

Since we are effectively using higher-order equations of motion, due to the higher-order phasing relations, we would have liked to include higher-order terms in the relative-to-center-of-mass (relative-to-COM) variable relation as well, for consistency. However, the resulting expressions for the far zone metric components are algebraically too complex for MAPLE to handle, so we had to forego including these terms. If one expands the contribution of the relative-to-center-of-mass relation to the (far or near zone) metric components consistently, then, to the order we have considered, all that one needs is the lowest-order Newtonian version of this relation, given in Eq. (4.3), and this is all we have used in the far zone metric. Fortunately, unlike the secular radiation reaction effects in the binary's phase and separation considered above, the neglected PN corrections to the relative-to-COM relation are numerically small in addition to being formally small: They first enter the metric at $O(v^8)$ (in the purely temporal component). Moreover, maximizing over mass ratio (all the PN corrections to the relative-to-COM relation vanish for an equal-mass binary), the magnitude of the largest of these is $\sim 5 \times 10^{-7}$ at the inner edges of the near-to-far buffer zone for a separation of $b = 10m$; for comparison, the uncorrected $(m_1/r)v_1^2 + (1 \leftrightarrow 2)$ term is $\sim 10^{-4}$ in this situation.

We were able to include these additional terms in the relative-to-center-of-mass relation in the near zone metric: For consistency, we include the same higher-order terms in the phasing and separation in the near zone metric as in the far zone metric, so it makes sense to

attempt to include the higher-order relative-to-COM relation there, even though we were unable to do so in the far zone metric. In fact, these corrections contribute to the near zone metric at one order lower than to the far zone metric [viz., $O(v^7)$ in the spatiotemporal components] and are numerically quite a bit larger: Maximizing over mass ratio, the magnitude of the largest of these corrections is $\sim 2 \times 10^{-3}$ at the inner edge of the inner-to-near buffer zone for a separation of $10m$; for comparison, the magnitude of the uncorrected $-4(m_1/r_1)v_1^k$ piece is ~ 0.2 in this situation.

Blanchet and Iyer give these corrections through 3PN in Eqs. (3.11)–(3.14) of [93]. We have specialized their result to a circular orbit by using the 2PN expression for ω to express v in terms of m , b , and η . Blanchet gives this relation specialized to a circular orbit through 2.5PN in Eq. (187) of [62], so we shall just quote the 3PN contribution to \vec{x}_A here:

$$\vec{x}_A^{3\text{PN}} = -\eta \frac{(m_1 - m_2)m^2}{b^3} \left[\frac{7211}{1260} + \eta - \frac{22}{3} \log \left(\frac{b}{r_0''} \right) \right] \vec{b}. \quad (6.7)$$

In this expression, r_0'' is another freely specifiable gauge constant which, though *a priori* different from r_0' , we shall take to have the same value, viz., m . [This is equivalent to taking the related gauge constants r_1' and r_2' to both be m —see Eqs. (3.15) and (3.19) in [93].] The expression for the binary's separation vector that we substitute into the resulting relative-to-center-of-mass relation to obtain the trajectories of the point particles is $\vec{b} = b(\hat{x} \cos \phi + \hat{y} \sin \phi)$, where b and ϕ are functions of t (in the near zone) or u (in the far zone).

VII. INCLUDING HIGHER-ORDER TERMS

Here we construct an extension to our data using various readily available higher-order terms. This extension includes all the $O(v^5)$ terms in the near and far zones, but also includes even higher-order terms that do not improve the data's formal accuracy. [We have to change our far zone order counting somewhat to be able to claim that we have all the $O(v^6)$ pieces of the spatiotemporal components of the far zone metric; these components are necessary to obtain initial data valid through $O(v^5)$.] The general philosophy is that adding higher-order terms can often improve the quality of the data in practice, even if it does not improve their formal accuracy. As we have seen in the previous section, this is particularly true in the far zone, where the binary's phase evolution depends sensitively on the inclusion of quite high-order radiation reaction terms.

There are also more specific reasons for including certain of these terms: We would like for a putative evolution of our data to be able to be compared directly with Kelly *et al.*'s evolution of their data [57]. (Such a comparison will give an indication of how much of the junk radiation is due to the failure of the initial data to

Zone	Attribute	Versions			
		04_No0ct	04	05	all
Inner	Time dependence	Perturbative	Perturbative	Full	Full
	Fourth order octupoles	No	Yes	Yes	Yes
Near	Metric order	$O(v^4)$	$O(v^4)$	$O(v^5)$	Full extended
Far					

TABLE II: An overview of the contents of the various data sets we considered.

include the correct tidal deformations.) Kelly *et al.* include the $O(v^5)$ pieces of the spatial metric in the near zone [though not the matching $O(v^6)$ pieces of the extrinsic curvature]. The extension we have constructed includes these terms, as well. It also includes (as noted above) the $O(v^5)$ terms in the far zone, along with the $O(v^6)$ terms in the extrinsic curvature in the near and far zones, so the extended data are valid through $O(v^5)$ in those zones. However, we have coded our data in such a way that one can easily produce a data set that only includes the pieces that Kelly *et al.* have, or some other subset of the pieces in the extension.

We would have liked to have included the $O(v^5)$ terms in the inner zone as well, for completeness, but it is not possible to obtain initial data in that zone that is formally $O(v^5)$ while still including the quadrupole pieces: We would need the $O(v^6)$ pieces of (the spatiotemporal components of) the inner zone metric. The quadrupole parts of these include hexadecapole tidal fields, and knowledge of how those fields enter the inner zone metric would require nonlinear black hole perturbation theory. However, we *are* able to calculate the polynomial parts of the fourth order octupole pieces—the results are presented in Appendix B2—and include them in the extension. (These pieces include the 1PN correction to the electric octupole tidal field.)

Moreover, we are also able to include the full time dependence of the tidal fields: See Appendix B2. It seems desirable to include these terms, since some of them are necessary for obtaining the pieces of the extrinsic curvature that describe how the tidal fields evolve: We already have the necessary, linear-in- t pieces for the lowest-order quadrupole fields, but not for their 1PN corrections, the explicit appearance of their time derivatives, or any of the octupole fields. As is discussed more fully in Appendix D, the additional time dependence we include in the tidal fields is only the lowest-order dependence on t alone, not the additional space-dependence that comes from the tidal fields' dependence on the Eddington-Finkelstein coordinate: The neglected dependence would generate contributions to the metric that combine with the unknown contributions from time derivatives of the tidal fields, while the t -dependent contributions are not entangled in this manner. We use t instead of T since the full time dependence of the tidal fields comes, in effect, from performing the matching at different (near zone coordinate) times t . We thus want these higher-order contributions to the tidal fields to depend on that time, instead of T (the inner zone time coordinate).

We have *not* attempted to obtain the full time dependence of the coordinate transformation, since this is a rather more involved task than obtaining that of the tidal fields. Moreover, our rationale for including the tidal fields' full time dependence was to improve the evolution of the tidal perturbations: Including the full time dependence of the coordinate transformation would only improve the agreement of the inner and near zone metrics in the buffer zone, while the largest effect of the tidal perturbations (e.g., in reducing the high-frequency junk radiation) presumably comes from closer to the horizons.

The other higher-order pieces we have added are all in the purely temporal components of the near and far zone metrics. We have included these since Blanchet, Faye, and Ponsot [58] give an explicit expression for the purely temporal component of the near zone metric through $O(v^7)$ and it is easy enough to calculate the matching terms in the far zone. The specifics of where we obtained all the extra terms are given in Appendix C, along with the accompanying caveats and new order counting in the far zone. We refer to these “state-of-the-art” versions of the near and far zone metrics as the full extended versions.

We have considered the effects of these additional terms on how well the metrics stitch together by putting together four versions of the data, as shown in Table II. While the versions in the table are given the labels we use for the corresponding MAPLE scripts and C code (available at [36]), we shall usually refer to them by the order of their near and far zone metrics [i.e., as $O(v^4)$, $O(v^5)$, and full extended]. This will not cause confusion, since we will almost always consider just the right-most three. While the 04_No0ct version is important, since it contains only the pieces that can be included consistently in the matching (except for the higher-order terms necessary to obtain the phasing in the far zone accurately and the analogous terms in the near zone), we only consider it in Fig. 21. Thus, when we refer to the $O(v^4)$ version without any qualifiers, we mean 04, the version including the fourth order octupole pieces. See Appendix D for the specific details of how all these metrics are calculated. (N.B.: The near zone metrics in all of these versions contain the background resummation detailed in Sec. VIII A.)

In the next section, we compare the extended data with their lower-order counterparts: The volume elements of the $O(v^4)$, $O(v^5)$, and full extended sets of data are compared in the near zone in Figs. 5 and 6 and in the far zone in Figs. 7 and 8. Their constraint violations are

compared in Figs. 17, 18, and 19. We compare the constraint violations of the different versions of the inner zone metric in Figs. 20 and 21. In general, the additional terms reduce the constraint violations and improve the overall matching, or at least do not affect them adversely. The only exception to this is the addition of the full time dependence in the inner zone, which increases the constraint violations in the inner zone. However, it does not increase them by much, and they were originally quite small: Our philosophy is thus to include these terms, which we think will improve the data's evolution, even at the cost of slightly higher constraint violations.

VIII. NUMERICAL CONSIDERATIONS

To get an idea of how well the matching is working numerically, we plot the volume elements of the various 4-metrics in the vicinity of their buffer zones. (In all these plots, we use the full extended version of the data discussed in the previous section, unless otherwise noted.) Of course, we first transform the inner zone metric using the coordinate transformation obtained from the algebraic matching above. To obtain a simple, easily interpreted plot, we choose the test system $b = 10m$, $m_1 = m_2$ (the mass is in arbitrary units) and restrict our attention to the $t = 0$ timeslice and the x -axis (i.e., we consider the spatial slice along the separation between the holes), concentrating on the portion near hole 1. (We expect this slice to provide the most stringent test of the matching, since it contains the portions of the buffer zones where the field is strongest and changes most rapidly.) We shall use this setup (or slight modifications thereof) for all of our later examples. The matching in the inner-to-near transition is shown in Figs. 5 and 6 (along with a comparison of different near zone volume elements). The first of these shows the volume elements themselves [along with the differences between the volume elements of the $O(v^4)$ and $O(v^5)$ versions of the near zone metric] and the second shows the differences between the volume elements of the various near zone metrics (along with the merged metric) and the inner zone metric. The volume elements in the near-to-far transition are shown in Fig. 7 (along with the volume element of the merged metric).

The inner zone metric we display here contains the fourth-order octupole pieces discussed in Appendix B 2. To avoid clutter, we did not plot the “plain” version without these additional pieces: It agrees very closely with the version we have plotted near and inside the horizon, but bends away from the near zone metric further away from the hole. The differences between the versions of the inner zone with full and perturbative time dependence would not appear in this plot, since we are looking at the $t = 0$ timeslice. We display the differences between the $O(v^4)$, $O(v^5)$, and full extended far zone metrics in Fig. 8, considering a binary with mass ratio 3 : 1 so that these differences are more pronounced. [In this plot, we have concentrated on the portion of the x -axis to the right of

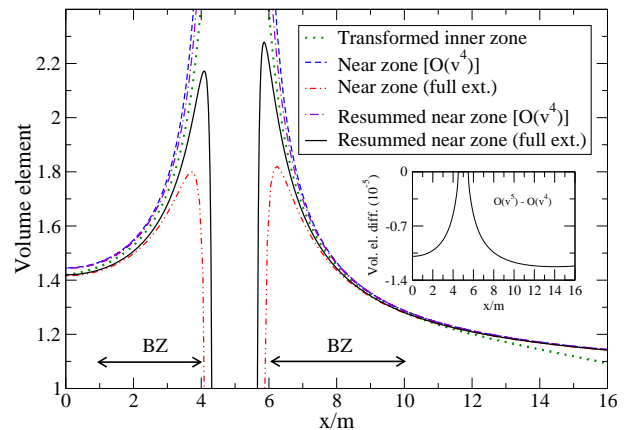


FIG. 5: The volume elements of the transformed inner zone metric (dotted line) along with those of the $O(v^4)$ and extended versions of the near zone metric. These are plotted both with [$O(v^4)$: dot-dashed line; extended: solid line] and without [$O(v^4)$: dashed line; extended: dot-dot-dashed line] background resummation. We have also displayed the differences between the volume elements of the $O(v^4)$ and $O(v^5)$ resummed metrics in the inset. We calculated all of these volume elements for our equal-mass test system and have plotted them along the x -axis near hole 1. (The associated point particle is at $x/m = 5$.) We have indicated the rough locations of the intersection of the x -axis with hole 1's inner-to-near buffer zone (BZ) using double-headed arrows.

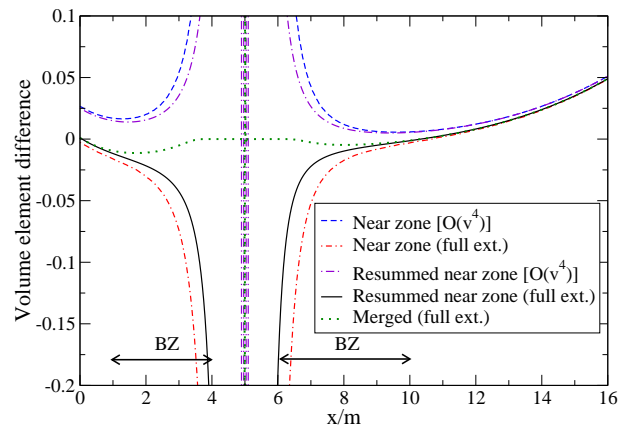


FIG. 6: The differences between the volume elements of various metrics with that of the full extended inner zone metric. The various metrics considered are the near zone metrics plotted in Fig. 5 (using the same colors and line styles as in that figure) as well as the merged metric constructed in Sec. VIII B. We have indicated the rough locations of the intersection of the x -axis with hole 1's inner-to-near buffer zone (BZ) using double-headed arrows.

the more massive hole, for clarity: The relations between the various metrics are qualitatively the same to the left of the less massive hole, except for differences in relative amplitude.]

In the near zone metric, the extension adds certain terms that become large when evaluated close to the holes

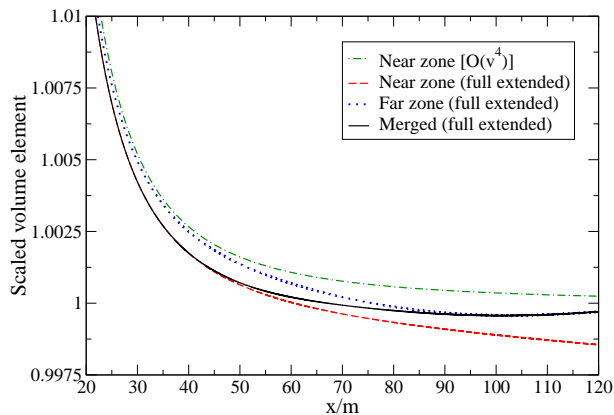


FIG. 7: The scaled volume elements of the (resummed) near zone [both $O(v^4)$ and extended], far zone, and merged metrics. These are calculated for our equal-mass test system and plotted along the x -axis in the portion of the near-to-far transition region that lies to the right of hole 1. To obtain a less crowded plot, we have scaled these by the contribution to the volume element of the lowest-order nontrivial pieces of the far zone metric, viz., $(1 + 2m/r)\sqrt{1 - 4m^2/r^2}$. The buffer zone is roughly the region in which we transition, which, in turn, is roughly the region plotted.

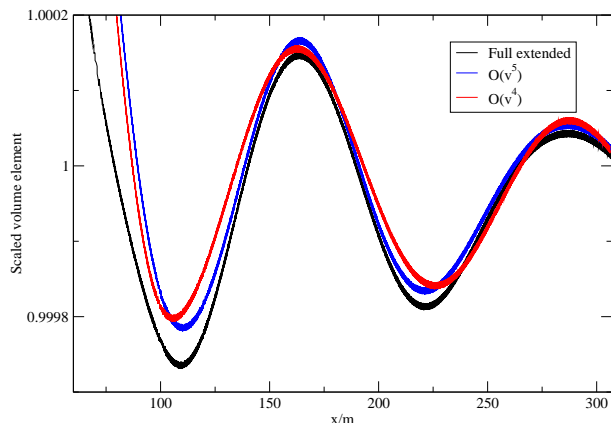


FIG. 8: The scaled volume element of the far zone metric for a binary with a separation of $10m$ and a mass ratio of $3 : 1$ along the x -axis to the right of hole 1 (the more massive hole). We display this for the extended data (the darkest curve—black in color) as well as the $O(v^5)$ and $O(v^4)$ versions of the data (the medium and lightest curves—blue and red in color, respectively) to illustrate their differences. (We considered an unequal mass binary to make these differences more pronounced.) As before, we have scaled these volume elements by the contribution from the lowest-order nontrivial piece of the metric, viz., $(1 + 2m/r)\sqrt{1 - 4m^2/r^2}$.

(e.g., $4m_1^2 m_2 / r_1^3$ in g_{00} , which equals $1/2$ at $r_1 = m$ for our test system) and others that grow rapidly as one moves away from the holes (e.g., $-m_1^2 m_2 r_1^3 / 4b^6$, also in g_{00} , which is about -0.03 at $r_1 = 100m$ for our test system). The terms that become large near the holes cause the $t = 0$ timeslice of the near zone metric to no longer be spacelike in a region that extends outside the

horizon. This can be seen in the rapid decrease of the volume element around the hole in Fig. 5. (Even though we do not display this in the plot, the volume element in fact decreases to zero.) However, for this separation, the timeslice is still spacelike in the buffer zone, so its bad behavior closer to the holes does not cause any problems in the merged metric.

N.B.: The unperturbed horizon is $m_1[1 - m_2/b + O(m_2^2/b^2)]$ away from the point particle associated with hole 1 in the new coordinates. For the test system, the correction is small, so hole 1's unperturbed horizon intersects the x -axis at $\sim 4.5m$ and $\sim 5.5m$ in the new coordinates. There are also corrections due to the tidal distortion, but for the test system these are even smaller than those due to the new coordinates: Taylor and Poisson [73] study the effect of the tidal distortion on the horizon (in their Sec. VIII) and find the expected quadrupolar deformation at lowest order.

In the inner-to-near transition, the volume elements generally behave in the expected manner: They differ when considered either too near or too far from the hole and approach each other in the buffer zone. Things look a bit more unusual in the near-to-far transition, since the two volume elements agree better in the region between $20m$ to $30m$ than they do further away from the holes. However, this should not be surprising: The reduced wavelength of the gravitational radiation is $\sim 16m$ for the equal-mass test system, and the difference between the near zone metric's perturbative treatment of retardation and the far zone metric's full treatment should become quite apparent beyond that radial distance. In fact, the oscillations we see in the far zone metric's volume element in Fig. 8 are due to the far zone metric's dependence on retarded time. (Even though the metric contains gravitational radiation, this is not the only source of these oscillations. However, it does contribute to them, as expected.) This plot also illustrates the phase differences between the various versions of data. Additionally, we expect the volume elements of the near and far zone metrics to differ dramatically close to the binary. This is indeed the case (particularly for $r < 10m$), though we did not show this in the plot, preferring instead to concentrate on displaying the details of the volume elements' behavior in the transition region.

A. Background resummation

In the inner-to-near transition, the volume elements do not agree as closely as we might like. In fact, the agreement is *worse* near the hole with the higher-order extended version of the near zone metric than it is with the original $O(v^4)$ version (though the agreement further away from the hole and outside the orbit is slightly better). However, even the agreement with the original version is not much better than that found in Paper II (see its Fig. 2), even though we have matched to higher

order.⁸ Part of the resolution of this apparent problem is that we have not yet used one of the “tricks” from Paper II, namely background resummation.

The idea of background resummation is to add higher-order terms to the near zone metric in order to improve its strong field behavior. If one considers the limit $m_2 \rightarrow 0$ ($\Rightarrow v_1 \rightarrow 0$) of the near zone metric, then one finds that it reduces to the far field asymptotic expansion of the unboosted Schwarzschild metric (with mass parameter m_1) in (PN) harmonic coordinates. This expansion, however, lacks the causal structure of the Schwarzschild metric—it has no horizon.

One method to restore this causal structure is to resum the PN metric. This resummation consists of adding an infinite number of higher-order terms, such that the metric reduces identically to the *full* (not the expanded) unboosted Schwarzschild metric in (PN) harmonic coordinates in the limit $m_2 \rightarrow 0$. *A priori*, there is no reason to suspect that adding such higher-order terms would increase the accuracy of the PN metric. *A posteriori*, however, it is usually the case that such resummed metrics are indeed closer to the exact solution, as was seen in Paper II. Moreover, we should stress that these higher-order terms are not arbitrary, but guided by the physical requirement of restoring the apparent horizons. Such physically informed resummations have met with great success in general relativity, notably in the effective one-body formalism (see, e.g., [94]).

It would also be possible to resum the far zone metric: One can calculate its Newtonian part without making a multipole decomposition by proceeding in the same manner as in the calculation of the Liénard-Wiechert 4-potential in electrodynamics (as given in, e.g., §14.1 in Jackson [95]). However, we have not pursued this line of investigation further. Simone *et al.* [96] performed a related resummation of the Newtonian pieces of the luminosity of an extreme mass-ratio binary, though they did this by first calculating the multipole expansion and then resumming directly, while the resummation of the metric we are suggesting here would involve computing the integral directly, with no multipole expansion of the Newtonian part.

With these points in mind, let us now describe the procedure in detail, exemplifying it using the purely temporal component of the metric. In PN harmonic coordinates, this component of the Schwarzschild metric takes the form $-(R - M)/(R + M)$. Here R is the harmonic radial coordinate and M is the hole’s mass. (As our use of “ R ” indicates, this is the same radial coordinate as in Cook-Scheel harmonic coordinates—see Appendix A for

a comparison of the two coordinate systems.) We expect to have $m_1 \rightarrow M$ and $r_1 \rightarrow R$ as $m_2 \rightarrow 0$, which suggests that the purely temporal component of the PN metric should approach $-(r_1 - m_1)/(r_1 + m_1)$ as $m_2 \rightarrow 0$. The far field asymptotic expansion of this metric component (i.e., for $r_1 \gg m_1$) is given by

$$-1 + \frac{2m_1}{r_1} - \frac{2m_1^2}{r_1^2} + O\left(\left[\frac{m_1}{r_1}\right]^3\right). \quad (8.1)$$

This identically reproduces all the terms in the PN near zone metric in the limit $m_2 \rightarrow 0$. We then resum the PN near zone g_{00} by taking

$$g_{00} - g_{00}^{\text{old}} = -\frac{r_1 - m_1}{r_1 + m_1} - \left(-1 + \frac{2m_1}{r_1} - \frac{2m_1^2}{r_1^2}\right) + (1 \leftrightarrow 2), \quad (8.2)$$

where g_{00}^{old} is the version of this component without resummation, given in Eq. (4.1a).

A similar procedure can be applied to the spatial sector of the metric. Carrying this out, we obtain

$$g_{kl} - g_{kl}^{\text{old}} = \frac{r_1 + m_1}{r_1 - m_1} n_{kl}^{(1)} + \left(1 + \frac{m_1}{r_1}\right)^2 \left[\delta_{kl} - n_{kl}^{(1)}\right] - \left[\left(1 + \frac{2m_1}{r_1} + \frac{m_1^2}{r_1^2}\right) \delta_{kl} + \frac{m_1^2}{r_1^2} n_{kl}^{(1)}\right] + (1 \leftrightarrow 2). \quad (8.3)$$

where $n_{kl}^{(1)} := x_1^{kl}/r_1^2$ and g_{kl}^{old} is given by Eq. (4.1c). One can check that g_{kl} reduces to g_{kl}^{old} identically as $m_2 \rightarrow 0$.

We have used the Schwarzschild metric in PN harmonic coordinates to resum the PN metric here, since it is this background that the PN metric approaches in the $m_2 \rightarrow 0$ limit. We thus cannot resum the spatiotemporal components of the metric, since they already match the background in this limit. If we had first transformed the PN metric to Cook-Scheel coordinates, then we would have been able to resum the background so that it exactly matched that of the inner zone metric. This would have guaranteed a better agreement, and would have probably also given a merged metric with smaller constraint violations, since there would be no coordinate singularity at the horizons in the resummed near zone metric.

However, if we had chosen this route, we would have had to pick some region surrounding the buffer zone for each hole in which to perform this transformation. This would have introduced further complications that we thought it best to avoid in this implementation, even at the possible cost of somewhat poorer matching. Moreover, the background resummation procedure that we have implemented has indeed improved the matching, as can be seen in Fig. 5: The improvement is particularly striking for the extended version of the near zone metric, where the region in which the $t = 0$ slice is no longer spacelike moves closer to the horizon and the graph of

⁸ The figures are not directly comparable, since the one in Paper II plots the xx components of the metrics, not their volume elements. However, the plot of just the xx components of this paper’s inner and near zone metrics displays the same behavior as that of the volume elements, including roughly the same numerical values for the difference between the metrics.

its volume element now crosses that of the near zone in the buffer zone outside of the orbit. But resummation also improves the matching of the original data: The resummed version of the $O(v^4)$ near zone metric agrees more closely with the inner zone metric than does the unresummed version.

B. Transition functions

We now turn to the process of stitching the inner and near zone metrics together numerically. It is necessary to interpolate between the various metrics in *transition regions* (located inside the buffer zones) in order to stitch the metrics together with no discontinuities. A simple way to do this is to use a weighted average of the metrics, where the precise way this average is carried out is determined by a C^∞ transition function $F_{AB} : \mathbb{R}^3 \rightarrow [0, 1]$. This function should have the property that $F_{AB}(\vec{x}) = 0$ if $\vec{x} \in C_A \cap O_{AB}^c$ and $F_{AB}(\vec{x}) = 1$ if $\vec{x} \in C_B \cap O_{AB}^c$. Here O_{AB}^c is the complement of the buffer zone between zones C_A and C_B . (These conditions guarantee that the transition takes place completely inside the buffer region.) If we just consider two metrics, $g_{\alpha\beta}^{(A)}$ and $g_{\alpha\beta}^{(B)}$, for simplicity, then the resulting merged metric is given by $[1 - F_{AB}]g_{\alpha\beta}^{(A)} + F_{AB}g_{\alpha\beta}^{(B)}$. (We have suppressed the position dependence of the transition functions and metrics, for notational convenience.)

In principle, these conditions are all one would impose on possible transition functions. (One might also want to stipulate that F_{AB} be “increasing as one moves from

C_A to C_B ,” where this would have to be interpreted in some appropriate sense.) One could then contemplate minimizing some appropriate norm of the constraint violations of the resulting merged metric (outside, say, the apparent horizons) over all possible transition functions satisfying these requirements [97]. Our approach will be significantly less ambitious, leaving a systematic study of transition functions to later work, probably that accompanying an evolution of the data.

However, as Yunes [35] realized, one can exclude from consideration *a priori* any transition functions that would induce larger (formal) constraint violations in the data than those due to the uncontrolled remainders of the individual metrics. The so-called Frankenstein theorems enunciated in [35] provide sufficient conditions on the transition functions to keep this from occurring: The first Frankenstein theorem tells us that the first and second derivatives of F_{AB} must be $O(\epsilon_A, \epsilon_B)$ and $O(\epsilon_A^0, \epsilon_B^0)$, respectively, if the merged metric is to satisfy the Einstein equations to the same order as the individual metrics. (Here ϵ_A represents the small parameters associated with zone A .) We have constructed our transition functions to respect the conditions of this theorem—we check this explicitly below.

We shall take our transition region and functions to be spherically symmetric, even though the optimal ones would surely be distorted—neither the binary nor the holes are spherically symmetric. Moreover, we shall only consider one particular form for the transition functions, viz., the same form used in Papers I and II:

$$f(r, r_0, w, q, s) := \begin{cases} 0, & r \leq r_0, \\ \frac{1}{2}\{1 + \tanh[(s/\pi)\chi(r, r_0, w) - q^2/\chi(r, r_0, w)]\}, & r_0 < r < r_0 + w, \\ 1, & r \geq r_0 + w, \end{cases} \quad (8.4)$$

where $\chi(r, r_0, w) := \tan[\pi(r - r_0)/2w]$. The full merged metric is thus

$$g_{\alpha\beta} = \{1 - f_{\text{far}}(r)\} \left\{ f_{\text{near}}(x) [f_{\text{inner},1}(r_1)g_{\alpha\beta}^{(3)} + \{1 - f_{\text{inner},1}(r_1)\}g_{\alpha\beta}^{(1)}] \right. \\ \left. + [1 - f_{\text{near}}(x)] [f_{\text{inner},2}(r_2)g_{\alpha\beta}^{(3)} + \{1 - f_{\text{inner},2}(r_2)\}g_{\alpha\beta}^{(2)}] \right\} + f_{\text{far}}(r)g_{\alpha\beta}^{(4)}, \quad (8.5)$$

where $g_{\alpha\beta}^{(A)}$ denotes the metric that lives in zone A (see Fig. 2 for the numbering system) and

$$f_{\text{far}}(r) := f(r, \lambda/5, \lambda, 1, 2.5), \\ f_{\text{near}}(x) := f(x, 2.2m_2 - m_1b/m, b - 2.2m, 1, 2.5), \\ f_{\text{inner},A}(r_A) := f(r_A, 0.256r_A^T, 3.17(m^2b^5)^{1/7}, 0.2, b/m). \quad (8.6)$$

[N.B.: We shall refer to the value of a parameter appearing in a particular transition function by trans-

ferring that transition function’s subscript to the parameter’s name, e.g., $w_{\text{inner},A} := 3.17(m^2b^5)^{1/7}$.] Here $\lambda = \pi\sqrt{b^3/m}$ is the Newtonian wavelength of the binary’s gravitational radiation. We have also used the “transition radius” r_A^T , given by taking the leading orders of the uncontrolled remainders of the approximations in the inner and near zones to be comparable. This gives $(m/b)(r_A^T/b)^4 = (m_A/r_A^T)^3$, and thus $r_A^T = (m_A^3b^5/m)^{1/7}$. With these choices for the parameters, the transition functions satisfy the hypotheses of the first Frankenstein

theorem [35], given above: For instance, the n th spatial derivatives of f_{near} and f_{far} scale as $w_{\text{near}}^{-n} \propto b^{-n} \propto v^{2n}$ and $w_{\text{far}}^{-n} = 1/\lambda^n \propto v^n$, respectively. Matters are a bit more complicated for $f_{\text{inner},A}$: Its spatial derivatives decrease rapidly as $v \rightarrow 0$ because they involve sech with an argument that goes to infinity as $v \rightarrow 0$ (since $s_{\text{inner},A} \propto v^{-2}$) and sech is rapidly decreasing at infinity.

We determined the parameters we use for the transition functions by experimenting with different choices: We found that the values given in Eq. (8.6) produced the smallest overall constraint violations along the x -axis for our equal-mass test system (with $b = 10m$) of all the choices we tried. Except for the near-to-far zone transition, which is completely new, these choices are very similar to those in Paper II. (In fact, despite the way it is written, our f_{near} agrees exactly with its analogue from Paper II, the function G .) The most important difference is the scaling of the transition width, $w_{\text{inner},A}$. Both Papers I and II took $w_{\text{inner},A}$ to scale with r_A^T , so it depends on the system's mass ratio; in particular, it goes to zero as $m_A \rightarrow 0$. (Note that our $f_{\text{inner},A}$ corresponds to F_A in Papers I and II.) We have found that this choice for $w_{\text{inner},A}$ results in large transition-induced constraint violations near the smaller black hole for unequal mass ratios. These constraint violations appear to increase without bound as the mass of the smaller hole goes to zero. This is as one would expect, since the gradient of the transition function blows up as the transition width goes to zero, leading to an unbounded increase in constraint violations—see [35] and the above discussion of the Frankenstein theorems.

We can obtain a better-behaved transition function by freezing the dependence of $w_{\text{inner},A}$ on the mass ratio, as we have done here. (We also have a slightly different coefficient of r_A^T than in Paper II, even for an equal-mass system.) The other differences between our $f_{\text{inner},A}$ and Paper II's F_A are a slightly different coefficient of the transition radius in $r_{0,\text{inner},A}$, in addition to a new transition radius that reflects the higher-order matching that we have performed here. (The transition radius, r_A^T , was slightly misleadingly called the matching radius and referred to as r_A^M in Paper II.)

The choices for the transition functions' parameters determine effective boundaries for the various zones: These are given in Table III for our equal-mass test binary. This table gives both the formal boundaries (i.e., the numerical values of the boundaries given in Sec. II) and the effective boundaries (i.e., the boundaries determined by our choices of parameters for the transition functions). What we call the complete effective boundaries are determined by the entire region in which we use a given metric, even if the coefficient of the metric (due to the transition functions) is very small in a portion of the region. What we refer to as the practical effective boundaries are cut off when the coefficient of the metric becomes smaller in magnitude than 10^{-4} [i.e., much smaller than the magnitude of the uncontrolled remainders, which are $\sim (b/m)^{-5/2} \simeq 3 \times 10^{-3}$].

Zone	Formal boundaries	Effective boundaries	
		Complete	Practical
Inner	$r_A \ll 10m$	$r_A \leq 17.4m$	$r_A \leq 11.2m$
Near	$\left\{ \begin{array}{l} r_A \gg 0.5m, \\ r \lesssim 15.8m \end{array} \right.$	$r_A \geq 0.985m, \quad r \leq 119m$	$r_A \geq 1.27m, \quad r \leq 109m$
Far	$r \gtrsim 15.8m$	$r \geq 19.9m$	$r \geq 30.4m$

TABLE III: The zone boundaries for our equal-mass test binary ($b = 10m$).

The effective inner zone boundaries given in Table III are not quite correct: Since even the practical effective boundaries of the inner zones are greater than half the distance between the holes for $b = 10m$ (as they are for an equal-mass binary, with our choice of transition functions, for $b \lesssim 165m$), one needs to introduce a third transition function, here called f_{near} , to effect the transition between the holes. (See Sec. VI B of Paper I for further discussion; this function is referred to as G in Papers I and II.) With our choice of parameters, f_{near} cuts off the complete effective inner zone when the x -coordinate is closer than $1.1m$ to (the x -coordinate of the point particle associated with) the other hole. The practical effective inner zone is cut off when the x -coordinate is $1.93m$ away from the other hole.)

In f_{far} , one might be concerned that even the practical effective transition region extends well outside of the standard outer boundary of the near zone, viz., $r \simeq \lambda$. Indeed, it is quite possible that blending in the near zone metric in a region where its perturbative treatment of retardation is not warranted will introduce significant phase errors in the binary's outgoing wave train. However, our choice of transition region is justified (at least for this preliminary construction of transition functions) by the (relatively) large constraint violations of the far zone metric at the inner edge of our transition region, as is shown in Fig. 13.

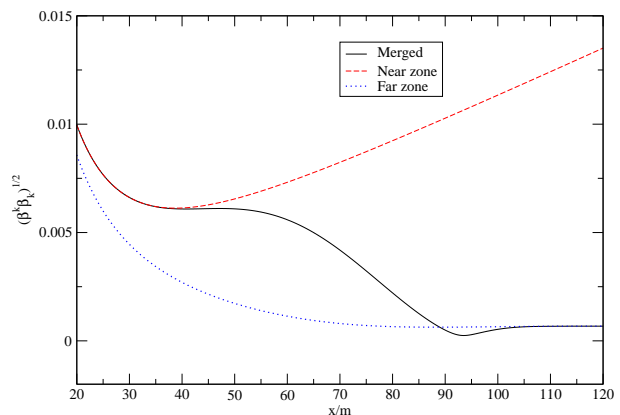


FIG. 9: The norm of the shift ($\sqrt{\beta^k \beta_k}$, with indices lowered by the metric under consideration) of the near zone, far zone, and merged metrics to the right of hole 1 along the axis between the holes. As usual, these are all calculated for our equal-mass test system.

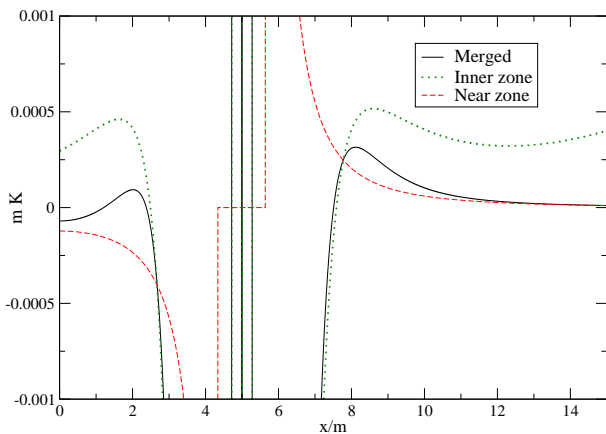


FIG. 10: The trace of the extrinsic curvature of the inner zone, near zone, and merged metrics near hole 1 along the x -axis between the holes. As always, these are all calculated for our equal-mass test system.

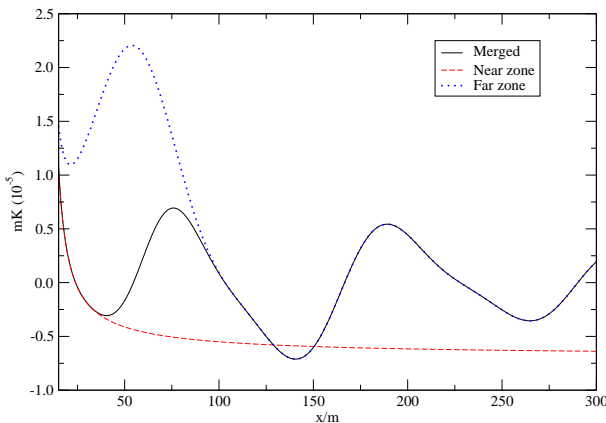


FIG. 11: The trace of the extrinsic curvature of the near zone, far zone, and merged metrics to the right of hole 1 along the x -axis between the holes. As usual, these are all calculated for our equal-mass test system.

To illustrate the matching, we have plotted the volume elements of each zone's metric along with that of the merged metric, all for our standard test system. (Recall that we use the full extended version of the data in all plots unless otherwise noted.) We did this for the inner-to-near zone transition in Fig. 6, plotting the difference between the merged and inner zone metrics' volume elements, for clarity. Similarly, the plot for the near-to-far transition was already given in Fig. 7. We also need to consider the matching of the shift (β^k) separately, since the volume element of the 4-metric equals the lapse times the volume element of the 3-metric [see, e.g., Eq. (E.2.25) in Wald [83]]. We display its norm ($\sqrt{\beta^k \beta_k}$, with indices lowered by the metric under consideration) in the near-to-far transition in Fig. 9. The analogous plot in the inner-to-near transition looks similar enough to that of the volume element (Fig. 6) that we do not include it. For the same reason, we do not show the matching of

the norm of the extrinsic curvature ($\sqrt{K^{lp} K_{lp}}$, with indices raised by the metric under consideration) in either transition region. The trace of the extrinsic curvature, K , behaves differently enough that we plot its matching in Figs. 10 and 11. Moreover, the trace of merged metric's extrinsic curvature is an intrinsically interesting quantity: It tells us how much our data's slicing differs from maximal slicing ($K = 0$).

C. Constraint violations

The constraint violations provide a much more sensitive check on how well the transition functions are working than the previous subsection's plots, in addition to giving a measure of the accuracy of the entire initial data construction. We compare the constraint violations (computed using BAM [98, 99]) of the individual metrics to those of the merged metric for our equal-mass test system along the x -axis in Figs. 12 and 13. (We have checked that the constraint violations behave roughly similarly—and are not significantly worse—in the y - and z -directions.) For the norm of the momentum constraint, M_k , we have chosen $\sqrt{M^k M_k}$, with indices raised by the (merged) metric. [See, e.g., Eqs. (14)–(15) in [21] for expressions for the constraint equations.] N.B.: As one can see by looking at the (norm of the) momentum constraint, the plot of the constraint violations in the inner-to-near transition (Fig. 12) does not cover the entire transition region. However, the portion we do not show is not particularly interesting: The momentum constraint violations of the near zone metric continue to decrease, and those of the merged metric rapidly become indistinguishable from the near zone metric's momentum constraint violations.)

The largest constraint violations in the merged metric outside of the horizons occur in the inner-to-near transition regions. These are likely due in part to the near zone metric's large constraint violations near the horizons due to the coordinate singularity at the horizons. (Recall that the horizons are approximately $.5m$ away from the positions of the point particles in our test system—the effects of the new coordinates and tidal distortion are small.) However, since the only knowledge we have about the size of the uncontrolled remainders is their scaling with v (and thus b), the magnitude of the constraint violations does not really provide us with a check that the uncontrolled remainders are in fact of the advertised orders. We can obtain such a check by considering how the constraint violations vary as the binary's separation (b) increases. As expected, they decrease at least as rapidly as $b^{-5/2}$ (the expected scaling of the largest uncontrolled remainders) as the binary's separation increases. This is illustrated in Figs. 14 and 15 in the inner and near zones, and in Fig. 16 in the far zone.

For a separation of $10m$, the relatively large constraint violations of the merged metric compared to those of the individual metrics are an indication that this separation

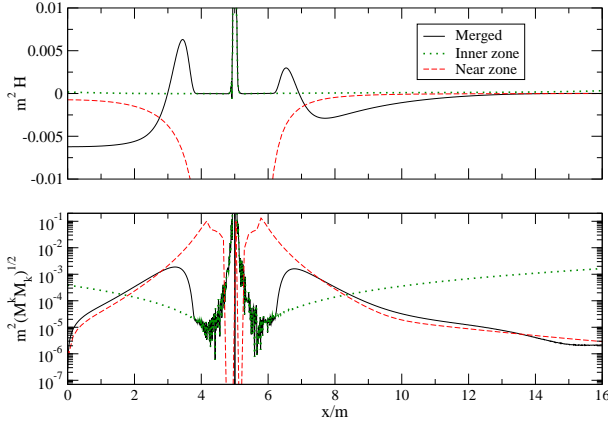


FIG. 12: The Hamiltonian constraint violations and norm of the momentum constraint violations of the merged, inner zone, and near zone metrics. These are plotted along the x -axis around hole 1 for our standard equal-mass test system.

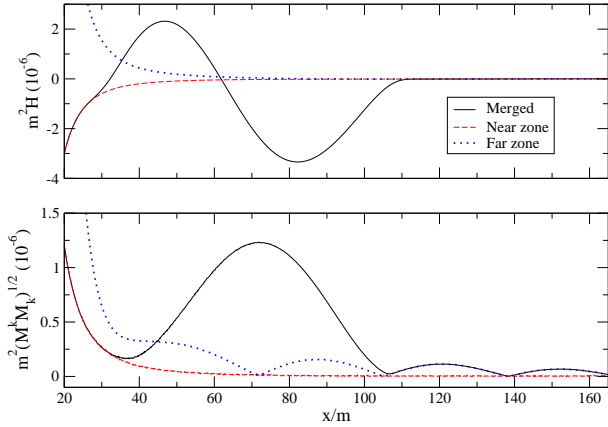


FIG. 13: The Hamiltonian constraint violations and norm of the momentum constraint violations of the merged, near zone, and far zone metrics. These are plotted along the x -axis in a region including the portion of the near-to-far transition region to the right of hole 1. As usual, this is done for our standard equal-mass binary test binary.

is close to the minimum for which the hypotheses underlying the data's construction are valid: For instance, as seen above, for this separation (and an equal-mass binary), the two inner-to-near transition regions overlap between the holes, meaning that much of the inner-to-near transition is effected by f_{near} —see Table III and the surrounding discussion. Moreover, as we have seen previously, the $t = 0$ slice of the near zone metric is not even spacelike at some points outside the holes' horizons for $b = 10m$. However, this does not adversely affect the merged metric with our choices of transition regions. If one tries closer separations, things are significantly worse. For instance, for a separation of $6m$, the maximum constraint violations are larger than those for $10m$ by a factor of 10 or more. Moreover, with our choices for the transition regions, the merged metric contains some of the

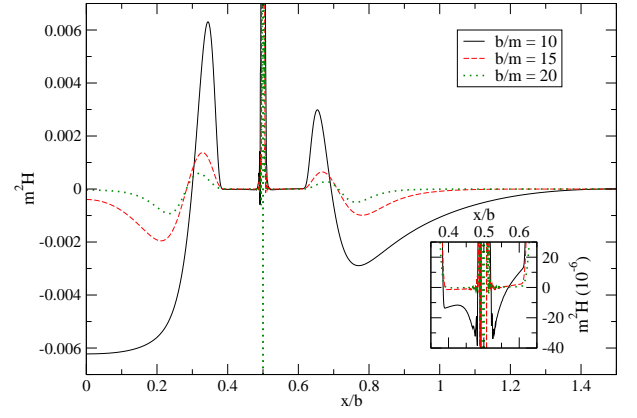


FIG. 14: The Hamiltonian constraint violations around hole 1 for an equal-mass binary with separations of $10m$, $15m$, and $20m$. For ease of comparison, we have scaled the x -axis by b so that (the point particle associated with) hole 1 is always at the same position. In the inset, we zoom in to show how the inner zone constraint violations vary with b .

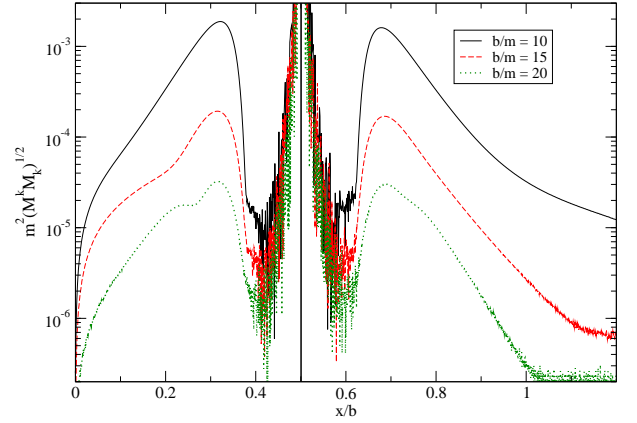


FIG. 15: The norm of the momentum constraint violations around hole 1 for an equal-mass binary with separations of $10m$, $15m$, and $20m$. For ease of comparison, we have scaled the x -axis by b so that (the point particle associated with) hole 1 is always at the same position.

portions of the near zone metric where its $t = 0$ slice is not spacelike.

In the near-to-far transition (as shown in Fig. 13), the relatively large constraint violations associated with the far zone metric are not unexpected at the distances from the binary at which we have made our transition: We have uncontrolled remainders of, e.g., $O(mb^4/r^5)$ in the multipolar expansion of the far zone metric, so we expect it to have (dimensionless) constraint violations of $O(m^3 b^3/r^7)$. For instance, at $r = 30m$, $m^3 b^3/r^7 \simeq 5 \times 10^{-7}$, reproducing the order of magnitude of the constraint violations at that point. We would have thus needed to transition somewhat farther from the binary if we wanted the near and far zone metrics' constraint violations be comparable in the transition region. However, we almost surely do not want to do this, since the

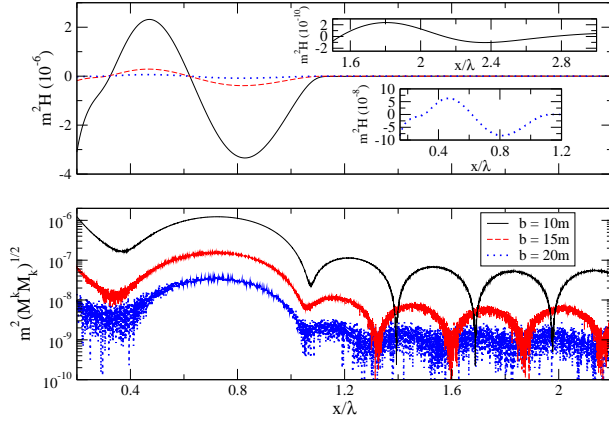


FIG. 16: The Hamiltonian constraint violations and norm of the momentum constraint violations along the x -axis in the portion of the near-to-far transition and far zone proper that lies to the right of hole 1. These are computed for an equal-mass binary with separations of $10m$, $15m$, and $20m$. For ease of comparison, we have scaled the x -axis by $\lambda = \pi \sqrt{b^3/m}$, the Newtonian wavelength of the binary’s gravitational radiation. In the two insets, we zoom in to better illustrate the behavior of the Hamiltonian constraint violation in two situations: In the lower inset, we consider the $b = 20m$ data in the transition region. In the upper inset, we consider the $b = 10m$ data in the far zone proper. (The other data sets also display similar oscillations in their Hamiltonian constraint violations in the far zone, though the amplitude of these oscillations is too small to be visible on the scale we use to display the oscillations of the $b = 10m$ data’s Hamiltonian constraint.)

near zone only accounts for retardation perturbatively, and thus accumulates large phase errors beyond $r \gtrsim \lambda$: It thus even has a considerable phase error in much of our current transition region. As was (briefly) discussed in the previous subsection, a resummation of the far zone metric might reduce its constraint violations closer to the binary, though we did not pursue this here.

We compared the constraint violations of the new data with the old data (for our standard test system) in Fig. 1 and Table I in the introduction, though we deferred a more detailed discussion to here: First, it is important to realize that the comparison is somewhat misleading, since each paper’s data are in a different coordinate system. (The data from Paper I are in the same harmonic coordinate system as this paper’s data in the near zone. However, this is only true perturbatively in the inner zone, where the black hole background is in a coordinate system that is not horizon-penetrating.)

Second, while our data’s Hamiltonian constraint violations are not appreciably better than those of the data from Paper II, even though we have matched to higher order, this is not unexpected: Even though we used horizon-penetrating coordinates for the black hole metrics, we used standard PN harmonic coordinates for the PN metric; these coordinates are singular at the horizon. While the merged metric has no coordinate singularities, the PN metric’s coordinate singularity increases

the constraint violations in the transition regions, making them comparable to those from Paper II: Paper II’s data use a PN metric with no coordinate singularity as well as even further resummation of the black hole backgrounds than we have employed here, leading to particularly small constraint violations.

Third, the increased momentum constraint violations near the hole in the new data, compared with either of the old papers’ data, come from the x -component: The y -component of the new data’s momentum constraint violations is much smaller than that of either of the two previous sets. However, the x -components of their momentum constraints vanish. (The x -component of the momentum constraint of Paper II’s data only vanishes before the transformation to horizon-penetrating coordinates; it develops two spikes after that transformation.)

Finally, if one compares Fig. 1 with, e.g., Figs. 14 and 17 in Paper II, one notices differences in the behavior of the data from Papers I and II close to the hole (and inside the horizon). This is because we have generated the plot using higher-order finite differencing (fourth order vs. second order) and a higher resolution ($0.002m$ vs. $0.008m$) in computing the constraint violations here than we did in first computing them in Paper II. It was necessary to do this to accurately resolve the constraint violations in the inner zone, since the metric components diverge rapidly there. Additionally, we have used the version of Paper II’s metric that is in horizon-penetrating coordinates, while Figs. 14 and 17 in Paper II were generated using the version of the data without that additional coordinate transformation: The transformation to horizon-penetrating coordinates introduces further structure in the data’s constraint violations in both the x - and y -components.

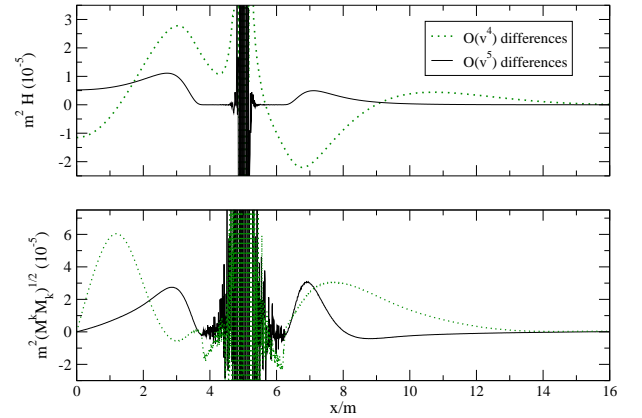


FIG. 17: The constraint violations of the $O(v^4)$ and $O(v^5)$ sets of data minus those of the full extended set of data. These are computed along the x -axis near hole 1 for our standard test binary.

We can also compare the constraint violations of the full extended data with those of the $O(v^4)$ and $O(v^5)$ versions. We do this in the inner-to-near transition in Figs. 17 and 18 for an equal-mass and 3 : 1 mass ra-

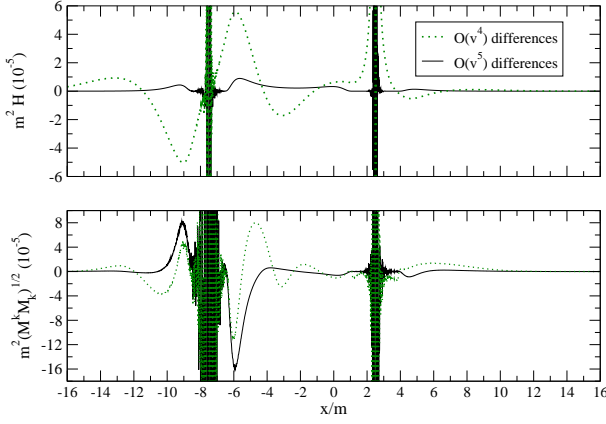


FIG. 18: The constraint violations of the $O(v^4)$ and $O(v^5)$ sets of data minus those of the full extended set of data. These are computed along the x -axis in the inner-to-near transition region for a binary with $b = 10m$ and a mass ratio of 3 : 1. (The more massive hole is on the right.)

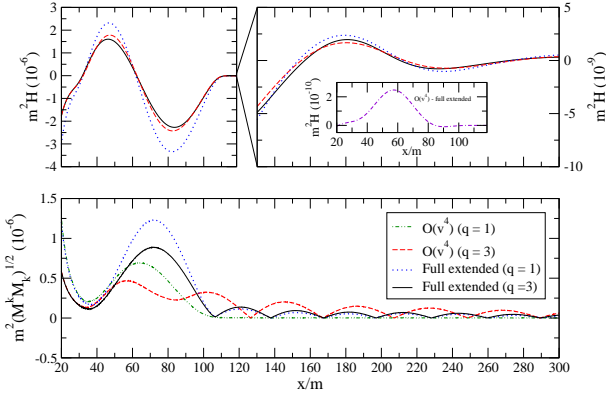


FIG. 19: The constraint violations of the $O(v^4)$ and full extended sets of data. These are computed along the x -axis in the near-to-far transition region (and far zone proper) to the right of hole 1 for binaries with $b = 10m$ and mass ratios of 1 : 1 and 3 : 1. (The more massive hole is on the right.) In the right-hand panel, we zoom in to show the differences in the oscillation of Hamiltonian constraint violations in the far zone proper. In the inset, we show the difference between the Hamiltonian constraint violations of the $O(v^4)$ and full extended versions of the data in the near-to-far transition for an equal-mass binary.

tio binary, respectively, and in the near-to-far transition, along with the far zone proper, for both of those binaries in Fig. 19. [We consider a unequal-mass binary to make the differences between the $O(v^4)$ and $O(v^5)$ versions more pronounced: Most of the $O(v^5)$ terms in the far zone metric vanish for an equal-mass binary.]

In the latter plot (Fig. 19), we do not show the differences between the $O(v^4)$ and full extended versions' Hamiltonian constraint in the far zone proper, as they agree up to the level of numerical truncation error. We also do not show the differences between the $O(v^5)$ and full extended versions of the data. These two sets only

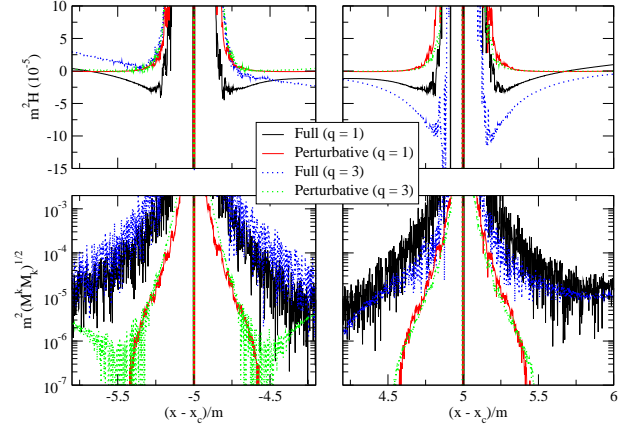


FIG. 20: The Hamiltonian constraint violations and norm of the momentum constraint violations of the versions of the inner zone metric with perturbative and full time dependence for binaries with $b = 10m$ and mass ratios of 1 : 1 and 3 : 1. We display these in the vicinity of both holes, which we shift in the 3 : 1 case so their associated point particles lie at $x = \pm 5m$. [In the figure, $x_c := [1/(q+1) - 1/2]b$.]

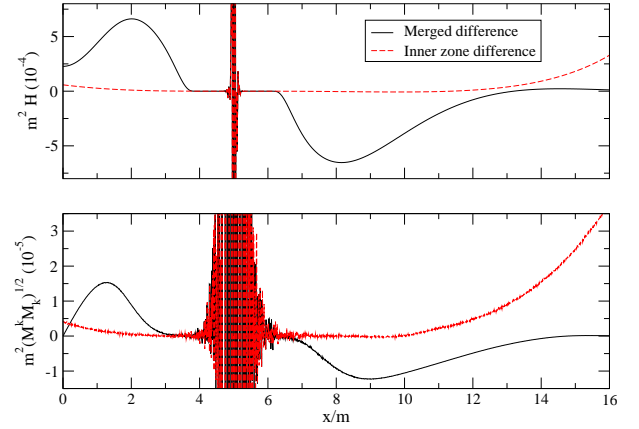


FIG. 21: The differences between the Hamiltonian constraint violations and norm of the momentum constraint violations of the version of the $O(v^4)$ data without fourth-order octupole terms (04_NoOct) in the inner zone and the version including those terms (04). These are computed along the x -axis near hole 1 for our standard test binary.

differ substantially in the far left-hand portion of the transition region, and even there the differences are several orders of magnitude less than those between the $O(v^4)$ and full extended versions. Additionally, we do not show the behavior of the constraint violations to the left of the smaller hole (hole 2): It is qualitatively similar to their behavior to the right of the larger hole shown here, except that for an equal-mass binary, the $O(v^4)$ version of the data has smaller Hamiltonian constraint violations than the full extended version in that region, and for a mass ratio of 3 : 1, there is no oscillation in the transition region in the $O(v^4)$ data's momentum constraint violations.

We compare the constraint violations of the different inner zone versions in Fig. 20 for binaries with mass ratios of 1 : 1 and 3 : 1. In this plot, we do not include the version of the inner zone with no fourth order octupole pieces, as the inclusion of those terms does not affect the constraint violations in the inner zone proper at a level above numerical truncation error. However, these terms *do* have a noticeable effect on the constraint violations in the inner-to-near transition, as can be seen in Fig. 21, which compares the $O(v^4)$ data with and without the fourth-order octupole terms in the inner zone. (The fact that including the fourth order octupole terms in the inner zone metric makes a much larger difference in the merged metric than in the inner zone metric itself in the transition regions suggests that the additional terms that have the most significant effect are those in the coordinate transformation, not those in the tidal fields.)

It is also interesting to consider how accurate the data are for different mass ratios. One finds that the constraint violations do not behave quite as well as might be desired in the inner-to-near transition regions as one increases the mass ratio. This is shown in Figs. 22 and 23, which plot the Hamiltonian constraint and norm of the momentum constraint for mass ratios of 1 : 1, 3 : 1, 5 : 1, and 10 : 1 ($q := m_1/m_2$). The worst behavior is that of the momentum constraint in the transition region near the more massive hole (hole 1), which increases as the mass of that hole increases. The Hamiltonian constraint also increases with mass ratio in the inner zones around both holes. (This is due to the inclusion of the full time dependence of the tidal fields—the inner zone constraint violations decrease with mass ratio if one only uses the version of the inner zone metric with perturbative time dependence.) The behavior of the other constraint violations is nonmonotonic. When one looks at the near-to-far transition and far zone proper one finds much better behavior: The constraint violations decrease with increasing mass ratio in all of those regions, except for a slight increase in the momentum constraint violations in the far zone proper for unequal mass ratios. This is visible for a mass ratio of 3 : 1 in Fig. 19; we do not display the results for higher mass ratios, since they are not particularly interesting.

This behavior in the transition regions is primarily attributable to the choices we have made for the transition functions. For instance, it is possible to choose parameters so that the momentum constraint violations *decrease* around the more massive hole as its mass increases. This can be accomplished by taking $w_{\text{inner},A} \propto r_A^T$, as in Papers I and II. However, with this choice, the decrease in momentum constraint violations around hole 1 occurs at the cost of the aforementioned extreme increase in constraint violations around hole 2 as its mass goes to zero. It should be possible to combine the two choices for $w_{\text{inner},A}$ to obtain better behavior for unequal mass ratios. However, we have chosen to leave such fine-tuning of transition functions to future work, contenting ourselves with providing examples of workable transition functions here.

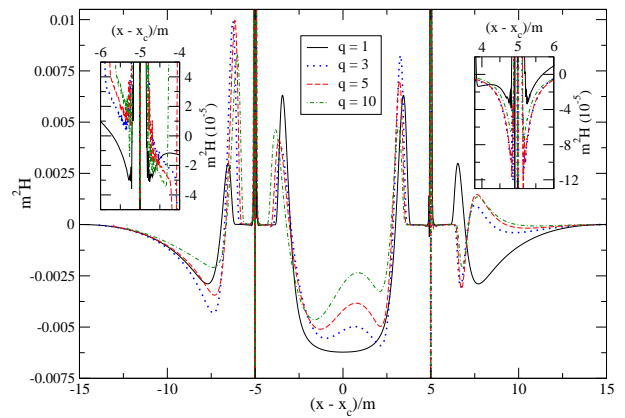


FIG. 22: The Hamiltonian constraint violations along the x -axis for a binary with a separation of $10m$ and mass ratios of 1 : 1, 3 : 1, 5 : 1, and 10 : 1 ($q := m_1/m_2$). (The more massive hole—hole 1—is on the right, and the less massive hole—hole 2—is on the left.) For ease of comparison, we have shifted all the data so that the point midway between the two particles is at $x = 0$. [In the figure, $x_c := [1/(q+1) - 1/2]b$.] In the two insets, we zoom in to show how the inner zone metric's constraint violations vary with q , looking at the region around each hole in the inset closest to it.

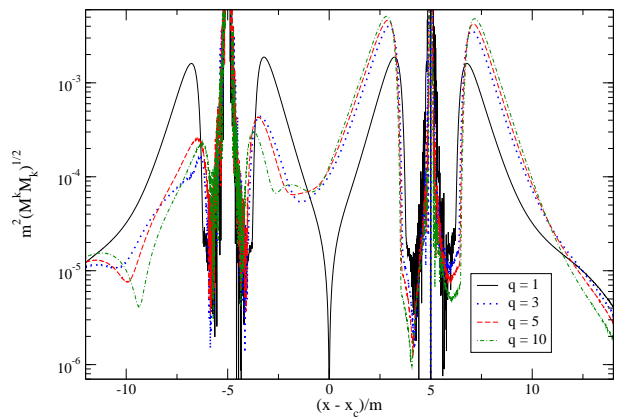


FIG. 23: The norm of the momentum constraint violations along the x -axis for a binary with a separation of $10m$ and mass ratios of 1 : 1, 3 : 1, 5 : 1, and 10 : 1 ($q := m_1/m_2$). (The more massive hole—hole 1—is on the right, and the less massive hole—hole 2—is on the left.) For ease of comparison, we have shifted all the data so that the point midway between the two particles is at $x = 0$. [In the figure, $x_c := [1/(q+1) - 1/2]b$.]

IX. CONCLUSIONS

A. Summary

We have constructed approximate initial data for a nonspinning black hole binary in a quasicircular orbit. This dSata set has uncontrolled remainders of $O(v^5)$ throughout the timeslice (including the far zone), along with remainders of $O(v^3[R/b]^4, v^5[R/b]^3)$ in the inner

zone. We have verified the scaling of the uncontrolled remainders with v by checking that the constraint violations decrease at least as rapidly as they should when the binary's orbital separation is increased. We constructed this data set by asymptotically matching perturbed black hole metrics onto a PN metric and creating transition functions to smoothly interpolate between the various metrics. The resulting data do not assume conformal flatness and contain the binary's outgoing radiation, in addition to the tidal deformations on the holes. (We have included the quadrupole deformations through 1PN along with the lowest-order octupole deformations.)

The results of the matching are given in Sec. V G and Eqs. (B1): Sec. V G gives directions for how to put together the coordinate transformation necessary to place the inner zone metric in the same coordinate system as the near zone metric (to the order we have matched). Eqs. (B1) give explicit expressions for the tidal fields we obtained. [We also found that the inner and near zone mass parameters—i.e., M and m_1 —agree through at least $O(v^3)$.] These tidal fields are then inserted into Detweiler's perturbed black hole metric, given in Cook-Scheel coordinates in Eqs. (3.5) and (3.6), to give the inner zone metric. The near and far zone metrics are given in Eqs. (4.1) and (6.6), respectively. We describe our method of computing the binary's past phase evolution, needed for the far zone metric, in Sec. VI A, and the specifics of how we put together the various zones' metrics in Appendix D. Workable (though surely not optimal) transition functions that smoothly interpolate between the various zones' metrics are given in Sec. VIII B.

We have also constructed an extension of these data that is accurate through $O(v^5)$ in the near and far zones. In addition, this extension includes other higher-order contributions to the temporal components of the near and far zone metrics that were readily available in the literature. We also calculated the fourth-order octupole pieces of the tidal fields (and the associated piece of the coordinate transformation) in Appendix B 2 and included them, as well. (The 1PN correction to the electric octupole tidal field is among the terms we calculated and add here.) Additionally, we calculated the full time dependence of the tidal fields (for times much less than the radiation reaction timescale) and included it in the inner zone metric. This is discussed in Appendices B 2 and D. See Appendix C for a discussion of how we put together the extension to the near and far zone metrics, and Eq. (B3) for the (polynomial part of the) coordinate transformation that accompanies the fourth-order octupole pieces of the tidal fields. See Table II (in Sec. VII) for an overview of the different versions of the metrics we considered in the paper. N.B.: While we did not include this in the table, for the sake of clarity, we considered all the versions of the near zone metrics with and without background resummation, displaying the resulting differences in the volume elements [for the $O(v^4)$ and full extended versions] in Figs. 5 and 6. We found the full extended (a11) data set (including background

resummation in the near zone) to be the best, overall, considering constraint violations as well as the inclusion of terms that we expect to improve evolutions.

In the process of obtaining these data, we have developed a method of fixing the matching parameters when matching a black hole onto a PN background that differs from that presented by Taylor and Poisson [73] and is more automatable. We have also obtained the 1PN corrections to the magnetic quadrupole and electric octupole for a circular orbit using this method, neither of which Taylor and Poisson computed.

The accurate description of the tidal deformations on the holes contained in these data should substantially reduce the high-frequency component of the initial spurious radiation; the use of a high-order PN metric should do the same for the low-frequency component. (The combination of the high-order PN metric, including accurate expressions for the trajectories, and the reduced junk radiation should also give a much better quasicircular orbit—see, e.g., [17, 19].) If these data do indeed reduce the initial spurious radiation, then they can be used to directly quantify the effects of using the conformally flat initial data currently employed, as opposed to data that include many more of the system's expected physical properties. In addition, the waveforms generated using these data would be ideal for the construction of hybrid numerical relativity/post-Newtonian waveforms (as in [100]): Since the initial data are directly connected to the PN approximation, the PN parameters and phasing that are input into the initial data should accurately describe the subsequent evolution.

Of course, one needs to evolve the data to see whether these putative improvements are indeed realized. We have already coded this data set into MAPLE scripts, which were then converted to C code. Both the scripts and codes are freely available online at [36] to anyone who is interested in evolving or otherwise studying the data. Any evolutions of these data will need to use either excision [30, 31], or the turducken approach [34]: The black hole perturbations are not valid all the way to the holes' asymptotically flat ends, preventing the use of standard puncture methods. Additionally, since the data only satisfy the constraint equations approximately, one may want to project them onto the constraint hypersurface before evolution. To do this, one would need to use a code such as [45, 63, 101, 102]: The standard solver for puncture data [103] requires conformal flatness. However, evolutions of data that only approximately solve the constraints are possible: See, e.g., [57, 65].

B. Possibilities for future initial data constructions with this method

With this work, the asymptotic matching method for generating initial data for nonspinning binary black holes in a quasicircular orbit first essayed by Alvi [41] and further developed in Papers I and II has been taken to the

highest order possible without further development in its constituent parts: Including higher multipole orders in the inner zone would require the input of nonlinear black hole perturbation theory. Iterating to higher orders in v would not only require the higher multipoles, but also an explicit expression for the $O(v^6)$ pieces of the purely spatial components of the near zone metric. Determining the higher-order-in- v pieces of the far zone metric would either require calculation of further contributions from the outer integrals in the DIRE approach [60], or obtaining the far zone metric via matching, following the post-Minkowskian approach of [76].

Nevertheless, it might still be possible to improve the initial data at the (formal) order presented here, as was done in Paper II for the data in Paper I. For instance, one could contemplate converting the near zone metric to Cook-Scheel coordinates (or some other horizon-penetrating coordinate system) in a neighborhood of each black hole. This would regain the complete agreement between background coordinates, with no coordinate singularity at the horizon in the near zone metric, that was found to improve the numerical agreement of the metrics in Paper II. One could also further tweak the transition functions, though this is not likely to produce any dramatic improvements in constraint violations. However, it is possible that different choices for the transition functions could improve the data's properties in evolutions. For instance, in the current near-to-far transition, the near zone metric is used (blended with the far zone metric) for $r \gg \lambda$, where its perturbative treatment of retardation leads to large phasing errors. It might thus be preferable to transition closer to the binary, even at the cost of greater constraint violations. (Resumming the far zone metric is a possibility for reducing these constraint violations, as was discussed briefly in Sec. VIII A.)

The prospects for generalizing this construction to include eccentricity or spin are good: The ingredients are nearly all readily available in the literature. Such generalization—particularly the inclusion of spin—would be an obvious next step if this initial data set indeed significantly reduces the spurious radiation. Including eccentricity would be straightforward, though algebraically involved, and can be carried out with the ingredients we have used here, perhaps supplemented with the results from [73]. (The evolution of the binary's phase and separation needed in the far zone metric can be obtained through 3.5PN order using the results of [104].)

However, it would only be possible to obtain the generalization of these data for a spinning binary to $O(v^2)$, formally, while still including all the formal quadrupole pieces in the inner zone. This is true even though the generalization of Blanchet, Faye, and Ponsot's metric to include spin (and spin-orbit coupling) is available [105],⁹

as are the expressions for the source multipoles necessary to obtain the matching far zone metric [107]. (The binary's evolution under radiation reaction is also known through 2.5PN [106].) The bottleneck is the available tidally perturbed Kerr metric [108], which only includes the quadrupole perturbations. We have seen that knowledge of the octupole perturbations is necessary to carry out the matching of all the formal quadrupole pieces at $O(v^4)$ [which one would need to do to obtain data that are formally valid through $O(v^3)$]. However, one could use the same philosophy we did when computing our extension and add the higher-order terms in the near and far zones without computing the matching inner zone terms.

Acknowledgments

We would like to thank Luc Blanchet, Steven Dettweiler, Lee Lindblom, Eric Poisson, Frans Pretorius, and Clifford Will for useful discussions and clarifications. This work was supported by the Penn State Center for Gravitational Wave Physics under NSF cooperative agreement PHY-0114375, as well as by NSF grants PHY-0555628 to Penn State, PHY-0652874 and PHY-0855315 to FAU, and PHY-0745779 to Princeton.

APPENDIX A: COMPARING COOK-SCHEEL AND PN HARMONIC COORDINATES

In the quasi-Cartesian form of Cook-Scheel coordinates [67], the Schwarzschild metric is

$$\begin{aligned} g_{00}^{\text{CS}} &= -\frac{R-M}{R+M}, \\ g_{0k}^{\text{CS}} &= \frac{4M^2}{(R+M)^2} \frac{X_k}{R}, \\ g_{kl}^{\text{CS}} &= \left(1 + \frac{M}{R}\right)^2 \delta_{kl} \\ &\quad + \frac{M^2}{R^2} \frac{R-M}{R+M} \left[1 + \frac{4MR}{(R+M)^2}\right] \frac{X_k X_l}{R^2}. \end{aligned} \tag{A1}$$

[The transformation from Schwarzschild to Cook-Scheel coordinates is given in Eq. (3.4).] For comparison, the Schwarzschild metric in PN harmonic coordinates is

$$\begin{aligned} g_{00}^{\text{har}} &= -\frac{R-M}{R+M}, \\ g_{kl}^{\text{har}} &= \left(1 + \frac{M}{R}\right)^2 \left(\delta_{kl} - \frac{X_k X_l}{R^2}\right) + \frac{R+M}{R-M} \frac{X_k X_l}{R^2}, \end{aligned} \tag{A2}$$

where $g_{0k}^{\text{har}} = 0$. (One obtains PN harmonic coordinates from Schwarzschild coordinates by $R = \mathcal{P} - M$, where \mathcal{P} is the Schwarzschild radial coordinate. This is just the spatial part of the Schwarzschild-to-Cook-Scheel transformation.) Obviously, these coordinates have preserved

⁹ Errata for the potentials and equations of motion in [105] are given in footnotes 6 and 10 of [106], respectively.

the coordinate singularity of the Schwarzschild metric in Schwarzschild coordinates.

Note that the purely temporal component of the Cook-Scheel version has the same form as in PN harmonic coordinates, but all the other components are different. In particular, the Cook-Scheel version has a nonzero shift component as well as a slightly more involved nondiagonal piece of the spatial metric. Explicitly, the differences between the PN harmonic and Cook-Scheel versions of the Schwarzschild metric components are

$$\begin{aligned} g_{00}^{\text{CS}} - g_{00}^{\text{har}} &= 0, \\ g_{0k}^{\text{CS}} - g_{0k}^{\text{har}} &= \frac{4M^2}{(R+M)^2} \frac{X_k}{R}, \\ g_{kl}^{\text{CS}} - g_{kl}^{\text{har}} &= -\frac{16M^4}{(R-M)(R+M)^3} \frac{X_k X_l}{R^2}. \end{aligned} \quad (\text{A3})$$

(Of course, this must be interpreted purely algebraically, since we are subtracting components in different coordinate systems.) The difference of the purely spatial components scales as $O([M/R]^4)$ as $M/R \rightarrow 0$, which is clearly higher order in the near zone. However, the dif-

ference of the spatiotemporal components is $O([M/R]^2)$, which is of the same order as the terms we do keep in the spatial metric. And, indeed, we do see the first term in this expansion appearing in our coordinate transformation—see Sec. V G. This shows that we have given up on the exact agreement of background metrics—which was seen to significantly improve the quality of the merged metric in Paper II—in order to have horizon-penetrating coordinates.

APPENDIX B: TIDAL FIELDS

1. Comparison with Taylor and Poisson's results

To facilitate the comparison of our expressions for the tidal fields with those obtained by Taylor and Poisson [73], we collect the results of our matching here. These include the results of the fourth order octupole matching from the next subsection, and are all put together using Eqs. (5.3) to give explicit expressions for the tidal fields about hole 1:

$$\mathcal{E}_{kl}(t) = \frac{m_2}{b^3} \left\{ \left[1 - \frac{1}{2} \frac{m_2}{b} \right] [\delta_{kl} - 3\hat{x}_k \hat{x}_l] + \frac{1}{2} \frac{m}{b} [4\hat{x}_k \hat{x}_l - 5\hat{y}_k \hat{y}_l + \hat{z}_k \hat{z}_l] - 6\sqrt{\frac{m}{b}} \frac{t}{b} \hat{x}_{(k} \hat{y}_{l)} + O\left(\left[\frac{m_2}{b}\right]^2, \frac{t^2}{b^2}\right) \right\}, \quad (\text{B1a})$$

$$\begin{aligned} \mathcal{B}_{kl}(t) &= \frac{m_2}{b^3} \sqrt{\frac{m_2}{b}} \left\{ \left[-6\sqrt{\frac{m}{m_2}} + \frac{m_2}{b} \left\{ 5\left(\frac{m}{m_2}\right)^{3/2} + 7\sqrt{\frac{m}{m_2}} - 3\sqrt{\frac{m_2}{m}} \right\} \right] \hat{x}_{(k} \hat{z}_{l)} - 6\frac{m}{m_2} \sqrt{\frac{m_2}{b}} \frac{t}{b} \hat{y}_{(k} \hat{z}_{l)} \right. \\ &\quad \left. + O\left(\left[\frac{m_2}{b}\right]^{3/2}, \frac{t^2}{b^2}\right) \right\}, \end{aligned} \quad (\text{B1b})$$

$$\mathcal{E}_{klp}(t) = \frac{m_2}{b^4} \left\{ \left[1 - 3\frac{m_2}{b} \right] [15\hat{x}_k \hat{x}_l \hat{x}_p - 9\delta_{(kl} \hat{x}_{p)}] - 3\frac{m}{b} [\hat{x}_k \hat{x}_l \hat{x}_p - 4\hat{y}_{(k} \hat{y}_{l} \hat{x}_{p)} + \hat{z}_{(k} \hat{z}_{l} \hat{x}_{p)}] + O\left(\left[\frac{m_2}{b}\right]^2, \frac{t}{b}\right) \right\}, \quad (\text{B1c})$$

$$\mathcal{B}_{klp}(t) = \frac{9}{2} \frac{m_2}{b^4} \sqrt{\frac{m}{b}} \left\{ 5\hat{x}_{(k} \hat{x}_l \hat{z}_{p)} - \delta_{(kl} \hat{z}_{p)} + O\left(\left[\frac{m_2}{b}\right]^{1/2}, \frac{t}{b}\right) \right\}. \quad (\text{B1d})$$

Here, for the purposes of comparison with Taylor and Poisson's results, we have included the time dependent pieces we know in the quadrupole fields (the time dependence falls into the uncontrolled remainders in the octupole fields). These are ordinarily contained in $\dot{\mathcal{E}}_{kl}$ and $\dot{\mathcal{B}}_{kl}$, since we usually treat them as independent tidal fields.

Taylor and Poisson give explicit expressions for the quadrupole tidal fields for a binary in a circular orbit in their Eqs. (1.10)–(1.14) [and with alternate notation in Eqs. (7.25)–(7.29)]. The parts of the quadrupole fields that Taylor and Poisson and we have both computed agree: These consist of the electric quadrupole, including its 1PN corrections; the time derivative of the electric quadrupole with no corrections; and the magnetic quadrupole with no corrections, all evaluated at

$t = 0$. In fact, we can recover all of Taylor and Poisson's expressions for the tidal fields, including the full time dependence, if we evaluate our expressions for the tidal fields at $t = 0$ and then make the substitutions $\hat{x}_k \rightarrow \hat{x}_k \cos \omega t + \hat{y}_k \sin \omega t$ and $\hat{y}_k \rightarrow -\hat{x}_k \sin \omega t + \hat{y}_k \cos \omega t$. (This is, of course, only accurate for times much less than the radiation reaction time scale.) Thus, even though we are not given the full time dependence directly from the matching, we can obtain it from our results, since they are true for any point in the orbit.

While we have computed certain higher-order contributions to the tidal fields that Taylor and Poisson did not, we cannot improve upon the formal accuracy of their result for the tidal heating [given through 1PN in their Eq. (9.4)]. This is the case even though Poisson gives the contribution of the octupole fields to the tidal heating in

Eq. (12) of [68]: The 2PN correction to the expression for the tidal heating involves the unknown 2PN correction to the electric quadrupole (along with the known 1PN correction to the magnetic quadrupole and the Newtonian piece of the electric octupole).

We can also check the lowest-order pieces of all the tidal fields we found are the expected Newtonian ones: The Newtonian pieces of the tidal fields can be computed independently using Eqs. (5.45), (5.50), and (5.56) in [77], along with the obvious generalization of that reference's Eqs. (5.45) and (5.50) for the magnetic octupole, viz., $\mathcal{B}_{klp}^{\text{Newt}} = -(3/8)\epsilon^{su}{}_{(k}\partial_{l)p)s}\beta_u$, where β^k is given by Eq. (5.56b) of [77]. (To reproduce our results exactly, one needs to evaluate all of these expressions for the Newtonian parts of the tidal fields at $r_1 = 0$. Also, since these expressions for the Newtonian parts of the tidal fields are valid in the rest frame of hole 1, we need to use the relative velocity of the holes in calculating β^k .) Our expression for the 1PN correction to the magnetic quadrupole can be checked in the extreme mass ratio limit against that computed by Poisson in [109]: This result is given in an appropriate form for comparison in an unnumbered equation in Sec. VII E of Taylor and Poisson [73] and agrees with our computation.

2. 1PN corrections to the fourth order octupole fields

Even though we cannot obtain all the inner zone octupole pieces at fourth and fifth orders without including

the hexadecapole fields (since these will give octupolar contributions to the nonpolynomial part at these orders), it *is* possible to match only the polynomial parts, and, in doing so, read off the 1PN corrections to the octupolar tidal fields. As an illustration, we shall read off the 1PN correction to the electric octupole (along with the lowest-order piece of the time derivative of the magnetic quadrupole) by matching the octupole parts of the polynomial pieces at fourth order.

Except for the added algebraic complication of keeping higher-order multipole terms, this calculation proceeds precisely analogously to the fourth order calculation involving the quadrupole-and-lower multipoles of the polynomial part in Sec. V F. The only subtlety that we should mention is one that was already present in our original fourth order calculation. However, it was not a potential source of confusion there because we were computing both the polynomial and nonpolynomial parts at once. Now that we want to compute the polynomial part by itself, we need to bear in mind that two nonpolynomial pieces can produce a polynomial piece when multiplied together (e.g., \tilde{r} is a nonpolynomial piece, but \tilde{r}^2 is a polynomial piece). Therefore, contributions to the near zone metric involving terms such as $n_1^{(k}n_{12}^{l)}/S^2$ will contain polynomial pieces, since n_1^k contains a factor of $1/\tilde{r}$, and $1/S^2$ contributes a factor of \tilde{r} [see Eq. (4.5)]. The final results are

$$(\dot{\tilde{\mathcal{E}}}_{kl})_2 = 0, \quad (\tilde{\mathcal{E}}_{klp})_2 = 9[3\delta_{(kl}\hat{x}_p) - 5\hat{x}_k\hat{x}_l\hat{x}_p] - \frac{m}{m_2}[3\hat{x}_k\hat{x}_l\hat{x}_p - 12\hat{y}_{(k}\hat{y}_l\hat{x}_p) + 3\hat{z}_{(k}\hat{z}_l\hat{x}_p)], \quad (\text{B2a})$$

$$(\dot{\tilde{\mathcal{B}}}_{kl})_1 = -6\frac{m}{m_2}\frac{1}{b}\hat{y}_{(k}\hat{z}_{l)}, \quad (\tilde{\mathcal{B}}_{klp})_1 = 0, \quad (\text{B2b})$$

with an accompanying polynomial piece of the coordinate transformation of

$$\begin{aligned} (X_\alpha^{\text{P}})_{4,3} = & \frac{\tilde{x}t}{b^3} \left\{ \left[\frac{3}{2} \frac{m}{m_2} - 2 \right] \tilde{x}^2 - \frac{m}{m_2} \frac{t^2}{6} + \left(\frac{3}{2} - \frac{9}{2} \frac{m}{m_2} \right) y^2 + \frac{1}{2} \left(1 - \frac{m}{m_2} \right) z^2 \right\} \hat{t}_\alpha \\ & + \frac{1}{b^3} \left\{ \left[\frac{m}{m_2} \left(\frac{t^2}{4} + \frac{\tilde{x}^2}{8} + y^2 - \frac{3}{2} z^2 \right) + y^2 + z^2 \right] \tilde{x}^2 - \frac{m}{m_2} \left[\frac{t^4}{24} + \frac{y^4 - z^4}{8} + \frac{(y^2 + z^2)t^2}{4} \right] - \frac{(y^2 + z^2)^2}{4} \right\} \hat{x}_\alpha \\ & + \frac{\tilde{x}y}{b^3} \left\{ 3\tilde{x}^2 - \frac{9}{4}(y^2 + z^2) + \frac{m}{m_2} \left[\frac{t^2}{2} - \frac{5}{2}\tilde{x}^2 + \frac{9}{4}y^2 + \frac{3}{4}z^2 \right] \right\} \hat{y}_\alpha \\ & + \frac{\tilde{x}z}{b^3} \left\{ 3\tilde{x}^2 - \frac{9}{4}(y^2 + z^2) + \frac{m}{m_2} \left[\frac{t^2}{2} - \frac{\tilde{x}^2}{2} + \frac{7}{4}y^2 + \frac{z^2}{4} \right] \right\} \hat{z}_\alpha. \end{aligned} \quad (\text{B3})$$

Continuing on to fifth order to obtain the 1PN corrections to the magnetic octupole and time derivative of the electric quadrupole would be algebraically more compli-

cated, but would otherwise proceed as above. At sixth order we are not so fortunate. If we tried to carry out even the quadrupolar part of the sixth order polynomial

matching, so as, e.g., to read off the 2PN correction to the electric quadrupole, we would be stymied by our lack of knowledge of $(X_\alpha^{\text{NP}})_{4,3}$: The \tilde{r} -times-a-polynomial-in- \tilde{x}^α pieces of $(X_\alpha^{\text{NP}})_{4,3}$ (which we expect to be present, as there have been such terms at all lower multipole orders) will contribute to $(h_{\alpha\beta}^{\text{P}})_6$ via the $b(1/R)_4$ term.

APPENDIX C: HIGHER-ORDER TERMS

1. Discussion

Let us first catalogue all the higher-order near and far zone pieces that are readily available in the literature (besides those already discussed in Sec. VI A): Blanchet, Faye, and Ponsot [58] give an explicit expression for the near zone 2.5PN metric with the standard PN order counting—i.e., with remainders of $O(v^8)$ in g_{00} , $O(v^7)$ in g_{0k} , and $O(v^6)$ in g_{kl} . The expression Pati and Will give for the far zone metric perturbation in terms of derivatives of the multipoles [reproduced here in Eq. (6.1a)] has remainders of at least $O(v^6)$ in all components. Additionally, Pati and Will express the metric in terms of the metric perturbation through 3.5PN order (with the standard PN order counting) in, e.g., Eqs. (4.2) of [60]. Further contributions to the far zone metric perturbation can be obtained from the full expression for the field multipole expansion of the near zone contributions to the far zone [Eq. (2.13) in [60]], combined with the expressions for the field multipoles, M^Q , in terms of the source multipoles, \mathcal{I}^Q and \mathcal{J}^Q , in Eqs. (4.7) of [60].

The lowest-order (Newtonian) pieces of all the source multipoles are known—see Eq. (D1) in [61]. Additionally, further PN corrections to the source multipole moments than we used in Sec. VI can be found in various places: Higher-order corrections to \mathcal{I} can be obtained from the system’s binding energy, which Blanchet gives through 3PN in Eq. (170) of [62]. Similarly, one can get higher-order corrections to \mathcal{J}^k from the expression Kidder, Will, and Wiseman give for the system’s angular momentum (through 2PN) in Eq. (2.13b) of [110]. We gave the 1PN correction to the mass quadrupole in Eq. (6.2c), even though we did not need it to construct our $O(v^4)$ data. The 1PN correction to the mass octupole can be obtained (up to the caveats mentioned below) from the expression for the three-index Epstein-Wagoner (EW) moment given in Eq. (6.6b) in Will and Wiseman [71]. This EW moment also yields the 1PN correction to the current quadrupole. Even further corrections to various source multipoles can be obtained from the expressions for the two- and four-index EW moments that Will and Wiseman give.

We can use Blanchet, Faye, and Ponsot’s results to obtain initial data in the near zone that are formally valid through $O(v^5)$. However, to obtain $O(v^5)$ initial data in the far zone, one needs the $O(v^6)$ pieces of the spatiotemporal components of the metric. As mentioned in

Sec. VII, including these is slightly problematic: There is an outer integral term in h^{0k} that is $O(v^6)$ with the order counting used in Sec. VI and is not known at present. This term looks, schematically, like $\mathcal{I}\mathcal{J}^k/r^3$ and comes from the first term in the general expression Pati and Will give for Λ^{0k} in Eq. (4.4b) of [60]. [Here $\Lambda^{\alpha\beta}$ gives the contributions of the gravitational field to $\tau^{\alpha\beta}$, the “effective” stress-energy pseudotensor. See Eqs. (2.5)–(2.7) in [60] for the explicit definitions.] However, it is *not* present in the explicit expression for Λ^{0k} in the far zone that Pati and Will give in Eq. (6.5b) of [60]. This is not a problem, since Pati and Will derive this expression specifically for computing the contributions to the near zone field from the outer integrals. They have thus used the “quick and dirty” rule from their Eq. (4.9) to eliminate any pieces that do not contribute there to the order considered. This piece is one of those eliminated, as it will contribute an \mathcal{R} -independent term only through a time derivative:¹⁰ Since both \mathcal{I} and \mathcal{J}^k are constants of the motion, up to radiative losses, the resulting contribution would be of considerably higher order than Pati and Will are keeping. However, the “quick and dirty” rule is not applicable to the far zone, and we indeed have to consider this term.

While it would be, in principle, reasonably straightforward to compute the unknown term, following the procedure given by Pati and Will in [60], the calculation would be involved enough that we do not attempt it here. In fact, it is possible to argue that we can ignore this term entirely: Recalling that, in practice, extra factors of $1/r$ always make a term smaller by at least a factor of v in the far zone [see Eq. (6.3) and the surrounding discussion], we can choose to count *all* powers of $1/r$ after the first as $O(v)$, disregarding post-Minkowskian considerations. This “practical” order counting is justified numerically, since the factors of $1/r$ will make the highest-order near zone terms (whose far zone analogues will not be present) similarly small when evaluated in the buffer zone. Since this is where we stitch the near and far zone metrics together numerically, it is thus the only place where we are concerned with their agreement, in practice.

We therefore disregard post-Minkowskian powers of G in our counting, giving, e.g., $(\mathcal{I}/r)^2 = O(v^5)$, as opposed to $O(v^4)$, as it was before. Nevertheless, this new order counting still allows us to keep all the outer integral contributions that we know (and, indeed, all the terms we calculated in Sec. VI), since we are now keeping terms to one order in v higher than before. It also gives $\mathcal{I}\mathcal{J}^k/r^3 = O(v^7)$, so we can safely ignore this unknown term. Thus, all we need to consistently calculate initial data through $O(v^5)$ in the far zone are the 1PN corrections to the current dipole and the contributions to h^{0k}

¹⁰ Here \mathcal{R} is the artificial radius of separation between the near and far zones in the DIRE approach, which, as Pati and Will demonstrate in Sec. II I of [60], cannot appear in any final results.

from the mass hexadecapole and current quadrupole. As mentioned above, all of these are easily obtainable.

Now, even though we can obtain initial data that are formally accurate to $O(v^5)$ in the near and far zones (with the new far zone order counting), this does not utilize the $O(v^6)$ and $O(v^7)$ terms in the purely temporal component of the metric that Blanchet, Faye, and Ponsot give us. While including these terms does not increase the formal accuracy of the data, even just in the near and far zones, it is nevertheless possible that adding such terms will improve the data's quality in practice. Of course, if we include terms through $O(v^7)$ in the purely temporal component of the near zone metric, it seems desirable to also include them in the purely temporal component of the far zone metric, and it is possible to do so, up to outer integral terms. Here we shall simply neglect the outer integral terms we do not know, since there appear to be some in h^{00} that are $O(v^7)$ even with the new “practical” order counting, e.g., ones that look like $\mathcal{I}\tilde{\mathcal{I}}^{kl}\hat{n}^{<kl>}/r^2$. [See Eq. (6.5a) in [60].¹¹] Since we are already adding pieces without regard to formal accuracy, it does not make much sense to go to the trouble of calculating these outer integral terms here. This is particularly true since we are not even sure that we have all the terms we need in the 1PN correction to the mass octupole. (We *do* know some even higher-order contributions to the far zone metric, but do not include those, since we do not know the matching near zone contributions.)

This uncertainty arises because the EW moments presented by Will and Wiseman are missing any pieces that are pure traces in the first two indices: Will and Wiseman were only interested in using their results to compute the gravitational waveform [via their Eq. (2.18)], which is transverse and tracefree. For instance, the $(7/4)m_1m_2b\delta^{kl}$ term present in the 1PN correction to \mathcal{I}^{kl} in Eq. (6.2c) is not present in the expression for I_{EW}^{kl} in Eq. (4.17) of [71]. If not for the missing trace term, these two expressions would be identical, up to a surface term, as can be seen from their definitions: I_{EW}^{kl} and \mathcal{I}^{kl} are defined in Eq. (2.19a) of [71] and Eq. (4.5b) of [60], respectively. Unlike for \mathcal{I}^{kl} , we do not have an independent calculation of the 1PN corrections to \mathcal{I}^{klp} . It is thus possible that we are missing terms such as $m_1^2b\delta^{kl}x_1^p + (1 \leftrightarrow 2)$ in I_{EW}^{klp} , which (as demonstrated in the next subsection) would contribute to the 1PN correction to \mathcal{I}^{klp} and thus to the $O(v^7)$ pieces of g_{00} .

¹¹ This equation only contains the parts of Λ^{00} that contribute to the near zone metric. But one can check, starting from the general expression for Λ^{00} Pati and Will give in Eq. (4.4a) of [60], that there are not any lower-order contributions that only appear in the far zone.

2. Outline of the calculation

For the far zone metric, we first calculate the higher-order multipole contributions that need to be added to the expression for $h^{\alpha\beta}$ given in Eq. (6.1a). The $O(v^6)$ and $O(v^7)$ pieces of h^{00} are

$$\frac{1}{6}\partial_{klps}\left[\frac{\mathcal{I}^{klps}(u)}{r}\right] - \frac{1}{30}\partial_{klpsv}\left[\frac{\mathcal{I}^{klpsv}(u)}{r}\right], \quad (\text{C1})$$

and the $O(v^6)$ pieces of h^{0k} are

$$-\frac{1}{6}\partial_{lps}\left[\frac{\dot{\mathcal{I}}^{klps}(u)}{r}\right] + \frac{1}{2}\epsilon^{lkp}\partial_{psv}\left[\frac{\mathcal{J}^{lsv}(u)}{r}\right]. \quad (\text{C2})$$

These were obtained by substituting the expressions for M^Q (in terms of \mathcal{I}^Q and \mathcal{J}^Q) from Pati and Will's Eqs. (4.7) into their Eq. (2.13) (both from [60]). One also needs higher-order contributions to the expression for g_{00} in terms of $h^{\alpha\beta}$. We do not need to add any other new terms to the expression for $g_{\alpha\beta}$, since the expressions required to obtain the $O(v^6)$ pieces of g_{0k} and $O(v^5)$ pieces of g_{kl} are the same as those given previously in Eq. (6.5). This follows because we already included the $-(1/2)h^{00}$ term in g_{0k} for formal consistency, even though it only gives $O(v^6)$ terms in actuality with our order counting. The expression we need to obtain g_{00} consistently through $O(v^7)$ is

$$g_{00} = -\left[1 - \frac{1}{2}h^{00} + \frac{3}{8}(h^{00})^2 - \frac{5}{16}(h^{00})^3\right] + \frac{1}{2}\left[1 - \frac{1}{2}h^{00}\right]h^{kk}, \quad (\text{C3})$$

taken from Eq. (4.2a) in [60].

We also need the 2PN corrections to the mass monopole, along with the 1PN corrections to the mass quadrupole, mass octupole, and current dipole. As discussed previously, all of these except the 1PN correction to the mass octupole are given directly in the literature: The corrections to the mass monopole come from Blanchet's Eq. (170) [62] and those to the current dipole from Eq. (2.13b) in [110]; the corrections to the mass quadrupole are given in our Eq. (6.2c). However, it is possible to obtain a very simple expression for its time derivative (up to the caveats mentioned above) in terms of the three-index EW moment I_{EW}^{klp} [which is given in, e.g., Eq. (6.6b) in [71]], viz., $\dot{\mathcal{I}}^{klp} = 3I_{\text{EW}}^{(klp)}$. Here the equality holds up to surface terms (i.e., ones involving \mathcal{R}), which we can neglect here. To obtain this equality, take a time derivative of the definition of the mass octupole, use the conservation law $\partial_\beta\tau^{\alpha\beta} = 0$ to write $\partial_0\tau^{\alpha 0} = -\partial_k\tau^{\alpha k}$, and integrate the result by parts, giving an expression that equals $3I_{\text{EW}}^{(klp)}$ up to surface terms.

We can now antidifferentiate the resulting expression for $\dot{\mathcal{I}}^{klp}$ to obtain \mathcal{I}^{klp} (up to the caveats mentioned in the previous subsection). If we do this for an arbitrary orbit,

we do not need to worry about missing terms due to the constant of integration: As we shall demonstrate below, any contributions to \mathcal{I}_{klp} that are constant at Newtonian order vanish for a circular orbit. (It also turns out that any terms that are time-independent for a circular orbit also vanish.) For a generic orbit, it is easiest to start from the explicit 2-body reduction Will and Wiseman give in Eq. (6.6b). The resulting expression is exactly what one would expect from the forms of the 1PN corrections to the mass monopole and quadrupole, viz., $\mathcal{I}^{klp} = m_1 x_1^{klp} (1 + v_1^2/2 - m_2/2b) + (1 \leftrightarrow 2) + O(v^4)$.

To prove our claim that any terms in the 1PN correction to \mathcal{I}^{klp} that are constant at Newtonian order for an arbitrary orbit vanish for a circular orbit, we construct all such possible terms. To do so, we note that the binary's only (nonzero) vectorial Newtonian constants of the motion are its Newtonian angular momentum \vec{L} and Laplace-Runge-Lenz vector $\vec{A} := \vec{p} \times \vec{L} - \mu^2 m \hat{b}$. (Here \vec{p} is the momentum of the reduced mass $\mu := m_1 m_2 / m$.) Noting that these are $O(c^{-1})$ and $O(c^{-2})$, respectively, we can write down the only two possible $O(c^{-2})$ symmetric 3-index (Cartesian) tensors involving only those two vectors (and constants). These will then be the only possible 1PN contributions to \mathcal{I}^{klp} that are constant at Newtonian order. They are, up to numerical factors (which could include contributions of $\|\vec{A}\|/\|\vec{L}\|^2$), $A^{(k} \delta^{lp)}$ and $\|\vec{L}\| L^{(k} \delta^{lp)}/m$. The first of these vanishes for a circular orbit, since \vec{A} does. The second is odd under time reversal and is thus inadmissible, since \mathcal{I}^{klp} should be even, from its definition, given in Eq. (4.5b) in [60].

With all these ingredients, we can put together the far zone metric in the same way as we did in Sec. VI. We thus obtain its various components to the same order as we are keeping the near zone metric (with the above caveats about missing terms), viz., with uncontrolled remainders of $O(v^8)$ in the purely temporal component, $O(v^7)$ in the spatiotemporal components, and $O(v^6)$ in the purely spatial components.

APPENDIX D: COMPUTATION OF THE METRICS

Here we detail exactly how the metrics are computed in the MAPLE scripts that were used (along with BAM) to compute the constraint violations and create the plots. (The scripts themselves, and the resulting C code that MAPLE outputs are available online at [36]).

1. Inner zone

To compute the inner zone metric around hole 1, we substitute the tidal fields given in Eq. (B1) into the expression for Detweiler's perturbed Schwarzschild metric in Cook-Scheel coordinates that we give in Eqs. (3.5) and (3.6), taking $M = m_1$. We then transform using

the coordinate transformation given in Sec. V G. The resulting metric thus includes the $O(v^5)$ terms in the purely temporal and spatial components, though these do not increase the formal accuracy of the initial data. We also do not perform any expansions after substituting the tidal fields and performing the coordinate transformation, so the final, transformed metric also contains various other higher-order-in- v terms. The inner zone metric around hole 2 is obtained by the same procedure, along with the transformations detailed at the beginning of Sec. V A.

We have considered three versions of the inner zone metric: The first version (contained in `04_NoOct`) comes directly from the matching performed in Sec. V and only contains the pieces that we were able to match onto the near zone metric while including all of the multipolar contributions at a given order [i.e., up to octupolar order through $O(v^3)$ and then only up to quadrupolar order through $O(v^5)$]. The second version (contained in `04`) also incorporates the results of the fourth-order octupole matching carried out in Appendix B 2—this includes the 1PN correction to the electric octupole, but only the polynomial part of the accompanying coordinate transformation. The third version (contained in `05` and `all`) adds on the time dependence of all the tidal fields (for a circular orbit), obtained in the manner described in Appendix B 2, though it still uses the same coordinate transformation as before. (We use the 1PN expression for ω when substituting for the unit vectors in obtaining the full time dependence. We leave off the known higher-order corrections to ω here since the expressions for the tidal fields we obtained by matching came from using the 1PN version of ω .)

We calculate the third version by substituting $T\dot{\mathcal{E}}_{kl} \rightarrow (T - t)\dot{\mathcal{E}}_{kl}(0)$ and similarly for $\dot{\mathcal{C}}_{klp}$ in Eqs. (3.6) before substituting in the tidal fields (with full time dependence). These substitutions are necessary because the $T\dot{\mathcal{E}}_{kl}$ and $T\dot{\mathcal{C}}_{klp}$ terms in Eqs. (3.6) come from the expansions of \mathcal{E}_{kl} and \mathcal{C}_{klp} (with full dependence on V , the ingoing Eddington-Finkelstein coordinate) about $V = 0$. We, however, are only including the full time dependence on t , the near zone time coordinate, in the tidal fields, due to our method of obtaining this dependence. These expressions will thus only contain the $t\dot{\mathcal{E}}_{kl}$ and $t\dot{\mathcal{C}}_{klp}$ pieces (when expanded about $t = 0$), so we make the above substitutions to retain the linear T -dependence given by the matching while not including the linear t -dependence twice. (We experimented with including the full time dependence of the tidal fields using T instead of t and found that the constraint violations increased.)

This method of computing the metric deliberately does *not* include the effects of the full time dependence on the spatial variation of the tidal fields' contributions to the metric [due to their dependence on V ; see the discussion following Eq. (3.6)], since these would enter at the same order as the unknown time derivatives of the tidal fields (second derivatives of the quadrupole fields, and first derivatives of the octupole fields). Of course, the

terms we are keeping are higher-order as well, but since they would enter with explicit factors of t in the multipole expansion, they would not be entangled with the explicit appearances of unknown time derivatives. (This follows because the Schwarzschild metric is time-independent in the coordinates we use.) What we have done is equivalent to repeating the matching we have performed at each value of (near zone time) t , up to orbital shrinkage effects, which are higher-order than the terms we are considering here. (We also have not attempted to include the full time dependence of the coordinate transformation for the reasons discussed in Sec. VII.)

2. Near zone

We compute the near zone metric by substituting the trajectories for the point particles [obtained in the manner discussed in Sec. VIA] into Blanchet, Faye, and Pontot's metric [given in Eqs. (7.2) of [58]], including the background resummation given in Sec. VIIIA. Here there are, again, three versions of the metric, one giving $O(v^4)$ data, one $O(v^5)$ data, and one containing the complete 2.5PN metric. Recall that one needs all the components through $O(v^4)$ [resp. $O(v^5)$] in addition to the $O(v^5)$ [resp. $O(v^6)$] terms in the spatiotemporal components in order to obtain $O(v^4)$ [resp. $O(v^5)$] data. N.B.: In order to perform background resummation on the purely temporal component of the complete 2.5PN metric, one needs to also subtract the $O([m_1/r_1]^3)$ portion of the expansion of the background, viz., $2m_1^3/r_1^3$, in Eq. (8.2). All these versions are constructed by truncating the metric components to the desired order before substituting in the trajectories. No expansions are performed after that substitution, since we do not want to drop the higher-order terms that we are keeping in the trajectories (discussed in Sec. VIA) for conformity with the far zone metric. Due to an oversight, we did not include the 3PN corrections to the relative-to-COM re-

lation in the $O(v^4)$ version of the near zone metric.

3. Far zone

The calculation of the far zone metric follows the DIRE approach, detailed in Sec. VI, differentiating multipole moments to obtain the metric. We have the same three versions of the far zone metric as for the near zone metric, and obtain them in the same manner: We expand to the desired order after performing all the substitutions except for ϕ , ω , and b (i.e., the contributions that vary due to secular radiation reaction effects and are discussed in Sec. VIA). We also do not include any of the terms due to derivatives acting on b : These would give nonzero contributions, due to the separation's retarded time dependence from orbital shrinkage, but these terms are quite small, both formally and practically—unlike those due to the radiation reaction effects in the phase or undifferentiated separation—so we neglect them. [For instance, the lowest-order contribution due to the nonzero time derivative of b in the $\partial_{kl}[\mathcal{I}^{kl}(u)/r]$ contribution to g_{00} is formally $O(v^9)$. It is also numerically small: The largest contribution has a magnitude of $\sim 10^{-7}$ when evaluated at the intersection of the x -axis and the inner boundary of the near-to-far transition for our equal-mass test binary, viz., $x \simeq 20m$ —see Sec. VIIIB. For comparison, the contribution of the uncorrected $(m_1/r)v_1^2 + (1 \leftrightarrow 2)$ term in that situation is $\sim 10^{-4}$.] The $O(v^4)$ version uses a slightly different order counting than the $O(v^5)$ and full extended versions: As discussed in Sec. VI, we choose to keep the outer integral terms—here these are the terms that look like $(m/r)^2$ —in the $O(v^4)$ data due to post-Minkowskian considerations, even though those terms are $O(v^5)$ if one interprets the Pati-Will order counting strictly. However, as mentioned in Appendix C, we do not know any of the higher-order outer integral terms, so we simply drop them in the $O(v^5)$ and full extended data.

-
- [1] F. Pretorius, Phys. Rev. Lett. **95**, 121101 (2005), gr-qc/0507014.
 - [2] M. Campanelli, C. O. Lousto, P. Marronetti, and Y. Zlochower, Phys. Rev. Lett. **96**, 111101 (2006), gr-qc/0511048.
 - [3] J. G. Baker, J. Centrella, D.-I. Choi, M. Koppitz, and J. van Meter, Phys. Rev. Lett. **96**, 111102 (2006), gr-qc/0511103.
 - [4] F. Pretorius, in *Physics of Relativistic Objects in Compact Binaries: from Birth to Coalescence*, edited by M. Colpi, P. Casella, V. Gorini, U. Moschella, and A. Possenti (Springer, Berlin, 2009), arXiv:0710.1338 [gr-qc].
 - [5] J. G. Baker, W. D. Boggs, J. Centrella, B. J. Kelly, S. T. McWilliams, and J. R. van Meter, Phys. Rev. D **78**, 044046 (2008), arXiv:0805.1428 [gr-qc].
 - [6] J. A. González, U. Sperhake, and B. Brügmann, Phys. Rev. D **79**, 124006 (2009), arXiv:0811.3952 [gr-qc].
 - [7] M. A. Scheel, M. Boyle, T. Chu, L. E. Kidder, K. D. Matthews, and H. D. Pfeiffer, Phys. Rev. D **79**, 024003 (2009), arXiv:0810.1767 [gr-qc].
 - [8] S. Husa, J. A. González, M. Hannam, B. Brügmann, and U. Sperhake, Class. Quantum Grav. **25**, 105006 (2008), arXiv:0706.0740 [gr-qc].
 - [9] B. Abbott *et al.* (LIGO Scientific Collaboration), arXiv:0711.3041 [gr-qc].
 - [10] L. Lindblom, B. J. Owen, and D. A. Brown, Phys. Rev. D **78**, 124020 (2008), arXiv:0809.3844 [gr-qc].
 - [11] *LISA: Laser Interferometer Space Antenna: A Cornerstone Mission for the observation of gravitational waves: System and Technology Study Report*, ESA-SCI(2000)11, URL

- http://www.srl.caltech.edu/lisa/documents/sts_1.05.pdf
- [12] M. Hannam *et al.*, Phys. Rev. D **79**, 084025 (2009), arXiv:0901.2437 [gr-qc].
 - [13] B. Aylott *et al.*, arXiv:0901.4399 [gr-qc].
 - [14] M. Boyle, D. A. Brown, L. E. Kidder, A. H. Mroué, H. P. Pfeiffer, M. A. Scheel, G. B. Cook, and S. A. Teukolsky, Phys. Rev. D **76**, 124038 (2007), arXiv:0710.0158 [gr-qc].
 - [15] L. Lindblom, arXiv:0907.0457 [gr-qc].
 - [16] H. P. Pfeiffer, D. A. Brown, L. E. Kidder, L. Lindblom, G. Lovelace, and M. A. Scheel, Class. Quantum Grav. **24**, S59 (2007), gr-qc/0702106.
 - [17] S. Husa, M. Hannam, J. A. González, U. Sperhake, and B. Brügmann, Phys. Rev. D **77**, 044037 (2008), arXiv:0706.0904 [gr-qc].
 - [18] B. Walther, B. Brügmann, and D. Müller, arXiv:0901.0993 [gr-qc].
 - [19] T. Bode, D. Shoemaker, F. Herrmann, and I. Hinder, Phys. Rev. D **77**, 044027 (2008), arXiv:0711.0669 [gr-qc].
 - [20] J. A. González, U. Sperhake, B. Brügmann, M. Hannam, and S. Husa, Phys. Rev. Lett. **98**, 091101 (2007), gr-qc/0610154.
 - [21] G. B. Cook, Living Rev. Relativity **3** (2000), URL <http://www.livingreviews.org/lrr-2000-5>.
 - [22] E.ourgoulhon, J. Phys. Conf. Ser. **91**, 012001 (2007), arXiv:0704.0149 [gr-qc].
 - [23] S. Brandt and B. Brügmann, Phys. Rev. Lett. **78**, 3606 (1997), gr-qc/9703066.
 - [24] P. Marronetti, W. Tichy, B. Brügmann, J. González, M. Hannam, S. Husa, and U. Sperhake, Class. Quant. Grav. **24**, S43 (2007), gr-qc/0701123.
 - [25] P. Marronetti, W. Tichy, B. Brügmann, J. González, and U. Sperhake, Phys. Rev. D **77**, 064010 (2008), arXiv:0709.2160 [gr-qc].
 - [26] W. Tichy and P. Marronetti, Phys. Rev. D **76**, 061502 (2007), gr-qc/0703075.
 - [27] W. Tichy and P. Marronetti, Phys. Rev. D **78**, 081501 (2008), arXiv:0807.2985 [gr-qc].
 - [28] W. Tichy, B. Brügmann, and P. Laguna, Phys. Rev. D **68**, 064008 (2003), gr-qc/0306020.
 - [29] W. Tichy and B. Brügmann, Phys. Rev. D **69**, 024006 (2004), gr-qc/0307027.
 - [30] M. A. Scheel, H. P. Pfeiffer, L. Lindblom, L. E. Kidder, O. Rinne, and S. A. Teukolsky, Phys. Rev. D **74**, 104006 (2006), gr-qc/0607056.
 - [31] D. Shoemaker, K. Smith, U. Sperhake, P. Laguna, E. Schnetter, and D. Fiske, Class. Quantum Grav. **20**, 3729 (2003), gr-qc/0301111.
 - [32] G. B. Cook and H. P. Pfeiffer, Phys. Rev. D **70**, 104016 (2004), gr-qc/0407078.
 - [33] A. Ashtekar and B. Krishnan, Living Rev. Relativity **7** (2004), URL <http://www.livingreviews.org/lrr-2004-10>.
 - [34] D. Brown, O. Sarbach, E. Schnetter, M. Tiglio, P. Diener, I. Hawke, and D. Pollney, Phys. Rev. D **76**, 081503 (2007), arXiv:0707.3101 [gr-qc].
 - [35] N. Yunes, Class. Quantum Grav. **24**, 4313 (2007), gr-qc/0611128.
 - [36] URL <http://www.physics.fau.edu/~wolf/Research/harmonics/>
 - [37] N. Yunes, W. Tichy, B. J. Owen, and B. Brügmann, Phys. Rev. D **74**, 104011 (2006), gr-qc/0503011.
 - [38] N. Yunes and W. Tichy, Phys. Rev. D **74**, 064013 (2006), gr-qc/0601046.
 - [39] A. Garat and R. H. Price, Phys. Rev. D **61**, 124011 (2000), gr-qc/0002013.
 - [40] J. A. Valiente Kroon, Class. Quantum Grav. **21**, 3237 (2004), gr-qc/0402033.
 - [41] K. Alvi, Phys. Rev. D **61**, 124013 (2000), gr-qc/9912113.
 - [42] S. Nissanke, Phys. Rev. D **73**, 124002 (2006), gr-qc/0509128.
 - [43] B. J. Kelly, W. Tichy, M. Campanelli, and B. F. Whiting, Phys. Rev. D **76**, 024008 (2007), arXiv:0704.0628 [gr-qc].
 - [44] L. Blanchet, Phys. Rev. D **68**, 084002 (2003), gr-qc/0304080.
 - [45] W. Tichy, B. Brügmann, M. Campanelli, and P. Diener, Phys. Rev. D **67**, 064008 (2003), gr-qc/0207011.
 - [46] G. Lovelace, Class. Quantum Grav. **26**, 114002 (2009), arXiv:0812.3132 [gr-qc].
 - [47] G. Lovelace, R. Owen, H. P. Pfeiffer, and T. Chu, Phys. Rev. D **78**, 084017 (2008), arXiv:0805.4192 [gr-qc].
 - [48] R. A. Matzner, M. F. Huq, and D. Shoemaker, Phys. Rev. D **59**, 024015 (1999), gr-qc/9805023.
 - [49] P. Marronetti and R. A. Matzner, Phys. Rev. Lett. **85**, 5500 (2000), gr-qc/0009044.
 - [50] P. Marronetti, M. Huq, P. Laguna, L. Lehner, R. A. Matzner, and D. Shoemaker, Phys. Rev. D **62**, 024017 (2000), gr-qc/0001077.
 - [51] U. Sperhake, Phys. Rev. D **76**, 104015 (2007), gr-qc/0606079.
 - [52] M. Hannam, S. Husa, B. Brügmann, J. A. González, and U. Sperhake, Class. Quantum Grav. **24**, S15 (2007), gr-qc/0612001.
 - [53] S. Dain, Phys. Rev. Lett. **87**, 121102 (2001), gr-qc/0012023.
 - [54] S. Dain, Phys. Rev. D **64**, 124002 (2001), gr-qc/0103030.
 - [55] H. P. Pfeiffer, G. B. Cook, and S. A. Teukolsky, Phys. Rev. D **66**, 024027 (2002), gr-qc/0203085.
 - [56] H.-J. Yo, J. N. Cook, S. L. Shapiro, and T. W. Baumgarte, Phys. Rev. D **70**, 084033 (2004), gr-qc/0406020.
 - [57] B. J. Kelly, W. Tichy, Y. Zlochower, M. Campanelli, and B. F. Whiting, in preparation.
 - [58] L. Blanchet, G. Faye, and B. Ponsot, Phys. Rev. D **58**, 124002 (1998), gr-qc/9804079.
 - [59] S. Detweiler, Class. Quantum Grav. **22**, S681 (2005), gr-qc/0501004.
 - [60] M. E. Pati and C. M. Will, Phys. Rev. D **62**, 124015 (2000), gr-qc/0007087.
 - [61] M. E. Pati and C. M. Will, Phys. Rev. D **65**, 104008 (2002), gr-qc/0201001.
 - [62] L. Blanchet, Living Rev. Relativity **9** (2006), URL <http://www.livingreviews.org/lrr-2006-4>.
 - [63] H. P. Pfeiffer, L. E. Kidder, M. A. Scheel, and S. A. Teukolsky, Comput. Phys. Commun. **152**, 253 (2003), gr-qc/0202096.
 - [64] M. Holst, L. Lindblom, R. Owen, H. P. Pfeiffer, M. A. Scheel, and L. E. Kidder, Phys. Rev. D **70**, 084017 (2004), gr-qc/0407011.
 - [65] T. Bode, P. Laguna, D. M. Shoemaker, I. Hinder, F. Herrmann, and B. Vaishnav, arXiv:0902.1127 [gr-qc].
 - [66] N. Jansen and M. Brügmann (unpublished).
 - [67] G. B. Cook and M. A. Scheel, Phys. Rev. D **56**, 4775 (1997).
 - [68] E. Poisson, Phys. Rev. Lett. **94**, 161103 (2005), gr-qc/0501032.

- [69] K. S. Thorne and J. B. Hartle, Phys. Rev. D **31**, 1815 (1985).
- [70] X.-H. Zhang, Phys. Rev. D **34**, 991 (1986).
- [71] C. M. Will and A. G. Wiseman, Phys. Rev. D **54**, 4813 (1996).
- [72] P. Jaranowski and G. Schäfer, Phys. Rev. D **57**, 7274 (1998), gr-qc/9712075.
- [73] S. Taylor and E. Poisson, Phys. Rev. D **78**, 084016 (2008), arXiv:0806.3052 [gr-qc].
- [74] P. Musgrave, D. Pollney, and K. Lake, *GRTensorII software* (1996), URL <http://grtensor.phy.queensu.ca/>.
- [75] C. M. Bender and S. A. Orszag, *Advanced Mathematical Methods for Scientists and Engineers* (McGraw-Hill, New York, 1978).
- [76] O. Poujade and L. Blanchet, Phys. Rev. D **65**, 124020 (2002), gr-qc/0112057.
- [77] J. B. Hartle, K. S. Thorne, and R. H. Price, in *Black Holes: The Membrane Paradigm*, edited by K. S. Thorne, R. H. Price, and D. A. Macdonald (Yale University Press, New Haven, 1986).
- [78] S. Detweiler (private communication).
- [79] R. Rieth, in *Mathematics of Gravitation. Part II: Gravitational Wave Detection*, edited by A. Królak (Polish Academy of Sciences, Institute of Mathematics, Warsaw, 1997), vol. 41 of *Banach Center Publications*, pp. 71–74, nearly identical to gr-qc/9603043.
- [80] T. Damour, P. Jaranowski, and G. Schäfer, Phys. Rev. D **62**, 084011 (2000), gr-qc/0005034.
- [81] J. A. Isenberg, Int. J. Mod. Phys. D **17**, 265 (2008), gr-qc/0702113.
- [82] J. R. Wilson, G. J. Mathews, and P. Marronetti, Phys. Rev. D **54**, 1317 (1996), gr-qc/9601017.
- [83] R. M. Wald, *General Relativity* (University of Chicago Press, Chicago, 1984).
- [84] H. Stephani, D. Kramer, M. MacCallum, C. Hoense-laers, and E. Herlt, *Exact solutions of Einstein's field equations* (Cambridge University Press, Cambridge, 2003), 2nd ed.
- [85] J. A. Schouten, *Ricci-Calculus: An Introduction to Tensor Analysis and its Geometrical Applications* (Springer, Berlin, 1954), 2nd ed.
- [86] L. Blanchet (private communication).
- [87] G. Schäfer, Ann. Phys. (N. Y.) **161**, 81 (1985).
- [88] L. Blanchet, Phys. Rev. D **47**, 4392 (1993).
- [89] N. Straumann, *General relativity: with applications to astrophysics* (Springer, Berlin, 2004), rev. ed.
- [90] L. Blanchet and T. Damour, Ann. Inst. Henri Poincaré Phys. Théor. **50**, 377 (1989).
- [91] S. Weinberg, *Gravitation and Cosmology: Principles and Applications of the General Theory of Relativity* (Wiley, New York, 1972).
- [92] T. Damour, B. R. Iyer, and B. S. Sathyaprakash, Phys. Rev. D **63**, 044023 (2001), gr-qc/0010009.
- [93] L. Blanchet and B. R. Iyer, Class. Quantum Grav. **20**, 755 (2003), gr-qc/0209089.
- [94] T. Damour, Int. J. Mod. Phys. A **23**, 1130 (2008), arXiv:0802.4047 [gr-qc].
- [95] J. D. Jackson, *Classical Electrodynamics* (Wiley, New York, 1999), 3rd ed.
- [96] L. E. Simone, S. W. Leonard, E. Poisson, and C. M. Will, Class. Quantum Grav. **14**, 237 (1997), gr-qc/9610058.
- [97] J. Pullin (private communication).
- [98] B. Brügmann, W. Tichy, and N. Jansen, Phys. Rev. Lett. **92**, 211101 (2004), gr-qc/0312112.
- [99] B. Brügmann, J. A. González, M. Hannam, S. Husa, U. Sperhake, and W. Tichy, Phys. Rev. D **77**, 024027 (2008), gr-qc/0610128.
- [100] P. Ajith *et al.*, Class. Quantum Grav. **24**, S689 (2007), arXiv:0704.3764 [gr-qc].
- [101] W. Tichy, *A new numerical method to construct binary neutron star initial data*, in preparation.
- [102] F. Pretorius, in preparation.
- [103] M. Ansorg, B. Brügmann, and W. Tichy, Phys. Rev. D **70**, 064011 (2004), gr-qc/0404056.
- [104] C. Königsdörffer and A. Gopakumar, Phys. Rev. D **73**, 124012 (2006), gr-qc/0603056.
- [105] H. Tagoshi, A. Ohashi, and B. J. Owen, Phys. Rev. D **63**, 044006 (2001), gr-qc/0010014.
- [106] G. Faye, L. Blanchet, and A. Buonanno, Phys. Rev. D **74**, 104033 (2006), errata in **75**, 049903(E) (2007), gr-qc/0605139.
- [107] C. M. Will, Phys. Rev. D **71**, 084027 (2005), gr-qc/0502039.
- [108] N. Yunes and J. A. González, Phys. Rev. D **73**, 024010 (2006), gr-qc/0510076.
- [109] E. Poisson, Phys. Rev. D **70**, 084044 (2004), gr-qc/0407050.
- [110] L. E. Kidder, C. M. Will, and A. G. Wiseman, Phys. Rev. D **47**, 3281 (1993).